A Dissertation

On

Cam Gear Walk off in a Diesel Engine

Submitted in partial fulfilment of requirements for the degree of

Master of Engineering

in

CAD / CAM Engineering

Submitted by

Naval Gupta

Registration No.: 801784011

Under the Supervisions of

Dr. Tarun Kumar Bera
Associate Professor
Mechanical Engineering Department
Thapar Institute of Engineering & Technology
(Deemed to be University), Patiala

Dr. Ashish Singla
Associate Professor
Mechanical Engineering Department
Thapar Institute of Engineering & Technology
(Deemed to be University), Patiala

Mr. Omkar D. Vaidya
Product Design Engineer
Technical Specialist EBU India
Eng. Systems Team
Cummins Technologies India Pvt. Ltd.

Mechanical Engineering Department
Thapar Institute of Engineering and Technology
(Deemed to be University)
Patiala-147004, India
July 2019

DECLARATION

I hereby declare that the work done in thesis report entitled, " ***Cam Gear Walk off in a Diesel Engine****" submitted towards partial fulfilment of award of* ***Master of Engineering*** *degree in* ***CAD/CAM Engineering*** *in* ***Mechanical Engineering Department of Thapar Institute of Engineering and Technology, Patiala*** *is an authentic record of work carried out by me under the supervision and guidance of* ***Dr. Tarun Kumar Bera, Associate Professor, Mechanical Engineering Department*** *of* ***Thapar Institute*** *of* ***Engineering and Technology, Patiala*** *and* ***Mr. Omkar D. Vaidya, Product Design Engineer, Technical Specialist, EBU India Engineering Systems Team, Cummins Technologies India Pvt. Limited, Pune.***

Naval

Naval Gupta

Date: 30/07/2019

This is to certify that above declaration made by the student concerned is correct to the best of my knowledge and belief.

Mr. Omkar D. Vaidya
Product Design Engineer
Technical Specialist EBU India
Engineering Systems Team
Cummins Technologies India Pvt. Ltd.

Tarun Kumar Bera 30/7/19

Dr. Tarun Kumar Bera
Associate Professor
Mechanical Engineering Department
Thapar Institute of Engineering & Technology
(Deemed to be University), Patiala

30/7/19

Dr. Ashish Singla
Associate Professor
Mechanical Engineering Department
Thapar Institute of Engineering & Technology
(Deemed to be University), Patiala

ACKNOWLEDGEMENTS

This thesis work was carried out in Cummins Technologies India Pvt. Ltd., Pune as an M.Tech. Intern and as a student of M.E. CAD/CAM at Thapar Institute of Engineering and Technology, Patiala. I am greatly obliged to Cummins and the authorities of Thapar Institute of Engineering and Technology, Patiala that I was given an opportunity to work as an intern in Cummins so that I could carry out my academic research work while honing my skills at the corporate life for the future readiness.

First and the foremost I would like to express my gratitude to my academic supervisors **Dr. Tarun Kumar Bera** and **Dr. Ashish Singla, Associate Professors, Mechanical Engineering Department, Thapar Institute of Engineering and Technology (Deemed to be University), Patiala** and my industry manager and mentors **Mr. Omkar D. Vaidya, Product Design Engineer – Technical Specialist, EBU India Engineering Systems Team, Cummins Technologies India Pvt. Ltd.** for their unfailing inspiration, fruitful suggestions, whole-hearted cooperation, thought provoking discussions and painstaking supervision during the entire period. Their continuous motivation and the ability to provide me with constructive suggestions made my work interesting and helped me improve the quality of my work at every step. I would also like to express my sincere thanks to the design and applied mechanics team of EBU to continuously motivate me and give constant support on whatever I needed help on. They kept me engaged in every team activity and taught me how to work as a team. They unfailingly helped me with all the analysis concepts and the methodology of the gear design without which I would not have been able to attain this quality of work.

I would take this opportunity to show regards to my parents, my brother and my friends for giving me inspiration, moral support and go get attitude in my life and for supporting me in every situation and giving me the energy to complete my goals.

(Naval Gupta)

ABSTRACT

A diesel engine, for the heavy commercial vehicles, employing a helical engine gear train which was developed by Cummins a few issues were observed with the cam gear while engine over speeding. A failure of cam gear walk-off was observed due to which the timing of the engine was affected leading to failure of the engine.

Current understanding for the root cause of failure is significant torsional vibrations introduced in the gear train at over-speeds. The preliminary tests and studies to the issue suggested changing the helical gear train to the spur gear train as this would fit into the gear cover with the same work envelope and without axial thrust but would require a thorough research so that it works properly with low vibrations. The gears are expected to work in various speed and load ranges, due to which they experience higher dynamic loads further giving rise to various failure modes like bending fatigue and surface wears which hamper the functioning and life of the gear train. Therefore, to improve the durability and reduce noise a thorough dynamic analysis of the system should be done. The dynamic response of the gear system is a lot sensitive to the modifications of the tooth profile from a perfect involute. Thus, intentional modifications to the micro design of the tooth profile is to be done to reduce the dynamic forces at some torque values.

In this project, the spur gear train will be designed so as the vibrations are least by checking the dynamic response of the model and further the micro design will be modified to reduce the wear of the teeth of the gears. The joint capacity analysis and the gear web design will also be done.

Keywords: gear train, over-speeds, vibrations, durability, noise, dynamic, micro design, joint capacity, web design.

LIST OF ABBREVIATIONS

3-D	Three Dimensional
rpm	Revolutions Per Minute
AC	Air Compressor
AGMA	American Gear Manufacturers Association
CAD	Computer Aided Design
CR	Contact Ratio
CSD	Contact Stress Distribution
DF	Dynamic Factors
DIN	Deutsches Institut für Normung
DTE	Dynamic Transmission Error
EAP	End of Active Profile
EFR	Equivalent Fully Reversed
FEA	Finite Element Analysis
FEM	Finite Element Methods
FP	Fuel Pump
HPSTC	Highest Point of Single Tooth Contact
ISO	International Organisation for Standardization
KTE	Kinematic Transmission Error
LDP	Load Distribution Program
LID	Load Intensity Distribution
LPG	Lube Pump Gear
LPI	Lube Pump Idler
LPSTC	Lowest Point of Single Tooth Contact
MTE	Manufacturing Transmission Error
RPH	Repairs Per Hundred
SAP	Start of Active Pitch
STE	Static Transmission Error
TD	Temperature Distribution
TDC	Top Dead Centre
TE	Transmission Error

NOMENCLATURE

a	Pre-Set Centre Distance (mm)
b	Width of the Gear (mm)
b_{h}	Hertzian Contact Half Width (mm)
d	Pitch Diameter (mm)
d_0	Outer Diameter of the Shaft (mm)
d_{b}	Base Diameter (mm)
d_{i}	Inner Diameter of the Shaft (mm)
d_{n}	Nominal Diameter of the Interference Fit (mm)
d_{w}	Working Pitch Diameter (mm)
h	Total Height of the Tooth (mm)
$h_{\mathrm{a1}}, h_{\mathrm{a2}}$	Addendum Height (mm)
i	Speed Ratio
inv	Involute
k	Nut Factor
l	Length of Interference (mm)
l_{a}	Length of Action (mm)
m	Module (mm)
p_{b}	Base Pitch (mm)
p_{i}	Pressure due to Interference (N/m^2)
p	Circular Pitch (mm)
q	Radius of Crank Throw / Rod Length (mm)
r	Instantaneous Value of Radius of Curvature of Tooth Profile at Pitch Point (mm)
$r_{\mathrm{a1}}, r_{\mathrm{a2}}$	Addendum Radius of Driven and the Driver Gear Respectively (mm)
r_{b}	Radius of base circle (mm)
$r_{\mathrm{b1}}, r_{\mathrm{b2}}$	Base Radius of Driven and the Driver Gear Respectively (mm)
r_{cr}	Crank Radius (mm)
$r_{\mathrm{p1}}, r_{\mathrm{p2}}$	Pitch Radius of Driven and the Driver Gear Respectively (mm)
r_{r}	Root Radius (mm)
s_{b}	Base Circular Tooth Thickness (mm)

t	Thickness of the Tooth at the Root Fillet (mm)
tt	Tooth Thickness (mm)
x_1, x_2	Addendum Modification Coefficients on Driven and Driver Gear Respectively (mm)
y	Centre Distance Modification Coefficient
y_p	Bending Arm Length (mm)
z	Number of Teeth
z_1, z_2	Number of Teeth of Driven and Driver Gear Respectively
A	Area of the Piston (mm^2)
C	Gear Contact Damping (N-s/mm)
D_b	Nominal Diameter of the Nut (mm)
E	Youngs Modulus (MPa)
F	Nominal Transverse Load (N)
F_c	Contact Force pressing the cylinder (N)
F_f	Frictional Force (N)
F_t	Tangential Force (N)
J	Mass Moment of Inertia (kg-m^2)
K	Contact Stiffness (N/mm)
L_c	Length of Contact Line (mm)
L_cyl	Length of Cylinders (mm)
M	Mass (kg)
P_max	Maximum Surface Pressure (N/m^2)
P_θ	Cylinder Pressure at Crank Angle θ (N/m^2)
T	Torque (N-m)
T_n	Nut Pre-Torque (N-m)
T_i	Inertia Torque (N-m)
T_p	Pressure Torque (N-m)
W_b	Bolt Clamp Load (N)
Y	Lewis Form Factor

Greek Characters

α_n	Normal Pressure Angle (°)

α_t	Transverse Pressure angle (°)
α_w	Working Pressure Angle (°)
δ_H	Hertzian Contact Deformation (mm)
δ_b	Elastic Deformation of the tooth (mm)
δ_i	Interference (mm)
θ_t	Taper Angle (°)
θ	Angle Moved by Crank (rad)
σ_b	Bending / Tooth Root Stress (MPa)
σ_c	Hertzian Contact Stress (MPa)
ζ	Damping Ratio
γ	Angle Moved by the Gear (°)
λ	Coefficient defining speed reducing or speed increasing gear pair
μ	Coefficient of Friction
ν	Poisson's Ratio
φ	Auxiliary Angle, (rad)
ψ	Helix Angle (°)
ω	Angular Velocity (rad/s)

LIST OF FIGURES

Fig. No.	Figure Captions	Page No.
1.1(a)	Picture showing cam gear walk off	1
1.1(b)	Picture showing cam gear out of place	1
1.2(a)	Schematic showing crankshaft and its nomenclature	4
1.2(b)	Schematic showing the crank throw configuration for a 6-cylinder engine	4
1.3	Schematic of a camshaft from a 4-cylinder diesel engine	5
1.4	3D model showing the timing gear train with crankshaft and the camshaft	6
1.5	Schematic showing nomenclature of spur gear	7
1.6	Schematic showing tooth profiles with zero, negative and positive addendum modification	11
1.7(a)	Schematic of Axial misalignment	12
1.7(b)	Schematic of Radial misalignment	12
1.7(c)	Schematic of Pitch misalignment	12
1.7(d)	Schematic of Yaw misalignment	12
1.8	Schematic depicting start of active profile (SAP) and end of active profile EAP	14
1.9	Schematic showing LPSTC and HPSTC of the low contact ratio (CR) and high contact ratio gears	14
1.10(a)	Schematic of Tooth tip and root relief	15
1.10(b)	Schematic of Profile crowning	15
1.11	Schematic of Lead crowning	16
3.1	Work flow process opted for achieving each objective	28
3.2	Layout of the engine gear train and the rotation direction of each gear	29

Fig. No.	Figure Captions	Page No.
3.3	3D model showing the gear train arrangement employing standard spur gears	30
3.4	Normalized graph of torque experienced by a single crank throw at rated rpm	35
3.5	Combined torques (normalized) acting on each cylinder	36
3.6	Crankshaft spring, mass damper system	37
3.7	Camshaft spring, mass damper system	38
3.8(a)	Schematic of Gear connection	38
3.8(b)	Gear inertia, contact, revolute joint and earthing components	38
3.9(a)	Schematic showing zone of action	40
3.9(b)	Schematic of Gear side nomenclature	40
3.10	Dynamic model map of the timing system of the engine	41
3.11(a)	Schematic of Deformation due to the Hertzian contact stress	44
3.11(b)	Schematic of Tooth elastic deformation	44
3.12(a)	Schematic showing Hertzian contact between two cylinders	46
3.12(b)	Schematic showing Hertzian contact between a pair of gear teeth	46
3.13	Schematic showing the tooth nomenclature while experiencing bending according to Wilfred Lewis	48
3.14	Spur gear graph for Lewis form factor	48
3.15	Schematic showing the taper fit assembly	51
4.1	3D CAD Model showing the Effect of Addendum Modification	53
4.2	3D CAD Model Showing Gear Train Employing Addendum Modified Spur Gears	54
4.3(a)	Without Backlash Contact Forces Comparison for Base Helical Model and Re-Constructed Helical Model (Normalized) of Crank-Cam Pair	55

Fig. No.	Figure Captions	Page No.
4.3(b)	Without Backlash Contact Forces Comparison for Base Helical Model and Re-Constructed Helical Model (Normalized) of Cam-AC Pair	55
4.3(c)	Without Backlash Contact Forces Comparison for Base Helical Model and Re-Constructed Helical Model (Normalized) of Cam-FP Pair	55
4.4(a)	Without Backlash Contact Forces Comparison for Re-Constructed Helical Model and Addendum Modified Spur Gear Model (Normalized) of Crank-Cam Pair	56
4.4(b)	Without Backlash Contact Forces Comparison for Re-Constructed Helical Model and Addendum Modified Spur Gear Model (Normalized) of Cam-AC Pair	56
4.4(c)	Without Backlash Contact Forces Comparison for Re-Constructed Helical Model and Addendum Modified Spur Gear Model (Normalized) of Cam-FP Pair	57
4.5(a)	With Backlash Contact Forces Comparison for Re-Constructed Helical Model and Addendum Modified Spur Gear Model (Normalized) of Crank-Cam Pair	57
4.5(b)	With Backlash Contact Forces Comparison for Re-Constructed Helical Model and Addendum Modified Spur Gear Model (Normalized) of Cam-AC Pair	58
4.5(c)	With Backlash Contact Forces Comparison for Re-Constructed Helical Model and Addendum Modified Spur Gear Model (Normalized) of Cam-FP Pair	58
4.6(a)	Comparison of Root Stresses (Von-Mises) on the Gear teeth of Crank Gear Using the Forces on the Crank-Cam Pair Tensile Root Stress LDP	56
4.6(b)	Comparison of Root Stresses (Von-Mises) on the Gear teeth of Crank Gear Using the Forces on the Crank-Cam Pair Compressive Root Stress LDP	59
4.6(c)	Comparison of Root Stresses (Von-Mises) on the Gear teeth of Crank Gear Using the Forces on the Crank-Cam Pair Maximum Root Stress LDP	59

Fig. No.	Figure Captions	Page No.
4.6(d)	Comparison of Root Stresses (Von-Mises) on the Gear teeth of Crank Gear Using the Forces on the Crank-Cam Pair Tensile and Compressive Root Stress ANSYS	59
4.7(a)	Comparison of Root Stresses (Von-Mises) on the Gear teeth of Cam Gear Using the Forces on the Crank-Cam Pair Tensile Root Stress LDP	60
4.7(b)	Comparison of Root Stresses (Von-Mises) on the Gear teeth of Cam Gear Using the Forces on the Crank-Cam Pair Compressive Root Stress LDP	60
4.7(c)	Comparison of Root Stresses (Von-Mises) on the Gear teeth of Cam Gear Using the Forces on the Crank-Cam Pair Maximum Root Stress LDP	60
4.7(d)	Comparison of Root Stresses (Von-Mises) on the Gear teeth of Cam Gear Using the Forces on the Crank-Cam Pair Tensile and Compressive Root Stress ANSYS	60
4.8(a)	Comparison of Root Stresses (Von-Mises) on the Gear Teeth of FP Gear Using the Forces on the Cam-FP Pair Tensile Root Stress LDP	60
4.8(b)	Comparison of Root Stresses (Von-Mises) on the Gear Teeth of FP Gear Using the Forces on the Cam-FP Pair Compressive Root Stress LDP	60
4.8(c)	Comparison of Root Stresses (Von-Mises) on the Gear Teeth of FP Gear Using the Forces on the Cam-FP Pair Maximum Root Stress LDP	60
4.8(d)	Comparison of Root Stresses (Von-Mises) on the Gear Teeth of FP Gear Using the Forces on the Cam-FP Pair Tensile and Compressive Root Stress ANSYS	60
4.9(a)	Comparison of TE between the Crank-Cam Gear Pair - TE Plot of Baseline Helical	62
4.9(b)	Comparison of TE between the Crank-Cam Gear Pair - TE Plot of Unmodified Spur	62
4.9(c)	Comparison of TE between the Crank-Cam Gear Pair - TE Plot of Microgeometry Optimized Spur	62
4.10(a)	Comparison of CSD between the Crank-Cam Gear Pair - CSD Plot of Baseline Helical	62

Fig. No.	Figure Captions	Page No.
4.10(b)	Comparison of CSD between the Crank-Cam Gear Pair - CSD Plot of Unmodified Spur	62
4.10(c)	Comparison of CSD between the Crank-Cam Gear Pair - CSD Plot of Microgeometry Optimized Spur	63
4.11(a)	Comparison of LID between the Crank-Cam Gear Pair - LID Plot of Baseline Helical	60
4.11(b)	Comparison of LID between the Crank-Cam Gear Pair - LID Plot of Unmodified Spur	64
4.11(c)	Comparison of LID between the Crank-Cam Gear Pair - LID Plot of Microgeometry Optimized Spur	64
4.12(a)	Comparison of TD between the Crank-Cam Gear Pair - TD Plot of Baseline Helical	64
4.12(b)	Comparison of TD between the Crank-Cam Gear Pair - TD Plot of Unmodified Spur	64
4.12(c)	Comparison of TD between the Crank-Cam Gear Pair - TD Plot of Microgeometry Optimized Spur	64
4.13(a)	Comparison of Maximum Root Stress (Von-Mises) of Crank Gear between the Crank-Cam Gear Pair - Root Stress Plot of Baseline Helical	65
4.13(b)	Comparison of Maximum Root Stress (Von-Mises) of Crank Gear between the Crank-Cam Gear Pair - Root Stress Plot of Unmodified Spur	65
4.13(c)	Comparison of Maximum Root Stress (Von-Mises) of Crank Gear between the Crank-Cam Gear Pair - Root Stress Plot of Microgeometry Optimized Spur	65
4.14(a)	Comparison of Maximum Root Stress (Von-Mises) of Cam Gear between the Crank-Cam Gear Pair - Root Stress Plot of Baseline Helical	66
4.14(b)	Comparison of Maximum Root Stress (Von-Mises) of Cam Gear between the Crank-Cam Gear Pair - Root Stress Plot of Unmodified Spur	66
4.14(c)	Comparison of Maximum Root Stress (Von-Mises) of Cam Gear between the Crank-Cam Gear Pair - Root Stress Plot of Microgeometry Optimized Spur	66

Fig. No.	Figure Captions	Page No.
4.15	Percentage Change in Maximum Value of Analyzed Attributes by Microgeometry Optimization in Crank-Cam Pair	67
4.16(a)	Comparison of TE between the Cam-AC Gear Pair - TE Plot of Baseline Helical	67
4.16(b)	Comparison of TE between the Cam-AC Gear Pair - TE Plot of Unmodified Spur	67
4.16(c)	Comparison of TE between the Cam-AC Gear Pair - TE Plot of Microgeometry Optimized Spur	67
4.17(a)	Comparison of CSD between the Cam-AC Gear Pair - CSD Plot of Baseline Helical	68
4.17(b)	Comparison of CSD between the Cam-AC Gear Pair - CSD Plot of Unmodified Spur	68
4.17(c)	Comparison of CSD between the Cam-AC Gear Pair - CSD Plot of Microgeometry Optimized Spur	68
4.18(a)	Comparison of LID between the Cam-AC Gear Pair - LID Plot of Baseline Helical	68
4.18(b)	Comparison of LID between the Cam-AC Gear Pair - LID Plot of Unmodified Spur	68
4.18(c)	Comparison of LID between the Cam-AC Gear Pair - LID Plot of Microgeometry Optimized Spur	68
4.19(a)	Comparison of TD between the Cam-AC Gear Pair - TD Plot of Baseline Helical	69
4.19(b)	Comparison of TD between the Cam-AC Gear Pair - TD Plot of Unmodified Spur	69
4.19(c)	Comparison of TD between the Cam-AC Gear Pair - TD Plot of Microgeometry Optimized Spur	69
4.20(a)	Comparison of Maximum Root Stress (Von-Mises) of Cam Gear between the Cam-AC Gear Pair - Root Stress Plot of Baseline Helical	70
4.20(b)	Comparison of Maximum Root Stress (Von-Mises) of Cam Gear between the Cam-AC Gear Pair - Root Stress Plot of Unmodified Spur	70

Fig. No.	Figure Captions	Page No.
4.20(c)	Comparison of Maximum Root Stress (Von-Mises) of Cam Gear between the Cam-AC Gear Pair - Root Stress Plot of Microgeometry Optimized Spur	70
4.21(a)	Comparison of Maximum Root Stress (Von-Mises) of AC Gear between the Cam-AC Gear Pair - Root Stress Plot of Baseline Helical	70
4.21(b)	Comparison of Maximum Root Stress (Von-Mises) of AC Gear between the Cam-AC Gear Pair - Root Stress Plot of Unmodified Spur	70
4.21(c)	Comparison of Maximum Root Stress (Von-Mises) of AC Gear between the Cam-AC Gear Pair - Root Stress Plot of Microgeometry Optimized Spur	71
4.22	Percentage Change in Maximum Value of Analyzed Attributes by Microgeometry Optimization in Cam-AC Pair	71
4.23(a)	Comparison of TE between the Cam-FP Gear Pair - TE Plot of Baseline Helical	71
4.23(b)	Comparison of TE between the Cam-FP Gear Pair - TE Plot of Unmodified Spur	71
4.23(c)	Comparison of TE between the Cam-FP Gear Pair - TE Plot of Microgeometry Optimized Spur	71
4.24(a)	Comparison of CSD between the Cam-FP Gear Pair - CSD Plot of Baseline Helical	72
4.24(b)	Comparison of CSD between the Cam-FP Gear Pair - CSD Plot of Unmodified Spur	72
4.24(c)	Comparison of CSD between the Cam-FP Gear Pair - CSD Plot of Microgeometry Optimized Spur	72
4.25(a)	Comparison of LID between the Cam-FP Gear Pair - LID Plot of Baseline Helical	73
4.25(b)	Comparison of LID between the Cam-FP Gear Pair - LID Plot of Unmodified Spur	73
4.25(c)	Comparison of LID between the Cam-FP Gear Pair - LID Plot of Microgeometry Optimized Spur	73

Fig. No.	Figure Captions	Page No.
4.26(a)	Comparison of TD between the Cam-FP Gear Pair - TD Plot of Baseline Helical	73
4.26(b)	Comparison of TD between the Cam-FP Gear Pair - TD Plot of Unmodified Spur	73
4.26(c)	Comparison of TD between the Cam-FP Gear Pair - TD Plot of Microgeometry Optimized Spur	73
4.27(a)	Comparison of Maximum Root Stress (Von-Mises) of Cam Gear between the Cam-FP Gear Pair - Root Stress Plot of Baseline Helical	74
4.27(b)	Comparison of Maximum Root Stress (Von-Mises) of Cam Gear between the Cam-FP Gear Pair - Root Stress Plot of Unmodified Spur	74
4.27(c)	Comparison of Maximum Root Stress (Von-Mises) of Cam Gear between the Cam-FP Gear Pair - Root Stress Plot of Microgeometry Optimized Spur	74
4.28(a)	Comparison of Maximum Root Stress (Von-Mises) of FP Gear between the Cam-FP Gear Pair - Root Stress Plot of Baseline Helical	75
4.28(b)	Comparison of Maximum Root Stress (Von-Mises) of FP Gear between the Cam-FP Gear Pair - Root Stress Plot of Unmodified Spur	75
4.28(c)	Comparison of Maximum Root Stress (Von-Mises) of FP Gear between the Cam-FP Gear Pair - Root Stress Plot of Microgeometry Optimized Spur	75
4.29	Percentage Change in Maximum Value of Analyzed Attributes by Microgeometry Optimization in Cam-FP Pair	75
4.30	Von-Mises Stresses (Normalized) on the Cam Gear Web Due to Loading on the Teeth	76
4.31	Von-Mises Stresses (Normalized) on the FP Gear Web Due to Loading on the Teeth	76
4.32(a)	EFR Stress Field During Forward Loading of Cam Gear	77
4.32(b)	EFR Stress Field During Forward Loading of FP Gear	77
4.32(c)	EFR Stress Field During Reverse Loading of Cam Gear	77

Fig. No.	Figure Captions	Page No.
4.32(d)	EFR Stress Field During Reverse Loading of FP Gear	77
4.32(e)	EFR Stress Field During Forward-Reverse Loading of Cam Gear	77
4.32(f)	EFR Stress Field During Forward-Reverse Loading of FP Gear	77
4.33	Torque Carrying Capacity (Normalized) for Crank Gear Press Fit Joint	78
4.34	Torque Carrying Capacity (Normalized) for Cam Gear Press Fit Joint	79
4.35	Torque Carrying Capacity (Normalized) for AC Gear Taper Fit Joint	80
4.36	Torque Carrying Capacity (Normalized) for FP Gear Taper Fit Joint	80

LIST OF TABLES

Table No.	Table Captions	Page No.
3.1	Error in the speed ratio and the centre distance of standard spur gear with original helical gear	30
3.2	Calculated values (normalized) for the addendum modification coefficient corresponding to the centre distances	32
3.3	Normalized values for addendum modification coefficients for each gear	33
3.4	Percentage change in attributes after addendum modification	34
3.5	Normalized values of torques and cylinder pressures obtained for every crank throw	35
3.6	Normalized stiffnesses and dampings for the helical and the spur gears	40
3.7	Normalized value of the calculated Hertzian deformation, the elastic deformation and the minimum tooth tip relief	45
3.8	Normalized values of Crank-Cam pair microgeometries	46
3.9	Values of the Lewis form factor Y, for 20° pressure angle, full-depth teeth, and unit diametral pitch in the rotation plane	49
3.10	Normalized values of calculated contact pressure, frictional force and torque capacity of press fit joint	52
3.11	The values of nut factor for various coatings	52

TABLE OF CONTENTS

DECLARATION i

ACKNOWLEDGEMENTS ii

ABSTRACT iii

LIST OF ABBREVIATIONS iv

NOMENCLATURE v

LIST OF FIGURES viii

LIST OF TABLES xvii

Chapter 1: Introduction 1–16

1.1 Background and Motivation 1

1.2 Problem Statement 2

1.3 Expected Rewards of the Proposed Project 2

1.4 Hypothesis Considered 3

1.5 Diesel Engine Timing System 4

1.5.1 Crankshaft 4

1.5.2 Camshaft 5

1.5.3 Timing Gear Train 5

1.6 Theoretical Background of Gear Design 7

1.6.1 Gear Nomenclature 7

1.6.2 Backlash 9

1.6.3 Contact Ratio 9

1.6.4 Addendum Modification 10

1.6.5 Misalignments 11

1.6.6 Transmission Error 12

1.6.7 Microgeometry 13

1.6.8 Types of Gear Microgeometries 14

Chapter 2: Literature Survey 17–26

2.1 Timing Gear Train in Engines 17

2.2 Effect of Backlash on the Dynamics of Gears 18

2.3 Contact and Root Stress 19
2.4 Design Optimization of Gear Train 20
2.5 Effect of Addendum Modification 21
2.6 Transmission Error 22
2.7 Microgeometry Optimization for Noise and Stresses 24
2.8 Observations from the Literature 25
2.9 Objectives of the Project 26
Chapter 3: Methodology 27–52
3.1 Scientific Rationale for the Methodology 27
3.2 Understanding the Design Space and the Gear Train Arrangement 28
3.3 Technical Requirements 29
3.4 Setting up the Base model of the Gear Train and Making 3D Model of the Same Using Creo 29
3.4.1 Modelling of Standard Gears 29
3.4.2 Modelling of Addendum Modified Gears 31
3.5 Using the Torsional Mass-Elastic Model and Excitation 34
3.6 Building the Gear Dynamic Model Using GT-Suite 36
3.7 No-Lash Dynamic Response 41
3.8 Lash Dynamic Response 42
3.9 Gear Design 42
3.9.1 Micro Geometry Optimization 42
3.9.2 Strength Calculations 46
3.10 Gear Web Design 49
3.11 Joint Capacity Analysis 50
Chapter 4: Results and Discussion 53–80
4.1 Result of Addendum Modification of Spur Gears 53
4.2 Without Lash Dynamic Response of the Gear Model Using GT-Suite 54
4.3 With Lash Dynamic Response of the Gear Model Using GT-Suite 57

4.4 Root Stress (Von-Mises) Evaluation of the Addendum Modified Gears Using Windows LDP and ANSYS 59
4.5 Effect of Microgeometry Modification on the Gears and their comparison with their Helical and Unmodified Counterparts 61
4.5.1 Crank-Cam Pair 62
4.5.2 Cam-AC Pair 67
4.5.3 Cam-FP Pair 71
4.6 Gear Web Fatigue Analysis 75
4.7 Determination of Torque to Slip Capacity of the gear and Shaft Joints 78
4.7.1 Press fitted Joints in Crank and Cam Gears 78
4.7.2 Taper Fit Joints in AC and FP Gears 79
Chapter 5: Conclusions and Future Work 77–78
5.1 Conclusions 81
5.2 Future Work 82
References 83–87

1.1 Background and Motivation

This project was initiated as a result of 11 months internship which was carried out in Cummins Technologies India Pvt. Ltd. Pune. The project came into existence due to Cummins Technologies India Pvt. Ltd. encountering a problem of cam gear walk off, shown in Fig. 1.1 (a) & (b), with the helical gear train of their particular diesel engine and decided to do research on the problem and resolve the issue as soon as possible.

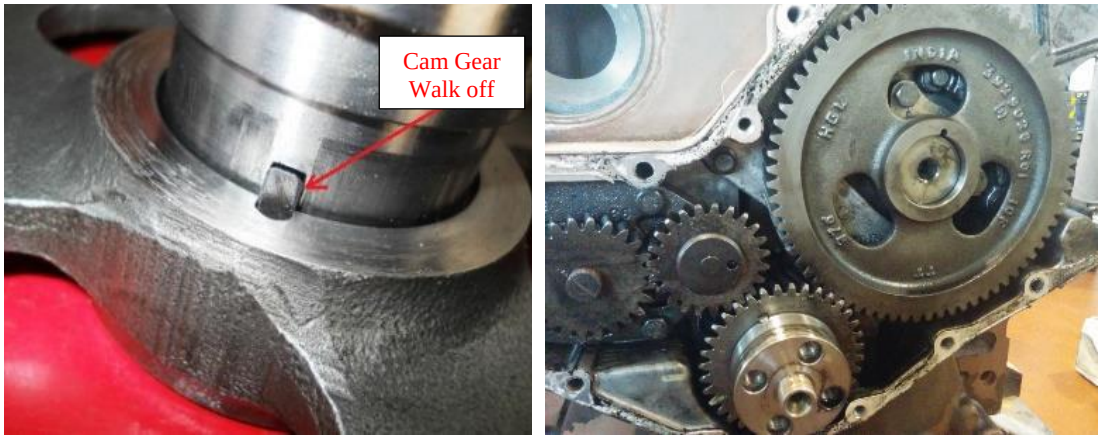

(a) (b)

Fig. 1.1 Picture showing (a) Cam gear walk-off and (b) Cam gear out of place [**Cummins Technologies India Pvt. Ltd.**]

Cummins designed a diesel engine, for the heavy commercial vehicles, employing a helical engine gear train. It was designed keeping in mind that the helical gear train, although costlier to manufacture than spur gear train, will give a better load carrying capacity and will produce lesser noise. Though, this worked out for every engine produced previously but did not for this engine. In this case, the helical gear train is not able to perform the basic task of being in place and powering the camshaft. During the overspeed testing at higher than the rated revolutions per minute (Rpm) it was diagnosed that the cam gear tends to slip from the camshaft. It came into picture that there is a problem of cam gear walk off from the camshaft due to the excessive axial thrust produced by the helical gear train, which is a big issue for the engine and the company, as without it the valves would not open and close and the engine would cease, which needs to be resolved as soon as possible. Current understanding of root cause of failure is significant torsional vibrations introduced in the gear train due to

ineffectiveness of engine damper at those speeds. The preliminary tests and studies to the issue gave rise to three ways to resolve the issue. The first one was to fit the gear on the shaft using shrunk heat press as it would not involve the changing of any design dimensions. But this method was dropped after testing as this gave an excessive process variation and posed a safety hazard to the worker. Second was to use a retainer plate and a bolt. But this proposal was also dropped as this was interfering with the gear housing cover and to fit the extra thickness, the size of the gear housing cover needed to be changed. This meant changing the dimensions of the work envelope in which the engine was to be fitted which is never desired as this is the customer requirement. The third and the best, but a time-consuming solution found out was changing the helical gear train to the spur gear train as this would fit into the gear cover with the same work envelope and without axial thrust but would require a thorough research so that it works properly with low vibrations.

1.2 Problem Statement

The sole intent of this study was to understand how to design a gear train from scratch, how to decide the number of teeth and the gear size, how dynamics of the gear train would be affected if changed from helical to spur gears, most importantly how the microgeometries affect the dynamics and the strength of a gear and how to design a fit between the gears and the shaft. The expected outcome of the project was to be able to design a spur gear train, maintaining the manufacturability, within the constraints which were defined by the pre-existing helical gear train employed in the diesel engine and to overcome the issue of the cam gear walk-off.

Additionally, the project also tries to answer the following questions

- What modifications should be made in a spur gear to have less contact forces *i.e.* contact forces almost similar to the helical gear train?
- What all modifications should be done to reduce the noise, root stress, contact stresses and the surface temperature of the gears?
- Would the joint capacities of the press fit joints be able to sustain the extra forces from the spur gears or changes will have to be made?

1.3 Expected Rewards of the Research

- The design passes the tests and be implemented on the engine: The design made would be tested for the maximum and minimum limits set by the company and if the design is found well inside the threshold limits, the design may be implemented for the upcoming engines
- The robustness of the engine would increase
- More efficient performance: The helical gear trains are less efficient than the spur gear trains because, the helical gear trains have sliding contact between the teeth due to which axial thrust is generated and more heat is generated which in turn contributes to more power loss
- Low manufacturing costs and easy assembly: As the spur gears have axial teeth, the design and manufacturing of the spur gears is far easier than any other type. Moreover, the gear teeth need not be properly aligned to stop the locking as is the requirement with the helical gears
- Customer satisfaction
- Warranty costs go down: A mature reliability data of 24 months shows that out of 247853 engines produced, a total of 213 engines had the issue of cam gear walk off bringing the repairs per hundred (RPH) to 0.085. Although RPH is well below the threshold limit, but as this issue affects the whole engine and may damage some neighbouring components, it is treated as a critical issue in terms of increasing the warranty costs and decreasing the reliability of the engine and is needed to be addressed as soon as possible
- Solving industry problem existing for over 2 years

1.4 Hypothesis Considered

The following hypotheses were considered while designing and analysing the spur gear train:

- The gear geometry points given by the Windows LDP (Load Distribution Program) tool are correct and thus the 3D model made using these points are accurate
- The forces on the gear pair shown using the GT-Suite software are correct

- The microgeometry optimisation to the original design enhances the stress distribution on the flank of the gear tooth
- The FEA software sometimes overestimate the stresses compared to the LDP software
- The centre distance between the gears are not to be altered

1.5 Diesel Engine Timing System

The timing gear trains, camshafts, rockers and the valves are the engine mechanical management train and are together known as the feedback assembly of the engine. The crankshaft, camshaft and the timing gears are the most important components of the timing system of the engine.

1.5.1 Crankshaft

The crankshaft, shown in Fig. 1.2 (a), is a shaft having the pistons connected to them via connecting rods attached to the journals or the offset throws of which the crankshaft is comprised of. The crankshaft's function is to convert the reciprocating movement of the pistons to the rotating movement just like the pedals of a bicycle. Crankshafts are designed to have dynamic balance using counterbalances to tackle the unbalance forces created by the piston movement which reduce as we increase the number of cylinders in an engine as the cylinder firing order produces a counter balancing effect *e.g.* in a 6-cylinder engine, the firing order generally is 1,6,5,2,3,4 which provide a balance to each other at a phase of 120 degrees as shown in Fig. 1.2 (b). Also, a viscous damper is provided on front end of crankshaft to curb the torsional vibrations [**Bennett, 2010**].

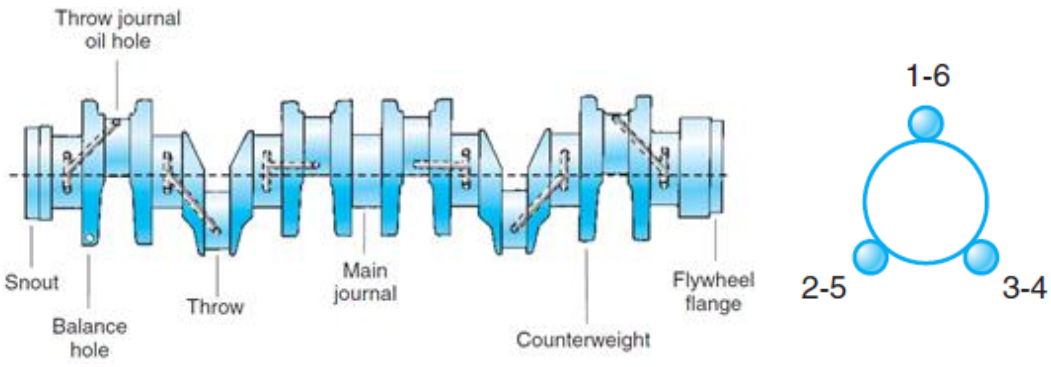

(a) (b)

Fig. 1.2 (a) Schematic showing crankshaft and its nomenclature and (b) Schematic showing the crank throw configuration for 6 – cylinder engine [**Bennett, 2010**]

1.5.2 Camshaft

This is the shaft responsible for operating the inlet and outlet valves in the engine through the cam follower mechanism. The camshaft, Fig. 1.3, is driven one revolution through one complete cycle of the engine *i.e.* as the crankshaft rotates through 720 degrees the camshaft rotates by 360 degrees in a four-stroke engine. This implies that the camshaft rotates at half the value of the speed of crankshaft. Therefore, the camshaft is preferred to be geared to the crankshaft to receive a perfect speed ratio of 1:2 [**Bennett, 2010**].

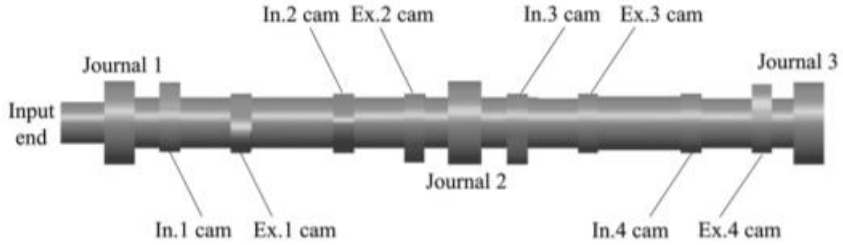

Fig. 1.3 Schematic of a camshaft from a 4-cylinder diesel engine [**Guo *et al.*, 2015**]

1.5.3 Timing Gear Train

These gears are responsible to provide torque to the camshaft to maintain the valve timing and all the accessories that are mounted to the engine. Therefore, it is important to constantly provide torque to camshaft to without any disruption so that the valves can function properly. Almost all the heavy duty and the medium duty engines have a gear train as the timing system instead of the belt or the chain drive since the gears can withstand higher torques, are much more reliable and have a comparatively long life [**Bennett, 2010**]. The gears used in the diesel engine are made by cast or forged steel alloys which are heat tempered and then surface hardened and the gear teeth are cut by milling or hobbing.

The engine has two ways in which the valves can be driven, one is to have a direct overhead camshaft to drive the valves and the other is the in-block camshaft, as present in the engine being worked on in this thesis, which employs push rods to drive the valve train. The over-head camshaft is more durable than the pushrod one as that has lesser number of moving members due to which the failure rate is low for the over-head camshaft. The layout of the gear train being worked on is shown in Fig. 1.4

The position of the crankshaft and the camshaft are the main factors governing the position of the gear train in the engine. The gear train can be placed in the front or the rear end of the engine. Majority of the heavy duty and some of the earlier engines have the gear train at the front, but it is advised to employ the gear train to the rear of the engine as the rear of the engine has the higher inertia due to the presence of the flywheel due to which there will be less twisting on the rear side of the crankshaft and thus less vibrations will be pertinent. Apart from this, the position also depends on the packaging prospects of the engine. Additionally, the gear train is also sometimes employed in the middle of the crankshaft, for the full gear train or just for oil pump or balancer shaft. The middle-mounted gear trains have been only implemented on motorbikes as it is quite challenging to be mounted on heavy duty engines. The bore in between the engine block would make this design as a pretty difficult design due to the reduced durability of the engine because of the reduced stiffness.

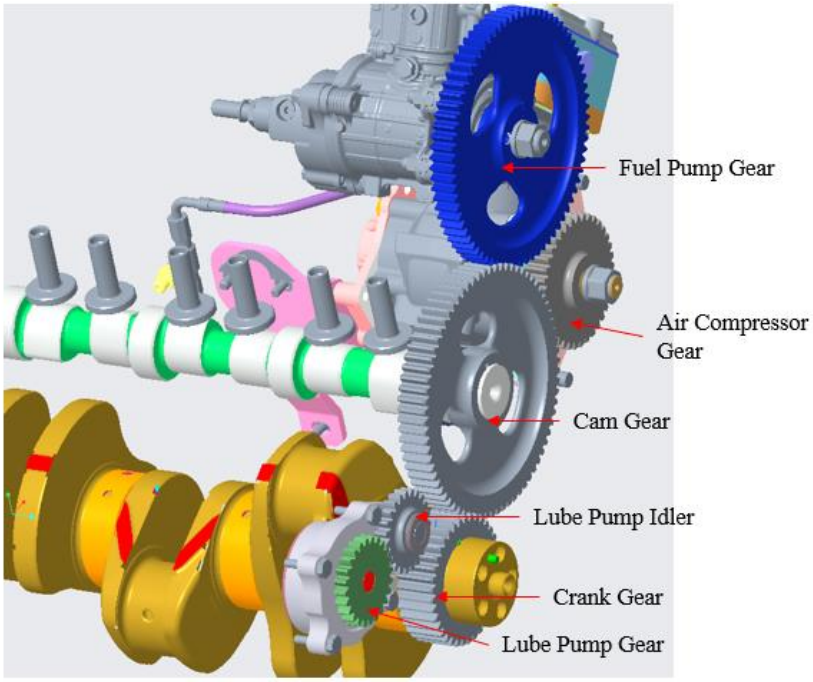

Fig. 1.4 3D model showing the timing gear train with crankshaft and the camshaft [**Cummins Technologies India Pvt. Ltd.**]

The power from the crankshaft is directly transmitted to camshaft using the crank and the cam gear pair. Both the cam gear and the crank gear are press fitted to the shafts and include a key which is for the positioning of the gears on the shafts. The torque variation from the combustion in the power cylinders produce the torsional vibrations in the crankshaft which are compensated by employing a viscous damper on the front

end of the camshaft so that the vibrations are not transferred to the engine gear train. As mentioned earlier, the auxiliaries also take power from the crankshaft. The lube pump is connected to the crankshaft using an idler gear. The lube pump's job is to maintain a constant oil supply to the engine components. The air compressor and the fuel pump are connected from the cam gear and as suggested by name they deliver fuel and compressed air respectively.

1.6 Theoretical Background of Gear Design

Gears are the mechanical components used to transmit the rotational motion between two shafts whether the shafts are parallel or intersecting. With a power transmission efficiency of about 94% to 98%, gear drives are regarded as the most efficient and long-lasting means for transmission of power amidst the variety of the mechanical drives [**KHK Stock Gears, 2015**] & [**Warner, 2017**].

The main intent of this section is to provide the introduction to the basics of the gear design, prioritising the nomenclature and the basic equations used to define the gears. Also, the various failures modes which can occur due to the incorrect design of the gears will also be briefly discussed in this section.

1.6.1 Gear Nomenclature

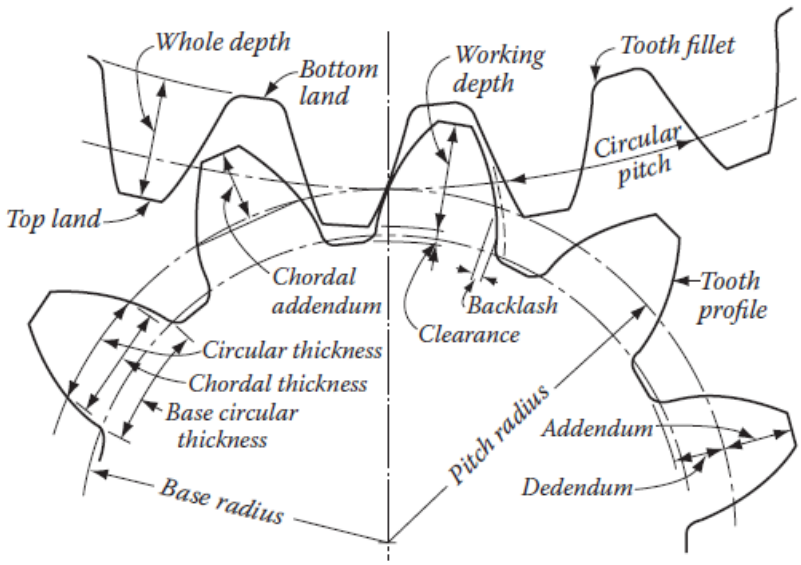

Fig. 1.5 Schematic showing nomenclature of spur gear [**Radzevich, 2012**]

The pitch circle is a hypothetical circle and probably the most important one, as all the calculations of contact are dependent on it. This can be elucidated as the rolling circle of the gear *i.e.* two mating gears can be thought of as two cylinders rolling with their diameters same as the pitch diameters of the gears. The pitch circle has a point where there is a pure rolling contact and no slippage, this point is called the pitch point. The distance between a point on one tooth to the corresponding point on the other tooth is called the circular pitch. The addendum and the dedendum are the distance of the top land and the distance of the root of the tooth from the pitch circle respectively. The addendum is generally taken same as the module used and the dedendum is used 15% to 25% more than module [**Budynas & Nisbett, 2011**]. The circle from where the involute curve starts is called the base circle of the gear and there should not be any contact below this circle [**KHK Stock Gears, 2015**].

The main deciding factor in defining the size of a gear are the number of the teeth on the gear, the module of the gear and the pressure angle in the SI system. The module indicates the size of the gear teeth and is evaluated as the pitch circle diameter to the teeth amount ratio. A gear pair can only function if the both the gears have the same module. Relation that can be used to define the module is given by

$$m = \frac{d}{z} \tag{1.1}$$

The number of teeth on each gear decides the speed ratio of a gear pair and this ratio further defines the relation between the angular velocities and the torques of the gears is given as

$$i = \frac{z_2}{z_1} = \frac{T_2}{T_1} = \frac{\omega_1}{\omega_2} \tag{1.2}$$

If the two gear wheels have same base pitch, then only they can transfer power. The base pitch is the distance between one point on the intersection of a tooth and the base circle and the corresponding point on the adjacent tooth. Numerically it can be defined by

$$p_b = \frac{2\pi r_b}{z} \tag{1.3}$$

Pressure angle, α, can be expound as the inclination in between the centre line connecting two gears and line connecting the point of intersection of the line of action (LOA) to the base circle of the gear [**KHK Stock Gears, 2015**]. In simple words, the pressure angle is the angle at which the tooth is slanted. The pressure angles these days is generally standardised to 20º but the angles in between 14.5º and 22º are also sometimes used for some special applications. The LOA is the line tangent to base circles of both the gears in mesh and the point created by the intersection of the line of action to the centreline of the gears is called the pitch point. The normal forces on the teeth of the gears always act along the LOA.

1.6.2 Backlash

Backlash is a need as well as the culprit in the design of gears. It is the space left between the surfaces of the two mating teeth. The backlash is generally not calculated but becomes the basis for the calculation of the tooth thickness as different applications need different amounts of backlash. It is necessary to include backlash into the design as zero amount of backlash would lock the rotation of the gears and very low amounts of backlash can cause insufficient lubrication leading to heat seizure and also the interference is also likely to occur. If the backlash is increased more than a level, it can cause excessive vibrations and noise. Therefore, to have a smooth operation, the backlash should be decided according to the application.

1.6.3 Contact ratio

The contact ratio can be defined as the average number of teeth in contact in a particular mesh cycle. When the teeth of the two mating gears mesh, the area falling under the length of the line of action is known as the zone of interaction. If the arc of action is equal to the circular pitch, then the matched set has a contact ratio of exactly 1 and if the circular pitch is less than the length of arc of action, then the contact ratio will be more than 1, which mean that the succeeding tooth contacts the tooth of the mating gear before the currently meshing tooth has left the contact [**Budynas & Nisbett, 2011**].

Every gear has to be designed to comply to a minimum contact ratio of 1.2, so that if it decreases due to mounting or assembly errors, the gear pair is still able to work

properly. The gear pairs with a low contact ratio become vulnerable to interference and get damaged due to the constant impact of teeth thus further resulting in the excessive production of noise. A value of 1.2 of contact ratio denotes that a single tooth is in mesh 80% of the time and two teeth will be in meshing for the rest 20% time. The gears having the contact ratio more than 2 are termed as the high contact ratio gears and low contact ratio gears for less than 2 [**Budynas & Nisbett, 2011**].

1.6.4 Addendum Modification

When the involute tip of the tooth of the mating gear touches the non-involute portion of the gear it is called interference. Interference is a non-conjugate action due to which the tip or the face of the mating gear chips off the flank of the driving gear and creates excessive vibrations and sudden jolt**.** Although, undercutting solves the problem of interference but, weakens the gear tooth in bending. Also, it tends to remove a small portion of involute portion near the base circle, which may cause serious shortening of the length of contact [**Bhandari, 2010**]. To avoid undercutting and eliminate interference addendum modification can be done on the gears.

When the addendum of tooth is expanded or reduced it is termed as the addendum modification and the factor by which the addendum is expanded or reduced is termed as the addendum modification coefficient or profile shift coefficient or correction factor. The aim of addendum modification is basically to avoid undercutting, rearranging the centre distance between the gear pairs, improvement in the load carrying capacity and the surface pressure of the gear teeth and also reducing the noise by changing the contact ratio of the gears [**Gunay *et al.*, 1996**].

Addendum modification is done using two ways, either positive or negative as shown in Fig. 1.6. For achieving a positive modification, the pitch line of the rack cutter is drifted apart from the gear centre and conversely for the negative correction, it is shifted towards the gear centre by the amount of profile shift coefficient.

There are limits in the profile correction both for positive and negative correction which are described as follows [**International Standard, 1982**].

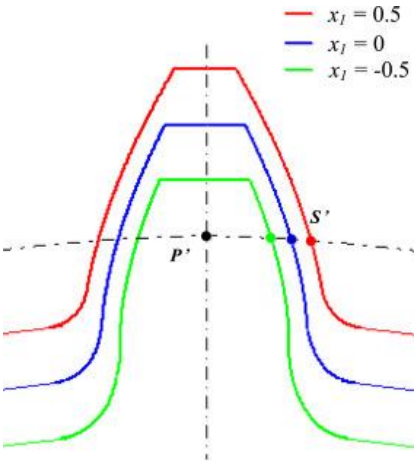

Fig. 1.6 Schematic showing tooth profiles with zero, negative and positive addendum modification [**Yu *et al.*, 2017**]

- **Positive Correction:**
  - Tooth thickness increases at the root, thus forming a tooth profile having an increased bending strength
  - The working pressure angle increases due to enlargement in the distance between the centres thus making the contact ratio smaller
  - The width of the tooth tip reduces and may become sharpen if the limit of correction is exceeded
- **Negative Correction:**
  - The thickness of the tooth on the root diameter gets reduced thus weakening the tooth in bending
  - The working pressure is reduced increasing the contact ratio
  - Undercut may occur if the limit of the correction is exceeded

1.6.5 Misalignments

Misalignment means the shift of the meshing surfaces of gear axially due to deflections because of vibrations or due to manufacturing errors. The contact locations of the tooth flank get altered due to the occurrence of any of these errors resulting in increased gear noise and production of large root stresses. Misalignments can be divided into three categories, parallel misalignment, angular misalignment parallel to the plane of action and angular misalignment perpendicular to the plane of action [**Houser, 2006**]. Another categorisation of misalignment shows that it can be categorised into axial, linear, pitch and yaw as shown in Fig. 1.7 (a), (b), (c) and (d).

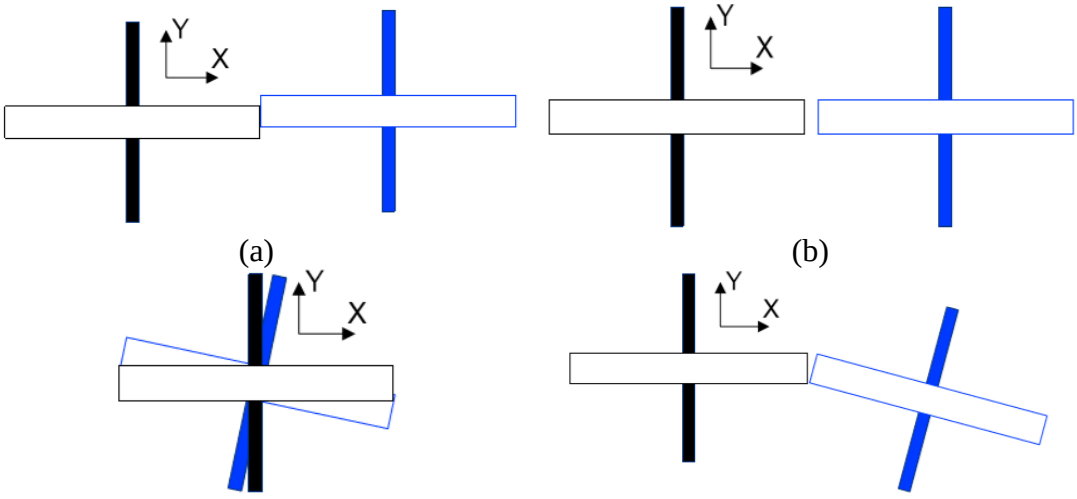

Fig. 1.7 Schematic of (a) Axial misalignment, (b) Radial misalignment, (c) Pitch misalignment and (d) Yaw misalignment [**Hu & Mao, 2017**]

1.6.6 Transmission error

Transmission error (TE) can be defined as "the difference between the actual position of the output gear and the position it would occupy if the gear drive was perfectly conjugate". Quite a few types of TE are given in by [**Tharmakulasingam, 2010**] on the effects of TE commonly. These types are more similar to each other and only have small differences between them.

The first type would be manufacturing transmission error (MTE). If there is a modification in the contacting point of the tooth due to manufacturing error, then it would be a MTE. This is the single transmission error which can be measured on a single gear whereas for others a pair of gears in mesh is needed. This is measured under low or no-load conditions and can be used to test the accuracy of gears on a production line. The second would be static transmission error (STE). The teeth under mesh deform elastically under low load conditions and the transmission errors caused because of these deflections are called STE. STE is measured under low load conditions while taking into account the stiffnesses of each and every member present within the system. While evaluating this error, the stiffnesses are assumed to be constant. The kinematic transmission error (KTE) is derived from MTE and considers the unevenness present on the tooth flank which cannot be seen by naked eyes. The unevenness takes the load on them and continue to misshape until the contact area is sufficient to support the load. This TE is also measured under low load condition.

The dynamic transmission error (DTE) considers that the components of the gear system have masses and variable stiffnesses. The designers, since ages have been adjusting their calculations using the dynamic factor, which is the ratio of dynamic load to the static load due to geometry errors of the tooth. The dynamic factor shows that the DTE is a result of the STE. The DTE is dependent on the celerity and can be portrayed mathematically by the multiplication of STE with a transfer function. The DTE is closest in relation to the TE in gears, but it is the most difficult type to obtain either by measurement or analysis and much harder to control. Hence, as learnt in the above paragraph, the DTE is excited by STE, it would be easy to control DTE if the STE is controlled. Therefore, the alternating nature of the STE is controlled by improving the microgeometry of the teeth which would compensate for the variation in the stiffnesses.

1.6.7 Microgeometry

The conjugate action from the perfect involute profiles of the spur and helical gears is shown only during the no load condition. As soon as the load is applied to the gear teeth, it gets deflected and the motion transfer does not remain conjugate any longer. So, the tooth profile is modified by removing some material from the tooth surface to bring motion back to some similitude of the conjugacy. This intentional removal of material from the gear tooth involute profile and the flank line is called the microgeometry modifications in gears [**Harianto & Houser, 2007**]. Microgeometry changes of the gear teeth are done intentionally to change the stress distribution, to minimize the transmission error, compensate for misalignments, minimization of scoring and pitting *etc*. Microgeometry modification is the very last step of the gear design and a perfect choice of microgeometry cannot compensate for a bad choice of macro geometry. It is not possible for a specific microgeometry change to fulfil all the objectives like noise, pitting, scuffing, service life, *etc.*

Roll angle is the angle whose arc on the base circle of radius unity equals the tangent of the pressure angle on a selected point on the involute. This is used to calculate the sum of addendum modification coefficient for the gears. Active profile can be understood as length of involute contour of the gear tooth that actually contacts with the mating tooth. Start of active profile (SAP) and end of active profile (EAP), as shown in Fig. 1.8 are the lowest and the highest point respectively on the profile of the gear

tooth that contacts the mating tooth. On the gears having no tooth tip chamfers SAP is defined by the outer diameter of the mating gears and is generally expressed as the degree of roll above the base diameter.

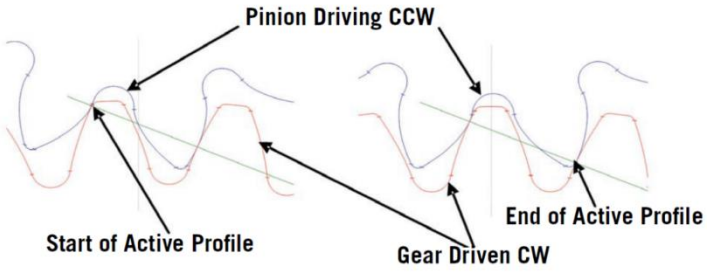

Fig. 1.8 Schematic depicting start of active profile (SAP) and end of active profile EAP [**Kuhr, 2009**]

The smallest diameter on which there is only a single tooth in contact with its mating gear is called lowest point of single tooth contact (LPSTC) and the largest diameter with the same condition is known as highest point of single tooth contact (HPSTC). These are also measured in degrees of roll above the base diameter. These diameters are important in the gear design, as the contact stress is calculated at LPSTC and the bending stress on the tooth is calculated on the HPSTC.

LPSTC for Pinion = HPSTC for Gear

HPSTC for Pinion = LPSTC for Gear

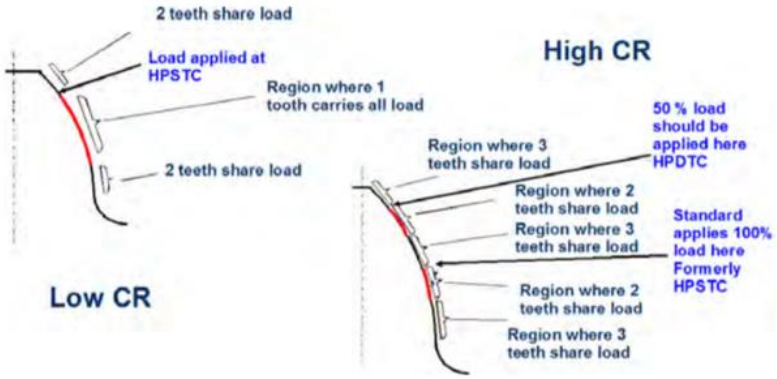

Fig. 1.9 Schematic showing LPSTC and HPSTC of the low contact ratio (CR) and high contact ratio gears [**Palmer & Fisch, 2010**]

1.6.8 Types of Gear Microgeometries

The type of microgeometry modification to be used for gear pair depends on what attribute of the gear we need to minimise. There are several types of microgeometry

modifications used for different changes in different attributes of the gears, of which only the ones used in this project are explained in this section.

a) Profile Modification

The calculations of the capacity of a gear under loading is based on the assumptions that the involute profile of the gear teeth is always perfect and there is no deflection of the teeth under load. These assumptions are not at all true in the real life. The deflection of the tooth under load generate transmission errors, which in turn is a cause for the excessive noise in the gear pair. So, to curb the increase of the transmission error, profile modifications to the gear teeth are done. Profile modification includes the tip relief and the profile crowning of the gear teeth.

Removal of material from the tip and the root of the gear teeth is known as the tip relief and the root relief respectively, shown in Fig. 1.10 (a). Providing of tip relief assumes that the tooth would not come into contact too soon if the tip of the teeth is made a little bit thin, due to which the driven gear tooth gets into the position of the line of action before coming in contact with the mating gear tooth. Thus, introducing tip relief to the gear helps in decreasing the transmission error. The tip relief tends to decrease the contact ratio during the no load condition; therefore, caution must be taken that the contact ratio does not fall below 1.2 at the condition of maximum centre distance and minimum material.

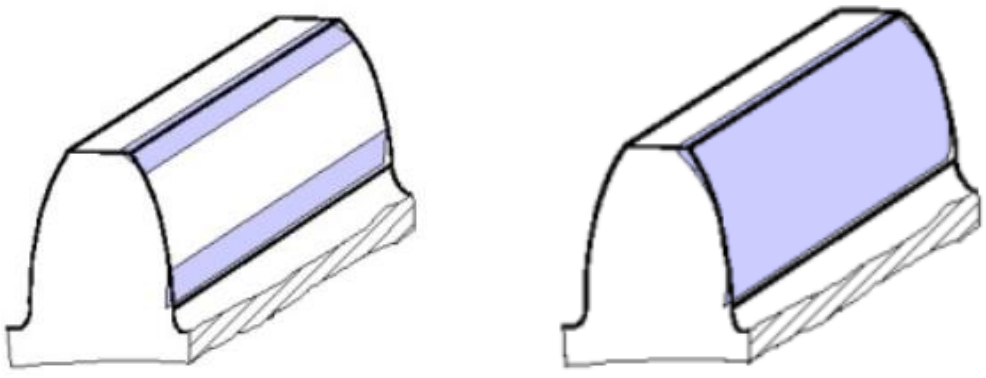

(a) (b)

Fig. 1.10 Schematic of (a) Tooth tip and root relief and (b) Profile crowning [**Recurdyn, 2019**]

Profile Crowning, shown in Fig. 1.10 (b), is where in the transverse section along the direction of the increasing addendum and dedendum, a constantly increasing

amount of material is removed starting at the middle of the tooth height. This technique is also termed barrelling as this gives a rounded shape to the tooth flank. This eliminates the backlash requirements in the gear thus leading to less transmission error and decreased vibrations, hence, leading to the longevity of the parts of the assembly.

b) Lead Crowning

Lead crowning, shown in Fig. 1.11, is the constantly increasing removal of material along the direction of the face width, starting generally at the middle of the face width. The material is removed in an arc like progression, giving rounded shape to the tooth along its face width. The modification can be done on the whole face or can be done only on the active face width if both the gears have equal face width, as, instead of using the roll angle as the starting parameter, a point is located along the face width in reference to the zero-face width. Noise increases if the mesh contact is forced to one end of the face by the lead errors. The condition worsens if both plus and minus lead errors are present on the gear tooth in an alternate fashion which can be reduced by crowning the gear teeth as it creates a relief on the edges of the teeth by creating a barrel shape. The lead crowning observes a little loss in the effectiveness of the gears as during a heavy load cycle the load pattern on the gear does spread out.

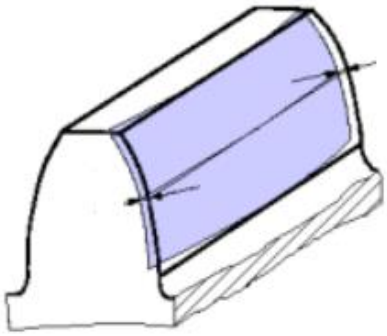

Fig. 1.11 Schematic of lead crowning [**Recurdyn, 2019**]

This chapter gives a lookout in the successive developments in the field of gear design for the engines and the controlling of the transmission error, contact stresses and the root stresses on the gear teeth using the microgeometries.

2.1 Timing Gear Train in Engines

As every gear in the gear train has a noteworthy amount of mass and moment of inertia, they contribute to the 3-D vibrations of the system. A four-cylinder diesel engine was used by [**Okamura & Yamashita, 1997**] to estimate the vibrations of the crankshaft due to the timing gear train present on the front end and the rear end of the engine. Holzer method was used to determine the natural frequencies and the torsional vibration modes for the crankshaft. They found out that in the torsional modes, the natural frequencies of the crankshaft reduce and the torsional vibration of the gear train increase because of the higher inertia of the gear train in the front-end gear drive. The results of the study declared that the gear train is recommended to be designed on the rear of the engine and as near as possible to the node point of the torsional vibrations of the crankshaft to minimize the upshot of the inertia of gears on crankshaft. Engine gear train adds to major power losses as it drives various engine accessories. Timing gear train is one of the most important components in an engine as it is used to transmit power to the camshaft from the crankshaft while regulating the valve operation timing and to drive the auxiliaries. Most of the diesel engine timing system is driven by a gear train as this is capable to withstand higher loads and has added robustness [**Bennett, 2010**]. An elasto-dynamic behaviour study of the timing gear system of the engine of a motorcycle was performed by [**Rivola & Troncossi, 2014**]. The results showed a low value of transmission error which was taken as the measure for the appropriateness of the gear train for the engine to impart motion to the camshaft from the crankshaft rather than the belt and the chain drives. They also prepared a numerical model using finite element analysis (FEA) to obtain the non-measurable quantities like the forces, tooth separation *etc.* and to ascertain the dynamic characteristics of the gear train. It is mentioned by [**Wright, 2018**] that the job of the camshaft is to keep the valves from colliding with the piston when it reaches top dead centre (TDC) as the valves or the piston can be damaged with even the modest delay in the timing therefore the correct

modelling of the timing gears is very important while building the total timing system of the engine.

2.2 Effect of Backlash on the Dynamics of Gears

The equation of motion for a gear system to ascertain the dynamic characteristics of the gear train by considering backlash was created by [**Sato *et al.*, 1985**]. They found out that when the gear pair is having a small backlash, then the inertia force becomes large and the torsional vibration gives a sinusoidal plot and the as the frequency of rotation increases, the torque is transmitted by the colliding gears. A major cause of the noise in the gear pairs is the impacts between the gear teeth due to the presence of backlash or due to the presence of alternating torques. [**Wilhelm *et al.*, 1990**] studied the vibrations arising the timing gears of a three-cylinder diesel engine. To determine the noise, they compared the acceleration of the gear teeth which were equipped with the accelerometers and the impacts measured with sensors on the bearings of the gears. The result portrayed that the injection pumps attached to the gear trains sometimes produce a fluctuation in functioning due to the hydraulic forces which in turn causes the gear teeth to cause impact. It was found suggested that to reduce these excitations and the noise levels, either the backlash needs to be eliminated or the fluctuations in the rotary gear train must be minimised by applying an added torque which is constant and higher than the reversal torque.

A simulation in ADAMS software was done by [**Croker *et al.*, 1995**] to determine the responsiveness of the rattle noise to different parameter changes in the front-end gear train of the engine and due to the highly non-linear nature of the gear train, the results were highly non conclusive. But the found that the rattle did not change much while increasing or decreasing the inertias but if the gears had a less amount of backlash, the rattle increases when the backlash is increased and then after a threshold it suddenly falls. They also found that if the water pump and alternator is attached to the gear train, then the rattle can be decreased. Also, to overcome the rattle noise in the power take off gearbox of a tractor, [**Shim *et al.*, 2008**] employed an anti-backlash gear as the driving and the driven member. They concluded that if there is zero relative angular displacement between the above two gears, the rattle noise will be reduced and also can be further reduced by increasing the stiffness of the spring. Further an experiment to

study the efficiency of anti-backlash gear was done by [**Joshi & Kelleher, 2014**] which employed 2 types of spur gear trains, one having two spur gears and one having a spur gear and an anti-backlash spur gear. After the tests they, came to a conclusion that Regular gear is more power efficient than the anti-backlash gear as the latter has higher gear friction and a greater amount of mesh loads and with the anti-backlash gear, gear train consumes higher torque than the one with normal spur gear. Analysis of torsional vibrations due to the crank nose and the timing gears was done preparing a multibody dynamics model of a 6-cylinder diesel engine's timing gears depicting gear tooth stiffness and damping by considering the time varying forces applied on the cylinder during combustion concluding that errors in the vibration data can be reduced using non-linear damping coefficient and sampling more torque data from the accessories [**Foltz *et al.*, 2016**].

2.3 Contact and Root Stresses

A circular dynamic model of the spur gear system with backlash and added involute tooth profile was made enabling to consider material compliance and energy dissipation. This made interpenetration of impact force of gears in mesh making stiffness linear, making it easy to use for studying dynamics in the gears with high speed and intermittent motions [**Yang & Sun, 1985**]. A study done by [**Andrews, 1991**] on the finite element model for determining the root stresses in the spur gears and comparing it with photo elastic experimental method concluded that FEA can produce accurate results. Also, it suggested that the maximum root stress decreases as the point of application of load is moved down from the highest point of contact to the lowest point of contact. A study was conducted for ascertaining the effect of variation in the rim thickness of the gears on the root stresses. It was concluded by [**Bibel *et al.*, 1994**] above a backup ratio of 1.3 no changes were observed in the root stress compared to a solid gear but the tensile root stress decreased with decrease in backup ratio up till 0.7 and after that it increased which concluded that the stiffer the rim is the lower will be the backup ratio which meant increased stresses.

Contact stresses are generated when two curved bodies roll or slide over each other. The excessive contact stresses lead to surface durability problems due to wear. The contact stresses can be calculated using various standardized methods viz. AGMA and

ISO. But the basis of method for the calculation of the contact stresses is the Hertzian contact theory. A technique to check the contact stresses in the gears using the Hertzian theory as the base was developed and the variation of the contact stresses with the change the point of the contact and the contact ratio was also examined [**Hassan, 2009**]. According to theoretical point of view, there should be infinite pressure existing between the two surfaces which would cause for immediate yielding of both surfaces. But this is not the case, instead the deformation during mating creates a small contact area, therefore making the stress to be considered. These contact stresses generated due to the small contact area are known as the Hertz contact stresses as this phenomenon was studied by Hertz first in 1881. The Hertzian theory assumes the contact patch to be elliptical, which translates the maximum stress concentration to be in the very middle [**Budynas & Nisbett, 2011**]**.** The deformation of the gear and the contact stresses are the key parameters to consider while designing the gears as the gears often fail when the working stress overreach the maximum stress. The authors aim was to minimise the contact stresses and the deformations to arrive at the best combination for the driven and the driver gear [**Mehta *et al.*, 2018**].

2.4 Design Optimization of Gear Train

A study was carried out by committed towards teaching and training for the process of gear design. Several combinations of parameters for gear design which need to be optimised by iteration and due to these combinations, gear design was quite a complex and time exhausting process for manual designers, therefore, a computer program was made so that designing a gear experiencing specific working condition is made possible and using that a gear was designed using the requirements of static load, dynamic load and the wear load [**Madhusudan & Vijayasimha, 1987**]. An algorithm was presented using two stage process for the easy optimisation of a constant speed multi spindle gear train choosing minimum size, overall centre distance, minimum gear volume or any other desired criteria for the optimization, reducing the design dimensions by 100 mm compared to the existing [**Prayoonrat & Walton, 1988**]. A new technique using finite element methods (FEM) was used to build dynamic non-linear analysis of gear train and obtained results from this model were used to design various variables like contact

forces, deflection of tooth and load distribution. Further these results were animated, enabling the real time scrutiny of the gear train [**Farhani, 1994**].

[**Ramamurti *et al.*, 1997**] described a methodology to fix the leading dimensions of gearbox which transmitted for a given speed a particular horse power. They calculated the module, dimensions of the shaft and bearing for the shaft support. Also, they compared the design stresses obtained from the FEA model of the gear with the traditional calculations. While designing a gear pair, it's geometrical volume and the meshing vibrations should be kept in mind as both are conflicting, and the design is always a trade-off between these. Therefore, [**Chong *et al.*, 2001**] proposed a design method to evenly distribute the above design parameters. They concluded that the light gears have more tendency of having noise and vibrations in them. During meshing, teeth experience the stresses and tend to deform due to the normal and the tangential forces acting on it. Resistance to this deformation is called meshing stiffness. Increasing mesh stiffness evaded undercut and changed centre distance, increased tooth strength because of modification coefficient on the rack cutter. Mesh stiffness varies with the contact point and is maximum in the middle, larger the modification coefficient, larger the mesh stiffness induced [**Shiau *et al.*, 2011**]**.** Author presented a pragmatic approach for the single as well as multi objective optimisation of the spur gear train developing a software named gear train optimisation which resulted in 22% reduction in occupied volume of gear train in far lesser time [**Marjanovic *et al.*, 2012**]. Different forms of failures may occur on the surface of gears while in operation and sometimes multiple failures appear simultaneously making it hard to determine the prime cause. These failures tend to reduce the longevity of the gears or may damage the gear to such extent that they may no longer work. A criterion should be matched by the designer in the modelling of the gear train to keep the wear and the noise levels of the gear minimum and make the life of the gears maximum [**Radzevich, 2012**]**.**

2.5 Effect of Addendum Modification

The variation in the root stresses due to the addendum modification was inspected using the finite element method by [**Gunay *et al.*, 1996**] taking into account the positive and the negative addendum modifications. They compared the stresses on the root of the gears of the standard and the addendum modified which concluded that the load

carrying capacity is increased by using a proper addendum modification coefficient. By increasing the modification, the tooth thickness increases at the root, thus giving the tooth a better bending strength and also due to the thinning of the teeth in the positive modification, the undercutting is prevented. Moreover, the centre distances of the gears can be reduced or increased by positive modification and negative modification respectively. A study to scrutinize the probability of decreasing the difference between the number of teeth between the internal and the external gear pair with simple corrections was done by [**Maiti & Roy, 1996**]**.** They concluded that the centre distances modification can be used to reduce the difference in the number of teeth and increase the contact ratio but only up to a level because of tip interference. Author presented approximate equation for the relation between the addendum modification of the gear and pinion. This estimate equation was devised when a condition of balanced specific sliding was present. With this study [**Pedrero *et al.*, 1996**] concluded that the equations made were valid for every value of the addendum and the pressure angle. The positive shifted addendum gear is called S-Plus gear and the negative shifted addendum gear is known as S-Minus gear. If gear and the pinion both have been corrected then this type of gear is called S-gearing. The sum of the corrections on the gear and pinion may be +ve or -ve, but in practice the sum is always taken as positive to harvest the advantages of the positive corrections. The sum of corrections can also be made to zero which is termed as S_0-gearing. This type of gearing is used when a huge reduction ratio is required. In S_0-gearing generally the pinion is made positively corrected and the gear is made negatively corrected. This type of gear arrangement is not suitable when reduction ratios are small as this makes the teeth of the gears weak [**Maitra, 2008**].

2.6 Transmission Error

The effect of the TE on the gear pairs was first stipulated by [**Hariss, 1958**] which can be applied to any gear type various profile deviation at any amount of load transfer. The definition of transmission error can be seen as given by [**Munro, 1990**] “the deviation in position of the driven gear (for any given position of the driving gear), relative to the position that the driven gear would occupy if both gears were geometrically perfect and undeformed.” Harris in 1958 showed that the spur gear operation at low speeds can be defined by the contours of transmission error which can combinedly plotted on a plot

and can ascertain how the transmission error is affected by the loading. This was only for the no load transmission errors. Later a program named Load Distribution program (LDP) was introduced by the Ohio State University in conjunction with Gear Labs which gave the plot for the loaded transmission error and the peak to peak transmission error. [**Houser *et al.*, 1994**] sampled the sound data from various helical and spur gear pairs for both low contact ratio and the high ones as well and tested them using the LDP software. Further they concluded that at any frequency level the transmission correlate to the sound levels of the gears and that for the high contact ratio gears, the transmission error is less sensitive to load change. At various rpms, for different contact ratios and torque, computation of dynamic transmission error (DTE) and dynamic factor (DF) based on tooth loads, gear mesh forces and bending stresses were calculated by building a model to predict the DTE and provide a direct link to DF like the contact stresses and the root stresses [**Tamminana *et al.*, 2007**]. The methods of gear design assume the geometry and alignment to be perfect so that there is perfect conjugacy between the gear pair which is attained using involute profile on the teeth. As, the gear teeth need to transmit large loads, they tend to deflect elastically causing transmission error and early tip contact, leading to scuffing and uncontrolled vibrations and noise. The transmission error can also be a result of manufacturing errors like the non-involute profile and pitch errors [**Palmer & Fisch, 2010**].

The noise due to transmission error is not directly related to the angular speed variations in the gear pair, but, the torsional vibrations caused due to this gets transferred to the bearings, which transfer them to the gearbox, thus propagating noise by the pulsating casing wall. The peak-to peak transmission error is the direct relative to the noise levels in the gears [**Kissling, 2010**]. The transmission error can be empirically defined as

$$TE = r_{b2}\gamma_2 - r_{b1}\gamma_1 \tag{2.1}$$

$$\frac{r_{b1}}{r_{b2}} = \frac{z_1}{z_2} \tag{2.2}$$

The study done for highlighting the factors responsible for the generation of TE and their effect on the gear pairs was done by [**Malviya & Sharma, 2014**]**.** They

concluded that TE is the effect of the misalignments of the gears due to which the gears provide a non-conjugate action which make the gears slip on each other and collide with each other thus producing noise.

2.7 Microgeometry Optimisation for Noise and Stresses

The removal of material from the teeth of the gears to reduce the contact stresses, bending stresses, transmission error (TE) and the surface temperature of the gears is called the microgeometry modification of the gears.

A method was developed by [**Litvin *et al.*, 1987**] to make a crowned surface on the gear tooth so that it provides a contact bearing on the surface of the tooth and also, they discussed the type of transmission error plot that would be most suitable for the correcting of the misaligned gears. They emphasised that the saw tooth type transmission error is not favourable for the reduction of the misalignments and the noise in the gears rather the plot should be a smooth transiting curve for the proper modification. Later [**Munro *et al.*, 1990**] described the effects of short and long tip relief on the transmission error in gears. He described that the short tip relief is better for the reduction of noise for the designed load and the long tip relief is better for the reduction of noise in the wide range of loads but has only a little effect on the design loads.

Microgeometry modification is basically the last step in the design of the gears and a good design of the microgeometry cannot compensate for the bad choice of the microgeometry. The designer should keep in mind beforehand the primary objective *i.e.* noise, scuffing, pitting, service life or efficiency, for doing the microgeometry modification as all these optimisations are not possible to achieve simultaneously and some modifications will worsen some attributes while improving the others [**Kissling, 2015**]. Microgeometry changes of the gear teeth are done intentionally to change the stress distribution, to minimize the transmission error, compensate for misalignments, minimization of scoring and pitting *etc*. For minimization of every term above, a different type of modification is generally required. It is not always true that if a factor is minimized by a certain modification, the other factor will also be minimized by the same modification. There is often a conflict in the type of modification needed to

minimize one factor and minimization of the other. An interactive and graphical approach was shown for how to determine the gear micro geometry which best addresses the issue of noise and stresses in the helical gears. Moreover, it provided a walkthrough on how to proceed further step by step for the micro geometry modification of the helical gears [**Harianto & Houser, 2007**]. Explanation of existing valid theories and the experimental validations on how to control the transmission error by employing tip relief in the gear teeth is explained by [**Palmer & Fisch, 2010**]. They also described that how the relief that is applied on the gear teeth contributes to the transmission error in the gear pair. Also, a single value method of applying the tooth relies cannot be used universally, because every gear pair has different dynamic characteristics and tooth structure therefore responding to different microgeometry changes differently.

The function of the tip and the root relief is to decrease the shocks in the gear pair when the changeover from the single to the double tooth contact takes place and vice versa as during the changeover, the impacts cause noise, increase of the pitch inaccuracies and the increased tooth deformation. The effects of the tip relief modification were studied by building two identical finite element analysis (FEA) models one with tip relief and the other one without. This showed that applying the tip relief decreased the contact stresses and root stresses of the gears along with the increase in the contact ratio. But the disadvantages of tip modification were ruled out by applying the profile modification. The authors also defined a way to calculate the tooth tip modification by using the Hertzian deformation and the elastic deformation [**Marković & Vrcan, 2016**].

2.8 Observations from the Literature

- The gear train modelling with the perspective of employing in an engine is not present in any literature
- The gear train has been modelled freely without any constraints of the gear size for a particular application
- No literature shows the transformation of the helical gear train to the spur gear train and the various effects on their mechanical attributes

2.9 Objectives of the Project

- To model mass elastic static and dynamic model with and without considering backlash
- To optimize gear micro design and gear web design
- To analyze joint capacity for shaft and gear fit

This chapter summarises the method or the steps followed to achieve the desired results. It starts with presenting the scientific rationale for the strategy and further depicts that what steps were taken to fulfil the objectives of the study using a flow diagram. After this the steps taken are elaborated so as to give an insight to what each step was made for and what was done in the particular step.

3.1 Scientific Rationale for the Methodology

As the gear trains are expected to work at various speeds and the loading conditions, the dynamic response of the gear train would be one of the major concerns, as the vibratory response of the gear trains generate excessive noise and dynamic forces which may lead to various failures in the gears hampering the functionality of the gear train. Therefore, to improve the durability and to reduce noise, one should be familiar with the dynamic response of the system. Further, the loss of the profile of the tooth and the tooth thickness might result in much higher gear tooth forces, consequently, making bending fatigue and sliding wear more prominent. Therefore, the micro design of the gear tooth should also be optimised as the micro design improves the tooth wear resistance, noise reduction and reduce the contact forces, but it only has an advantage if the macro design of the gear is proper. So, the bending strength of the gear teeth will be calculated and accordingly the macro and the micro design of the gears would be modified. The main motive of the micro geometry modification in this research is to modify the tooth of the gear in such a way that the transmission error of the gear pair reduces while keeping the contact stresses, load distribution and the surface temperature distribution under the permissible limits. This will help in reducing the noise in the spur gear train and keep the gear train. The lesser the weight of the gear, the lesser will be the dead torque due to the gears. Therefore, the gears must be analysed using FEA and the pockets in the gears must be made to decrease the dead torque. Lastly, the gears are to be fitted in their respective positions on the shafts thus needing a joint capacity analysis to be done to assess the amount of the torque that the joint between the gear and the shaft could sustain without slippage.

The Fig. 3.1 shows the work flow process for achieving all the objectives that are to be completed in this project.

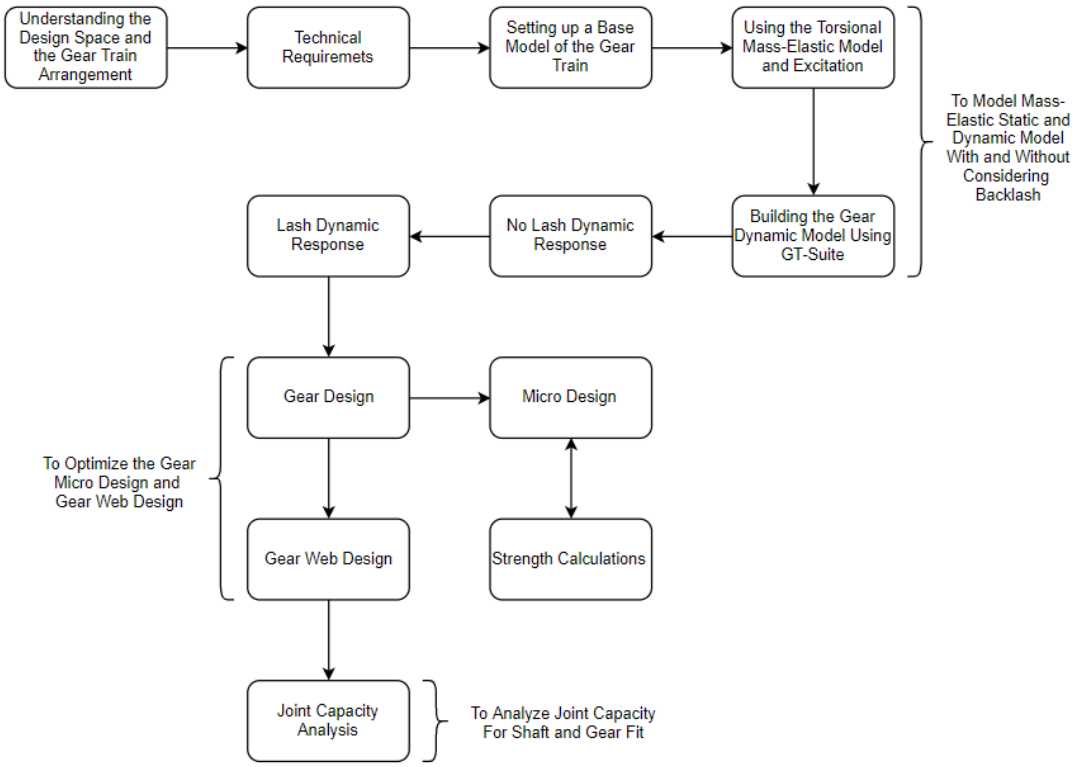

Fig. 3.1 Work flow process opted for achieving each objective

3.2 Understanding the Design Space and the Gear Train Arrangement

This is basically a requirement study process which was done to study the constraints in which the work has to be done. As the engine is already developed employing a helical gear train design according to the requirements of the customer, the constraint would be the space for the modelling of the spur gear train as every component is already designated a position and space which cannot be changed. Also this corresponds to doing a literature survey, documented in the Chapter 2 of this report, for gaining the knowledge of the previous work done in this field and building a base for the study by understanding the attributes of the timing system of the diesel engine and acquiring knowledge in the field of gear design and the various challenges that are to be overcome for a perfect timing gear train design. The Fig. 3.2 shows the 3D model of engine timing gear train on which the work was to be carried out. The model shows the placement of the various gears and the direction of rotation of each gear.

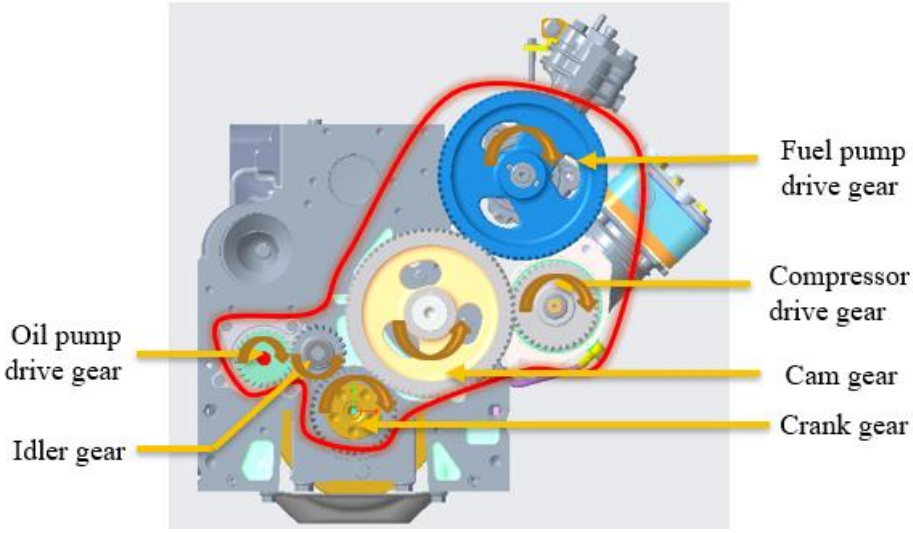

Fig. 3.2 Layout of the engine gear train and the rotation direction of each gear [**Cummins Technologies India Pvt. Ltd.**]

3.3 Technical Requirements

The technical requirements mean ascertaining the centre distances between the gear pairs, the angle at which the shafts are aligned, the required torques of each of the component that need to be run using the gear train *etc*. This is a constraint for the design that needs to be bound with and the output of the components in the engine and the engine itself, have been fixed as per the requirements of the customer which cannot be altered. So, this was the study which was done to define the boundaries of the project.

The centre distances and the angles between the mounting positions of the gears were measured on Creo and also on the engine. Then the torques needed for accessory drives like the compressor, fuel pump and the lube pump were sourced from the supplier.

3.4 Setting up the Base Model of the Gear Train and Making 3D Model of the Same Using Creo

3.4.1 Modelling of Standard Gears

Now, as the engine was previously employing a helical gear train, the pitch diameters were set according to the basic formulae of the helical gears which would now become totally obsolete as the requirement of the project was to not change the number of teeth

as that would imply changing the pitch diameters and the centre distances of the crankshaft and the camshaft, which was not desirable.

Therefore, the new number of teeth were calculated by the simple gear Eq. (3.1) and the percentage error in the speed ratio and the centre distance in comparison to the original dimensions was reported as in Table 3.1.

$$z = \frac{d}{m} \tag{3.1}$$

Table 3.1 Error in the speed ratio and the centre distance of standard spur gear with original helical gear

Gears Pairs	**Percentage Error in Speed Ratio**	**Percentage Change in Centre Distance**
Crank-Cam	0	-0.72025
Crank-LPI	2.7027	-1.77229
LPI-LPG	0	-3.41413
Cam-AC	0	-1.61458
Cam-FP	0	-0.97796

Now, as seen from the above data, all the speed ratios came out to be same except the Crank-LPI (Lube Pump Idler) gear. This percentage error was acceptable for this gear pair as the lube pump just need to provide a constant lubricant supply and the ratio is not critical for this operation. Further, from the same table it is evident that the centre distances are reduced drastically thus creating lot of space between the teeth of the gears. After finding the best fit model, all the gear parameters were calculated and verified with Windows LDP tool for the proper meshing.

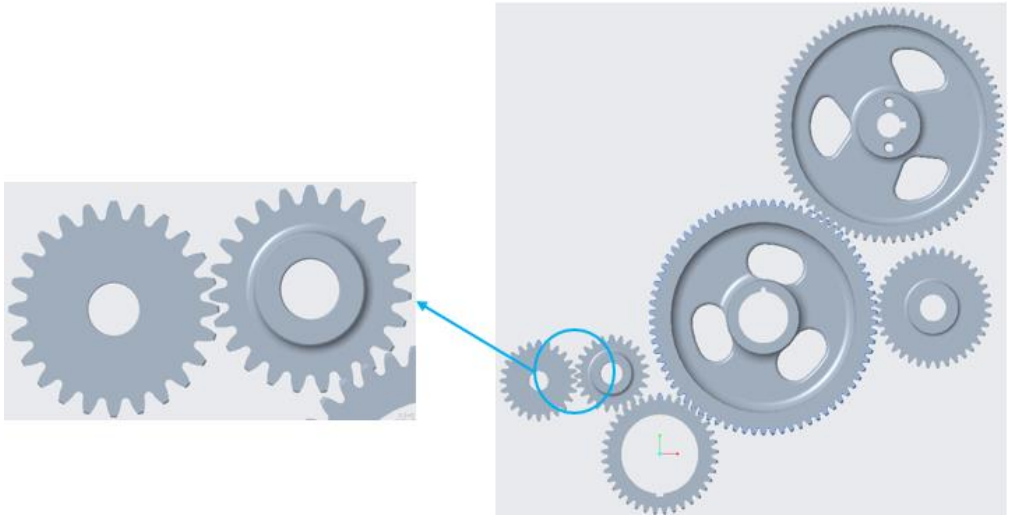

Fig. 3.3 3D model showing the gear train arrangement employing standard spur gears

This verification showed that although some gear pairs were meshing ok but others were not even coming close to each other which caused non-meshing. As shown in Fig. 3.3, the gears will not be having conjugate action as the pitch circles do not meet. This was verified by Windows LDP tool as well, thus leading to larger values of backlash and consequently leading to higher transmission error and noise.

Thus, to rectify the problem of the improper centre distance, literature was studied enlightening that the centre distance can be modified by a technique called addendum modification which has been discussed in Section 1.6.4.

3.4.2 Modelling of Addendum Modified Gears

The centre distance in this case needs to be increased, so, a positive profile shift coefficient is employed to all the gear pairs. This can be done using the calculation methodology given in DIN or ISO standards. In this case [**International Standard, 1982**] and [**International Standard, 2007**] is used for the calculations.

For the calculation of the addendum modification coefficient, firstly the centre distance modification coefficient was calculated for the gear pairs using Eq. (3.2) by keeping the centre distances between the gear pairs as constant as these were the parameters that were not to be changed.

$$y = \frac{a}{m} - \frac{z_1 + z_2}{2} \tag{3.2}$$

Then, as the modification coefficient is changed, it implies that the working pressure angle of the gears would also change because the overall effect of the change of the centre distance changes the involute angles of the profile of the gear tooth. The working pressure angle can be calculated as

$$\alpha_{\mathrm{w}} = \cos^{-1}\left(\frac{\cos\alpha}{\frac{2y}{z_1 + z_2} + 1}\right) \tag{3.3}$$

The sum of addendum modification coefficient on both the gears in mesh combinedly is calculated by the use of the involute normal and working pressure angles and the number of teeth of both the gears. This can be calculated as given by Eq. (3.4)

$$\Sigma x = \frac{(z_1 + z_2)(inv\ \alpha_w - inv\ \alpha)}{2 \tan \alpha} \tag{3.4}$$

Here, the $inv\ \alpha_w$ and $inv\ \alpha$ are the roll angles associated with the addendum modified and the non-modified gears and can be calculated by

$$involute\ of\ any\ angle\ X\ (inv\ X) = \tan X - \frac{\pi X}{180} \tag{3.5}$$

The Table 3.2 shows the normalized calculated values of the sum of addendum modification coefficients calculated for each of the gear pair.

Table 3.2 Calculated values (Normalized) for the addendum modification coefficient corresponding to the centre distances

Gear Pairs	**Centre distance (mm)**	**Sum of addendum modification coefficient (mm)**
Crank-Cam	0.74805	0.4287
Crank-LPI	0.40868	0.5974
LPI-LPG	0.32557	0.9645
Cam-AC	0.75485	1.0000
Cam-FP	1.00000	0.7853

After the calculation of the sum of addendum modification coefficient, the addendum modification coefficient for each gear was to be calculated in order to increase the addendum of the gears. This was done using the formulae given in [**International Standard, 1982**] & [**International Standard, 2007**] which are shown as below

$$x_1 = \lambda \frac{z_2 - z_1}{z_2 + z_1} + \Sigma x \frac{z_1}{z_2 + z_1} \tag{3.6}$$

$$x_2 = \Sigma x - x_1 \tag{3.7}$$

The above-mentioned formulae distribute the profile shift coefficients to both the gears which should be within limits defined in [**International Standard, 1982**] as given below in Eqs. (3.8 – 3.14)

Upper Limits:

$$for\ 10 < z \leq 50 \qquad x = 0.50 + 0.01z \tag{3.8}$$

$$for\ 50 < z \qquad x = 1 \tag{3.9}$$

Lower Limits

$$for\ 12 < z \leq 20 \qquad x = 0.0375(20 - z) \tag{3.10}$$

$$for\ 20 < z \leq 50 \qquad x = \frac{(20 - z)}{60} \tag{3.11}$$

$$for\ 50 < z \qquad x = -0.5 \tag{3.12}$$

Recommended Value of λ

$$0.5 \leq \lambda \leq 0.75 \qquad for\ speed\ reducing\ gears \tag{3.13}$$

$$0 \leq \lambda \leq 0.5 \qquad for\ speed\ increasing\ gears \tag{3.14}$$

Now, as the gear train has the speed reducing as well as the speed increasing gears, therefore the value of λ was used as 0.5 so as to maintain symmetry in the calculations. The Table 3.3 shows the calculated (normalized) addendum modification coefficients for each gear in the gear train. It can be verified that the sum of the addendum modification coefficients obtained from the Table 3.3. for a gear pair is equal to the sum given in the Table 3.2. This verifies that the addendum modification is done right.

Table 3.3 Normalized values for addendum modification coefficients for each gear

Gears	**Addendum modification coefficients (mm)**
Crank	0.3158
Cam	0.1130
LPI	0.2816
LPG	0.6829
AC	0.8870
FP	0.6723

Now, as soon as the addendum modification coefficient is applied to the gears, all the basic gear parameters like the pressure angle, pitch diameter, addendum height, tooth depth, tip diameter, root diameter and tooth thickness get changed that need to be calculated except the base diameter and reference pitch diameter that experiences no change in the dimensions. The parameters can be calculated according to the Eqs. (3.15 – 3.19) as shown below

$$d_{\mathrm{w}} = \frac{d_{\mathrm{b}}}{\cos \alpha_{\mathrm{w}}} \tag{3.15}$$

$$h_{\mathrm{a1}} = (1 + y - x_2)m \tag{3.16}$$

$$h_{a2} = (1 + y - x_1)m \tag{3.17}$$

$$h = \{2.25 + y - (x_1 + x_2)\}m \tag{3.18}$$

$$tt = \left(\frac{\pi}{2} + 2x \tan \alpha\right) m \tag{3.19}$$

Where, d_w is the working pitch diameter, h_{a1} & h_{a2} are the height of the addendum for the gear 1 & 2 in the pair, h is the tooth depth and tt is the tooth thickness at the working pitch diameter of the gear. The Table 3.4 shows the percentage change in attributes after the addendum modification. Although the working pressure angle and working pitch diameters have also changed but they remain different for the different meshing pairs.

Table 3.4 Percentage change in attributes after addendum modification

Gears	**Height of addendum**	**Tip diameter**	**Root diameter**	**Tooth thickness**
Crank	29.3710	1.5062	1.7650	14.4782
Cam	9.8175	0.2584	0.3047	5.1800
LPI	23.6815	1.8945	2.6493	12.9133
LPG	55.9124	4.3010	6.1251	31.3111
AC	80.1870	4.1122	4.9583	40.6726
FP	62.1910	1.6366	1.8133	30.8267

It is evident the after the positive addendum modification, the height of the addendum has increased drastically which compensates for the gap in the centre distance. Also, the tooth thicknesses at the working pressure angle also has increased quite a bit which gives the impression that the tooth will be much stronger in bending.

3.5 Using the Torsional Mass-Elastic Model and Excitation

The torsional mass elastic model uses stiffnesses of crank throws as obtained from ANSYS, the inertias from the 3D CAD models and the damping coefficients from calibration. The mass elastic model, cylinder pressures, and cylinder details (like bore diameter, connecting rod length, stroke, reciprocating mass, and firing order) were provided as an input to the Cummins proprietary tool. The combination of reciprocating inertia torque Eq. (3.20) and gas pressure torque Eq. (3.21) on the crankshaft from each cylinder, is calculated by this tool.

$$T_i(\theta) = -Mr_{cr}^2\omega^2\left[\frac{\sin\theta\cos\theta + q^2\sin\theta\cos\theta(2cos^2\theta - 1)\sqrt{1-(q\sin\theta)^2} + q\sin\theta(3cos^2\theta - 1)}{1-(q\sin\theta)^2}\right] \quad (3.20)$$

$$T_p(\theta) = P_\theta . A . r_{cr}\left[\frac{\sin\theta + q\sin\theta\cos\theta}{1-(q\sin\theta)^2}\right] \quad (3.21)$$

The normalized values of the torques on the crankshaft throw per cylinder were obtained for every degree of rotation of the crankshaft at rated rpm which are shown in the Table 3.5 for every 48 degrees of rotation along with the cylinder pressures.

Table 3.5 Normalized values of torques and cylinder pressures obtained for every crank throw

Crankshaft Rotation (°)	Inertia Torque (N-m)	Cylinder Pressure (N/m^2)	Gas pressure torque (N-m)	Total torque (N-m)
1	-0.04459	0.02042	0.00120	-0.00377
48	-0.86418	0.01522	0.03545	-0.05984
96	0.60085	0.01284	0.03213	0.10406
144	0.47847	0.01465	0.01688	0.07329
192	-0.15633	0.01482	-0.00566	-0.02411
240	-0.72849	0.01711	-0.03255	-0.11912
288	0.09294	0.04153	-0.11264	-0.11328
336	0.87507	0.27809	-0.37522	-0.31269
384	-0.87507	0.74113	1.00000	1.00000
432	-0.09294	0.13043	0.35374	0.37851
480	0.72849	0.06093	0.11594	0.21086
528	0.15633	0.02740	0.01047	0.02939
576	-0.47847	0.02180	-0.02512	-0.08235
624	-0.60085	0.01982	-0.04958	-0.12327
720	0.00000	0.02111	0.00000	0.00000

The graph of the total torques obtained at every degree of rotation of the crankshaft at the rated rpm is shown in the Fig. 3.4.

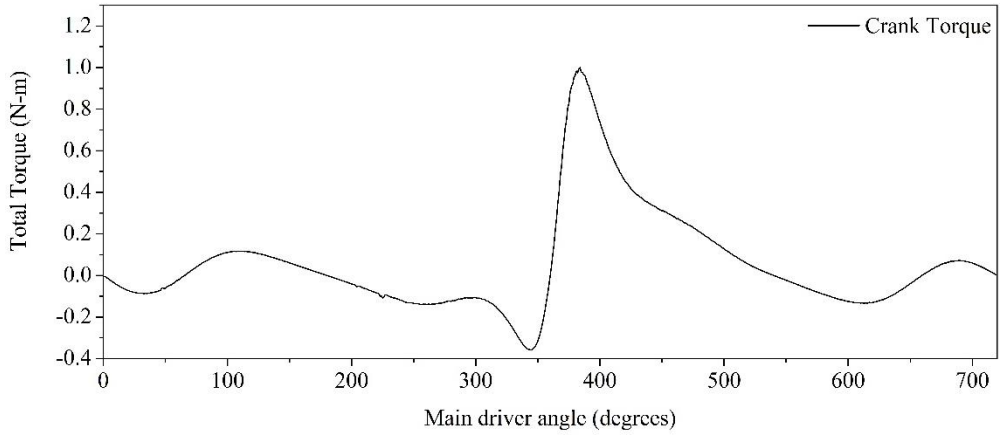

Fig. 3.4 Normalized Graph of torque experienced by a single crank throw at rated rpm

Similarly, the torques are obtained for every cylinder at every rpm band of the engine and then the data is prepared to be fed as an input to the dynamic model of the gear train which is to be prepared using GT-Suite. The torques in the Fig. 3.5 are flipped, *i.e.* the power stroke is shown in the negative side because this is the way that GT-Suite software requires the input for the dynamic model of the gear train.

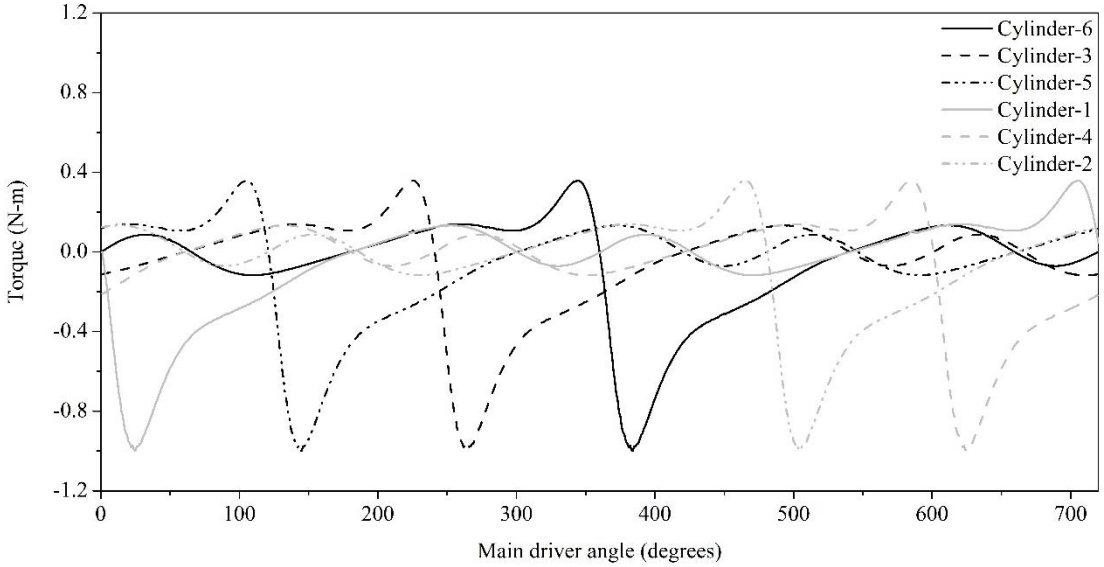

Fig. 3.5 Combined torques (normalized) acting on each cylinder at rated rpm

This model was used to obtain combined torques on the crankshaft throw at different rpms. But the further research here was done on the rated rpm of the engine.

3.6 Building the Gear Dynamic Model Using GT-Suite

GT-Suite is a simulation tool with a wide range of capabilities and vast libraries focused on various industrial applications. It can be used to design a concept, a detailed system or a sub-system analysis, optimization of the design and investigation of the root cause.

In this research this tool is used to build a dynamic model of the timing gear train and to ascertain the dynamic characteristics of the model and further to optimise the dynamics of the model. This tool takes the inertias, damping, stiffnesses, component torques and the crankshaft excitation as the input and gives, in this case, the contact forces, dynamic transmission error, torque, lash values, *etc* as the outputs.

To have an apple to apple comparison, a new gear Dynamic model for helical gear train was built using the same methodology which would be used for the spur gear train

dynamic model instead of the experimental methodology used in the original helical model. The torques on the crankshaft in Fig. 3.5 are used as the input torques to the crankshaft model here, which further produces an excitation through crank nose to the gear train from where measure the forces on the gear is recorded.

The dynamic model of the timing system of the engine is made firstly by making a mass stiffness model of crankshaft by identifying each part of the crankshaft as a separate inertia and the joining them by the spring and damper system. The inertias observed on the crankshaft are the damper ring, damper casepulley, crank nose (where the crank gear is fit), six separate throws of the crankshaft, flywheel and clutch (taken as a single inertia) and a dynamometer. Also, a speed boundary condition is given to the dynamometer for the rpm control. Then each throw is connected to a torque component for feeding the torque which was obtained in the Fig. 3.4 and the torque components are controlled by a time delay switch which is inputted with the degree of crank rotation at which the particular crank throw needs to actuate. All the actuation signals come from a signal generator which were provided at the very beginning of the circuit. The crankshaft model is shown in Fig. 3.6 below.

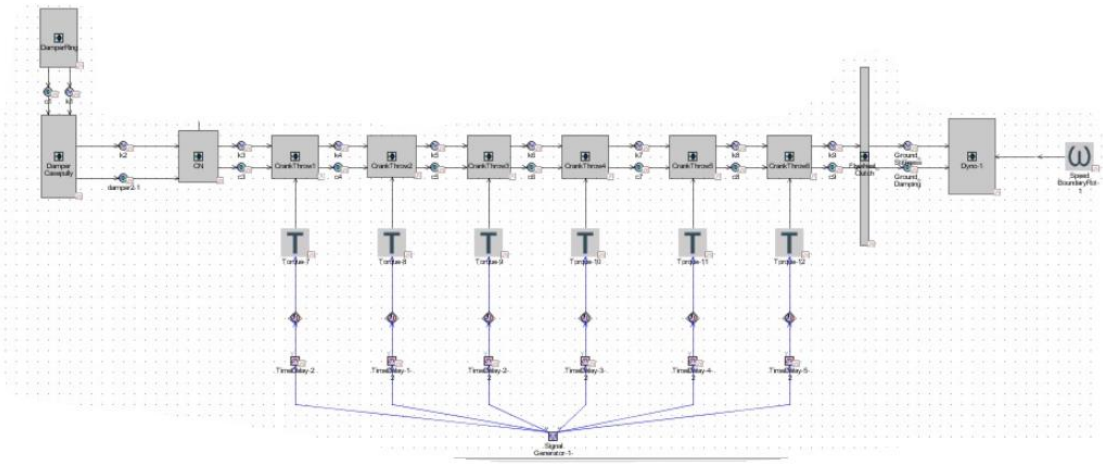

Fig. 3.6 Crankshaft spring, mass damper system

Similar to the crankshaft model, the model for the camshaft was also made as shown in Fig. 3.6. The only difference in the camshaft model is that we need not calculate the torques for the camshaft separately as this would be calculated by the software itself when the connections are built.

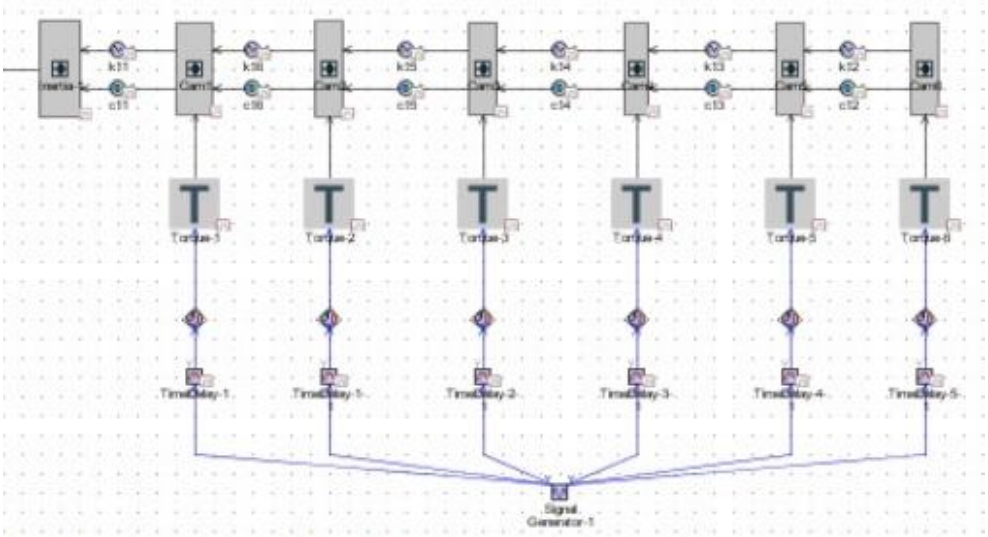

Fig. 3.7 Camshaft spring, mass damper system

Similarly, the inertia and the torque components for the air compressor, fuel pump and the lube pump are also laid out. The torque values in these components are not actuated using the signal generator as we have torque map already provided by the supplier company for these components.

Lastly, we connect the gears to the respective components. It is to note that the gears sit on a revolute joint and the revolute joint has an earth connection to it, specifying that the revolute joint is fixed in place. A gear connection is to be given between two gear inertias as this contains the values of stiffnesses and the dampings of the gear pair. The gear inertias contain the gear parameters and the material properties of the gears. This connection of gear to gear is shown in Fig. 3.8 (a) and the gear to revolute joint and the contact is shown in Fig. 3.8 (b).

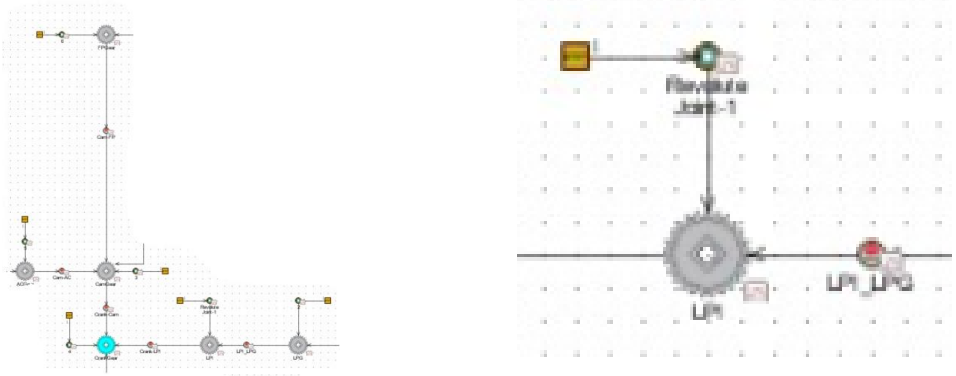

(a) (b)

Fig. 3.8 (a) Gear connection and (b) Gear inertia, contact, revolute joint and earthing components

The main calculations for the dynamic model were done for obtaining the stiffness and the dampings of the gear train as these were the parameters that were originally obtained experimentally. But, as this model was a preliminary one therefore, these parameters were to be calculated theoretically for both the helical and the spur gears. The contact stiffness of the gears is calculated when trying to obtain the dynamics and vibrations of the system as the gear's mesh region is much more flexible than the core region. To calculate the contact stiffness of the gears, a Cummins confidential formula was used which employed a constant multiplication with the length of line of contact. The length of contact line for the spur gears is the width of the gear tooth which is straightforward obtained from standard gear formulae. But the length of contact line for helical gears can be obtained from a formula given in NASA Technical Note by [**Coy & Zaretsky, 1975**] as shown in Eqs. (3.22 & 3.23)

For Helical $$L_c = 0.95\frac{b \times CR}{\cos\psi} \tag{3.22}$$

For Spur $$L_c = b \tag{3.23}$$

The 0.95 value is recommended for the calculation of contact stress and length, by American Gear Manufacturers Association (AGMA).

The calculation of length of contact is easy for spur gear but for helical gear we need the contact ratio which indicates the average number of pairs of teeth in contact. The contact ratio for any gears can be calculated by

$$\mathrm{CR} = \frac{\text{Length of zone of action}}{\text{Circular pitch}} \tag{3.24}$$

For the contact ratio, the length of line of action, shown in Fig. 3.9 (a) was need to be calculated as given in Eq. (3.25). The gear side nomenclature is shown in Fig. 3.9 (b). Further, when the contact stiffnesses are obtained we need to obtain the viscous damping coefficients for the gear mesh using the Eq. (3.26) as the damping has a major effect on the stress factor and the dynamic loads when the operating speeds are close to the critical speeds or half or one-third of the critical speeds otherwise it does not have much effect on rest of the speeds.

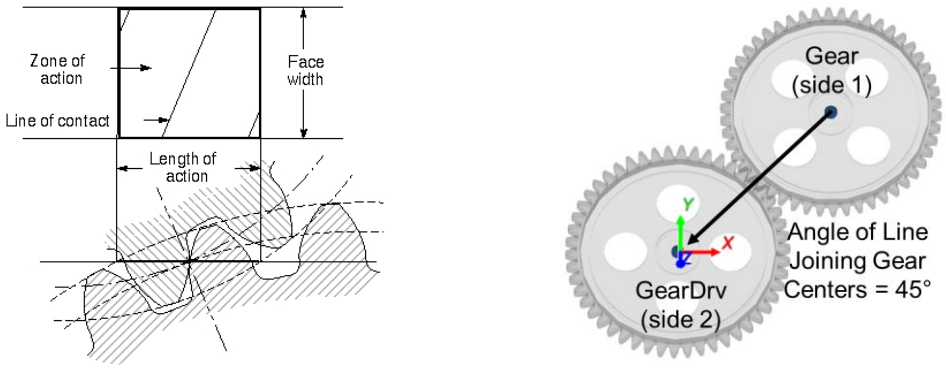

(a) (b)

Fig. 3.9 (a) Schematic showing zone of action [**Wikipedia, 2018**] and (b) Gear side nomenclature [**GT-Suite, 2018**]

$$l_a = \sqrt{(r_{a1})^2 - (r_{b1})^2} + \sqrt{(r_{a2})^2 - (r_{b2})^2} - (r_{p1} + r_{p2}) \sin\psi \tag{3.25}$$

$$C = 2\zeta\sqrt{K \times J_{eq}} \tag{3.26}$$

Where,

$$J_{eq} = \frac{J_1 \times J_2}{(J_1 r_{b2}^2 + J_2 r_{b1}^2)} \tag{3.27}$$

The value of damping ratio (ζ) was taken as 0.08 as it was directed by the Cummins technical data. The normalized values of all the calculated parameters are given in Table 3.6 for each of the gear pair.

Table 3.6 Normalized stiffnesses and dampings for the helical and the spur gears

Gear Pairs	**Contact Ratio Helical**	**Contact Ratio Spur**	**Contact Stiffness Helical (N/m)**	**Contact Stiffness Spur (N/m)**	**Damping Coefficient Helical**	**Damping Coefficient Spur**
Crank-Cam	1.5636	1.5095	0.3951	0.3077	0.2456	0.2172
Crank-LPI	1.5319	1.4546	0.3545	0.2818	0.1793	0.1655
LPI-LPG	1.6651	1.8032	1.0000	0.7312	0.8664	0.7399
Cam-AC	2.0185	2.0096	0.9091	0.5484	0.7428	0.5973
Cam-FP	1.7177	1.8813	0.8166	0.5789	1.0000	0.8147

Now, when all the parameters have been calculated, a GT- Map is to be made, like the one given in Fig. 3.10, by linking the inertia, gear, spring and the damper elements using the arrows along with the boundary conditions and inputting the above data to the respective contact member of the gears.

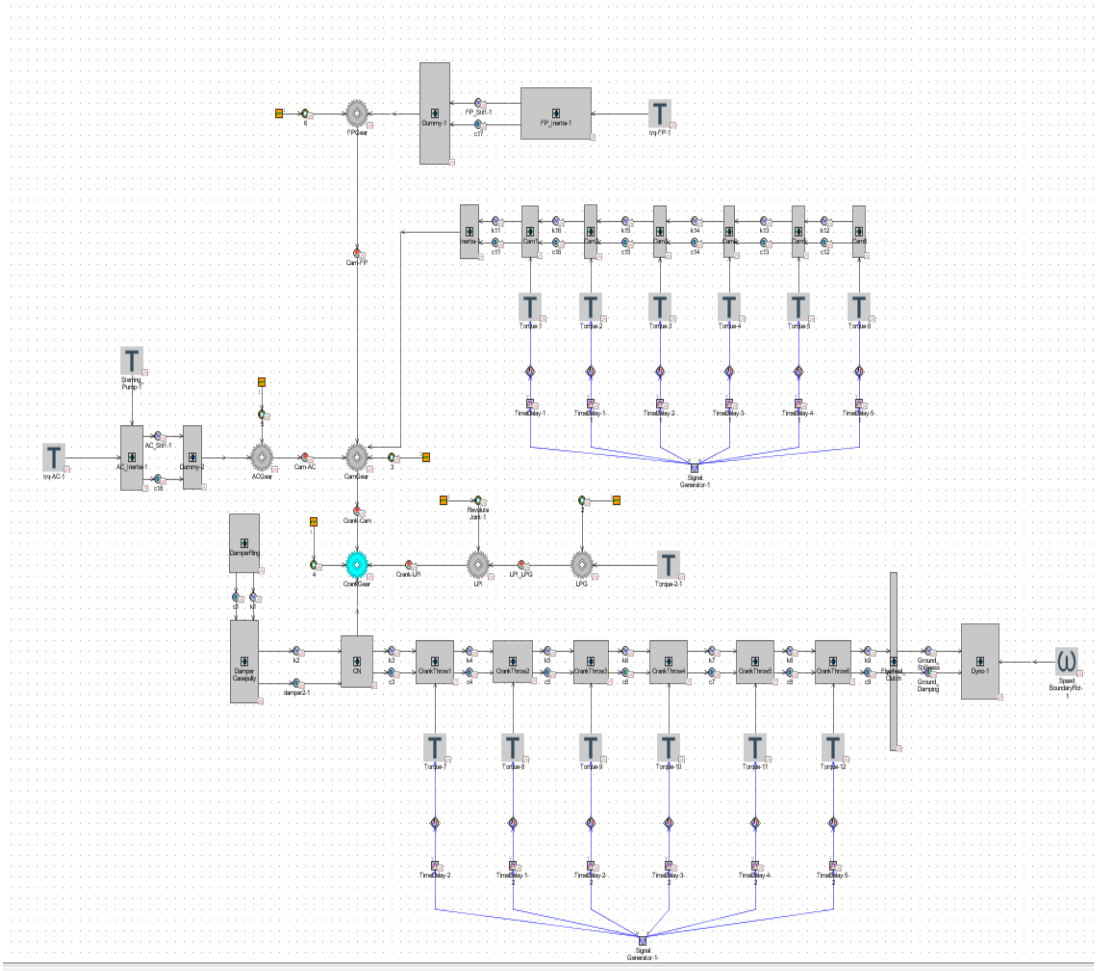

Fig. 3.10 Dynamic model map of the timing system of the engine

The torques obtained from the mass stiffness model, the torques of each of the component and the damping and the stiffnesses become the main inputs to the model and the total transverse contact loads and the thrust loads are the ones that needs to be matched to confirm that the model made is correct. After confirming that the dynamic model map in GT is correct, the dynamic model map for spur gear is built using the stiffnesses and the damping obtained by the calculation given by the formulae mentioned above. Also, the lash dynamic response and the no-lash dynamic response of each gear pair is also ascertained.

3.7 No-Lash Dynamic Response

The no lash dynamic response is obtained using the dynamic model by keeping backlash as zero. This is done to analyse any discrepancies in the model, like, if there is any abrupt behaviour in the results or the response of the model is not as it was

expected to be, it can be identified and rectified easily. This is done in the no lash condition as in this phase the dynamic model follows linearity and the unexpected behaviour is easily detected which cannot be detected in the lash dynamic response.

3.8 Lash Dynamic Response

In real life the gear train always behaves as a non-linear dynamic problem as backlash cannot be avoided. If the backlash is not present between a gear pair, then gears may get stuck and proper lubrication of teeth will be a problem. Therefore, it is important to analyse that what are the properties of a gear pair having backlash between them. This marks the completion of the first objective.

3.9 Gear Design

In the previous steps, the gear macro design was finalized by ascertaining the number of teeth and the size of the gears as per the available centre distances of the engine components. Also, by analysing the gear-train in GT-suite the gear macro design was also optimised, by changing the number of teeth and the addendum modification coefficients, to attain the best possible dynamic characteristics from the gear train.

In this step, the main motive was to reduce the noise of the gears by reducing the peak-to-peak transmission error side by side by maintaining the gear root stresses, contact stresses and temperature below the threshold limits. This was achieved by calculating the gear micro design using the standard formulae from [**International Standard, 2007**] and then optimising the gear micro-design using Windows LDP tool, which is a program that analyses a single pair of gear in mesh for predicting the load distribution in the gears using the AGMA standards for calculations. The gear designing included two steps which would be discussed in this section.

3.9.1 Micro Geometry Optimisation

The micro geometry calculations were done using the international standards by [**International Standard, 2007**] and then the calculated microgeometries were input into the Windows LDP tool to optimise the micro design for minimum attainable transmission error along with the acceptable contact stresses, root stresses, load

intensity distribution and surface temperature of the gears. The LDP model assumes the load distribution to be a function of the elasticity of the gear system and errors or modifications on the gear teeth. The major assumption in LDP are as given below

- The total elastic deformation is the sum of the individual elastic deformations.
- The elastic deformations are small; thus, tooth contact is assumed to remain on the line of contact.
- The gear bodies and supporting shafts behave as solid cylinders for determining the bending and torsional deformations.
- The deflections of any given tooth pair are not influenced by the loads on other tooth pairs.

The microgeometry modification carried out in this thesis revolves particularly on the idea to reduce the noise in the spur gear trains as the previous design employed a helical gear train which has the property of producing a less noise than any other gear train. Therefore, to get the noise levels equal to or at least near about the noise levels of the helical gears the modification was carried out. The microgeometry optimisation was done step by step as mentioned in the research by [**Harianto & Houser, 2007**]. According to them, the best methodology to obtain a good micro design for the noise reduction is to first provide the tip relief and the profile crowning on the gears, which would help in reducing the peak-to-peak TE in the gear pairs after which the lead crowning is to be done which helps in increasing the area of load intensity distribution so that the load does not gear concentrated in a single area and lead to micro pitting on the surface of the tooth.

To start with the microgeometry modification, the tip relief was applied on both the gears by first calculating the tip relief manually using the deformations due to the Hertzian contact stress and the elastic deformations as given by [**Marković & Vrcan, 2016**]. The calculation methodology first implied the calculation of the Hertzian deformation which is shown by the Fig. 3.11. (a) This deformation is caused as the result of the imposed contact loads on the two curved surfaces of the teeth and depends on the modulus of elasticity and the Poisson's ratio. The maximum deformation due to the Hertzian contact stresses and be calculated as given by Eq. (3.28). The elastic

deformation caused by the transverse load can be shown as in Fig. 3.11 (b) and can be calculated according to the formula given in Eq. (3.29).

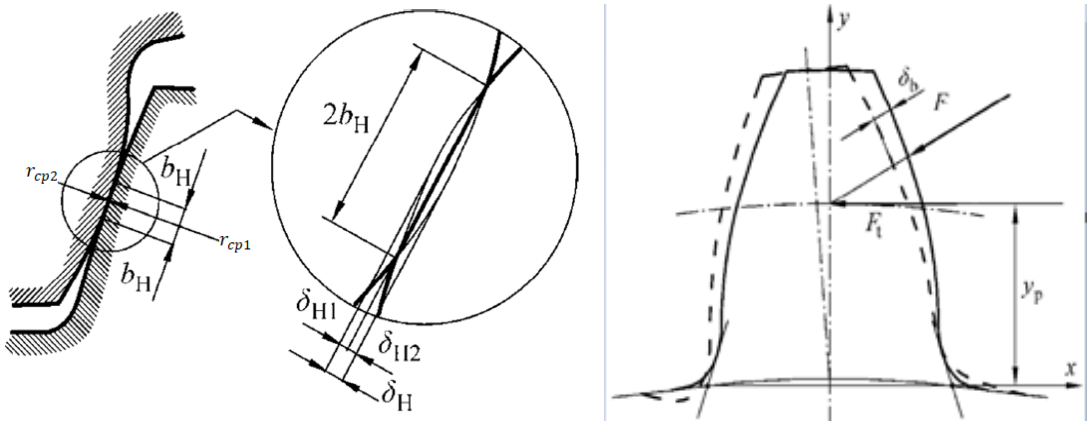

(a) (b)

Fig. 3.11 (a) Deformation due to the Hertzian contact stress and (b) Tooth elastic deformation [**Marković & Vrcan, 2016**]

$$\delta_{\mathrm{H}} = \frac{2F}{\pi b}\frac{(1-v^2)}{E}\left[1.27 + 0.78\ln\frac{m}{b_{\mathrm{h}}}\right] \tag{3.28}$$

$$\delta_{\mathrm{b}} = \frac{F}{b}\frac{(1-v^2)}{E}\left(\mathcal{A} + \mathcal{B}e^{\mathcal{C}.\bar{y}_{\mathrm{p}}} + \mathcal{D}\right) \tag{3.29}$$

Where,

$$\mathcal{A} = -1.05 + 153e^{-8.1x}.z^{-(1.75-1.6x)} \tag{3.30}$$

$$\mathcal{B} = 0.63 + (7.35 - 0.924x)z^{-1} \tag{3.31}$$

$$\mathcal{C} = 1.28 - (2.88 + 3.68x)z^{-1} \tag{3.32}$$

$$\mathcal{D} = -1.06 + 0.638\ln(mz) \tag{3.33}$$

$$\bar{y}_{\mathrm{p}} = \frac{y_{\mathrm{p}}}{m} = \frac{r_{\mathrm{p}}\cos(\alpha_{\mathrm{w}} - \omega_{\mathrm{b}}) - r_{\mathrm{r}}}{m} \tag{3.34}$$

$$\omega_{\mathrm{b}} = \frac{r_{\mathrm{r}}}{r_{\mathrm{b}}} - \varphi \tag{3.35}$$

$$\varphi = \frac{4x\tan\alpha_{\mathrm{n}}}{2z} + inv\alpha_{\mathrm{n}} \tag{3.36}$$

$$b_{\mathrm{h}} = \sqrt{\frac{2F_{\mathrm{c}}}{\pi L_{\mathrm{cyl}}} \times \frac{\frac{(1-\nu_1^2)}{E_1} + \frac{(1-\nu_2^2)}{E_2}}{\left(\frac{1}{d_1}\right) + \left(\frac{1}{d_2}\right)}} \tag{3.37}$$

Now, the total tooth tip relief is the same as the total deflection of the tooth given by the Eq. (3.38). The mod magnitude entered in the microgeometries of the LDP software should be greater than the calculated tip relief.

$$C_t = \delta_b + \frac{1}{2}\delta_H \tag{3.38}$$

The Table 3.7 shows the normalized value of the Hertzian deformation and the elastic deformation along with the minimum amount of tip relief required on the tooth tip of the spur gears in order to stop the early contact to the teeth and reduce the transmission error

Table 3.7 Normalized value of the calculated Hertzian deformation, the elastic deformation and the minimum tooth tip relief

Gear Pairs	**Hertzian Deformation (mm)**	**Elastic Deformation (mm)**		**Tip Relief (mm)**	
		Gear 1	**Gear 2**	**Gear 1**	**Gear 2**
Crank-Cam	1.0000	0.4127	1.0000	0.4975	1.0000
Crank-LPI	0.0882	0.0135	0.0458	0.4975	0.0519
LPI-LPG	0.0675	0.0114	0.0174	0.0519	0.0246
Cam-AC	0.9702	0.3264	0.1555	1.0000	0.2731
Cam-FP	0.5654	0.3861	0.1303	1.0000	0.1931

In this study, a linear tip relief has been used rather than the parabolic tip relief as this tip relief provides a less TE at the given loads in spur gears if the design is correct and the parabolic tip relief produces an increased TE [**Marković & Vrcan, 2016**]. While providing the tip relief, profile crowning is also provided to the tooth flank of the gear so the peak-to-peak transmission error (PPTE) is further reduced. After confirming the acceptability of the PPTE, the lead crowning is applied to the tooth flank to reduce the amount of contact stresses and the root stresses and to distribute the loads over the flank as scattered as possible.

The Table 3.8 shows the microgeometry optimization done on the crank-cam pair. Using these values, the contact stresses, load distribution, transmission error and the temperature distribution were optimized for their lowest values and the optimization with the best results were selected and then put into LDP to obtain the results. Similarly, all the microgeometries for each of the gear pair of spur and helical gear was optimized. Further, the optimized attributes for the spur gear along with the unmodified spur already present helical gear were compared for the percentage change.

Table 3.8 Normalized values of Crank-Cam pair microgeometries

Run No.	Microgeometries optimised											
	1st roll angle at start of EAP (degrees)		1st linear EAP mod mag. (mm)		Profile crown (mm)		2nd roll angle at start of EAP (degrees)		2nd linear EAP mod mag (mm)		Lead Crown (mm)	
	G1	G2	G1	G2	G1	G2	G1	G2	G1	G2	G1	G2
1	0.89	0.82	1.00	1.00	0.01	0.01	1.00	0.88	1.00	1.00	0.04	0.24
2	0.89	0.82	1.00	1.00	0.01	0.01	1.00	0.88	1.00	1.00	0.04	0.32
3	0.96	0.86	0.32	0.32	0.20	0.20	1.00	0.89	0.32	0.32	0.01	0.32
4	0.96	0.86	0.32	0.32	0.20	0.20	1.00	0.89	0.32	0.32	0.08	0.32
5	0.96	0.86	0.32	0.32	0.20	0.20	1.00	0.89	0.12	0.12	0.01	0.32
6	0.96	0.86	0.40	0.40	0.20	0.20	1.00	0.89	0.12	0.12	0.01	0.32

3.9.2 Strength Calculations

This is one of the major steps in the gear design as this decides whether the gear teeth will be able to sustain the loads that are being imposed on them during the work cycle. This includes the calculation of the root stresses and the contact stresses on each of the gears. The root stresses and the contact stresses were only analysed on the gear pairs which had high contact forces acting on them.

The calculations for the contact stresses were done with the help of the Hertzian contact theory. To calculate the Hertzian contact stress for gear teeth, the teeth are considered as 2 cylinders, shown in Fig. 3.12 (a) rolling over each other with diameters equal to the pitch circle diameters of the gears.

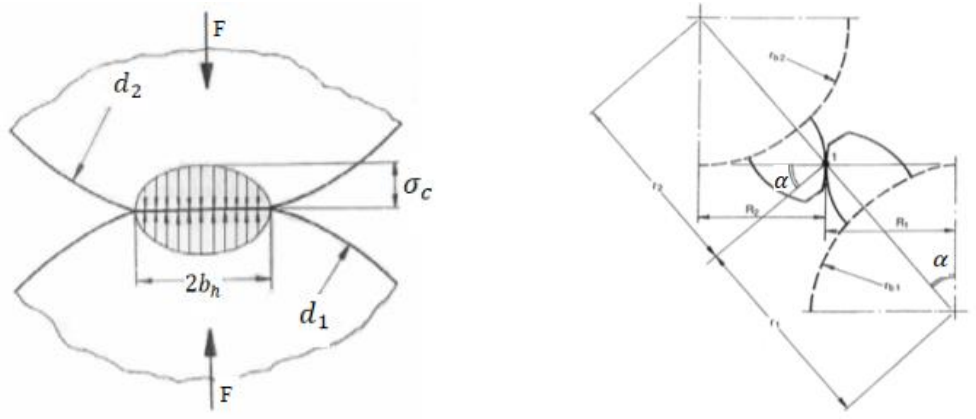

(a) (b)

Fig. 3.12 (a) Schematic showing Hertzian contact between two cylinders and (b) Schematic showing Hertzian contact between a pair of gear teeth [**Hassan, 2009**]

The maximum contact pressure between the teeth along the centre line of the rectangular contact area is given by Eq. (3.39) and the half width can be calculated as given in Eq. (3.37).

$$P_{\max} = \frac{2F_{\mathrm{c}}}{\pi b_{\mathrm{h}} L_{\mathrm{cyl}}} \tag{3.39}$$

The above stated equations need to be generalised for a gear pair according to the notations used in the gear nomenclature. The cylinder lengths L_{cyl} is replaced with face width b, F is changed to $F_{\mathrm{t}}/\cos\alpha$ and d is replaced by $2r$. The Hertzian theory assumes the contact patch to be elliptical, as shown in Fig. 3.12 (a), which translates the maximum stress concentration to be in the very middle. Therefore, substituting P_{max} in Eq. (3.39) by σ_{c} and substituting the value of b_{h} along with the changed notations, the contact stress can be given by

$$\sigma_{\mathrm{c}} = \sqrt{\frac{F_{\mathrm{t}}}{\pi b \cos\alpha} \times \frac{\left(\frac{1}{r_1}\right) + \left(\frac{1}{r_2}\right)}{\frac{(1-\nu_1^2)}{E_1} + \frac{(1-\nu_2^2)}{E_2}}} \tag{3.40}$$

Where,

$$r_1 = \frac{d_1 \sin\alpha}{2} \qquad r_2 = \frac{d_2 \sin\alpha}{2} \tag{3.41}$$

F_{t} can be calculated by dividing the drive torque by the pitch radius of the gear when there is no other load increment factor present.

Now, the calculation of the root stresses was done using the Lewis bending equation as it is considered as the basis for the calculation of the bending stresses in the root of the teeth. These were further evaluated for a true 3D results by analysing the gear designs in the tools like Windows LDP and ANSYS.

The gear tooth, shown in Fig. 3.13, is strong anywhere along the inscribed parabola except where the parabola meets the root of the tooth *i.e.* at point ‘a’ because of which the maximum bending stresses occur at that point. Therefore, the bending stress at the point ‘a’ can be written as in Eq. (3.42).

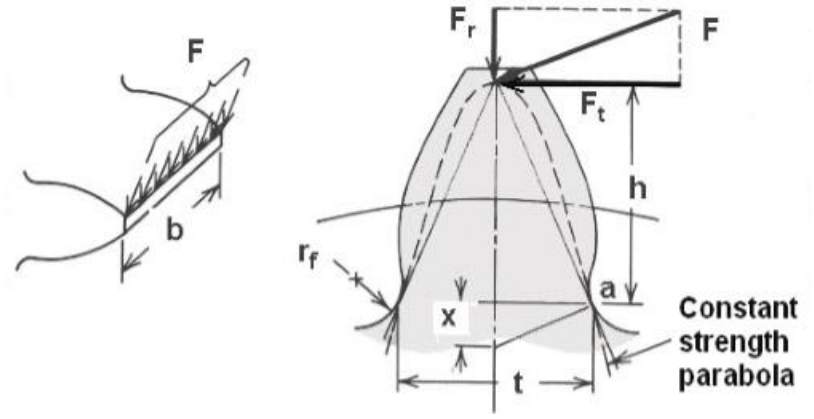

Fig. 3.13 Schematic showing the tooth nomenclature while experiencing bending according to Wilfred Lewis [**Gopinath & Mayuram, 2010**]

$$\sigma_b = \frac{F_t}{bYm} \tag{3.42}$$

Where, Y is known as the Lewis form factor and can be calculated using the Eq. (3.43).

$$Y = \pi \frac{2x}{3p} \tag{3.43}$$

$$x = \frac{t^2}{4h} \tag{3.44}$$

This equation for Y has been used as only the bending if tooth is taken into consideration and not the compression of the tooth due to the radial forces has been neglected. The Lewis form factor Y depends on the tooth shape and not the size, therefore, it varies with the change in the number of teeth. These values can be retrieved by using the Table 3.9 or the graph given in the Fig. 3.14.

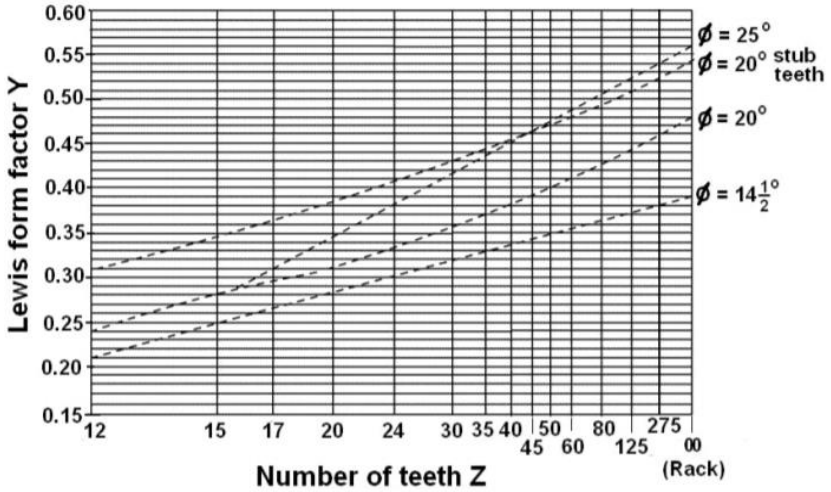

Fig. 3.14 Spur gear graph for Lewis form factor [**Gopinath & Mayuram, 2010**]

Table 3.9 Values of the Lewis form factor Y, for 20° pressure angle, full-depth teeth, and unit diametral pitch in the rotation plane [**Budynas & Nisbett, 2011**]

Number of Teeth	Y	Number of Teeth	Y
12	.245	28	.353
13	.261	30	.359
14	.277	34	.371
15	.290	38	.384
16	.296	43	.397
17	.303	50	.409
18	.309	60	.422
19	.314	75	.435
20	.322	100	.447
21	.328	150	.460
22	.331	300	.472
24	.337	400	.480
26	.346	Rack	.485

3.10 Gear Web Design

The gears are generally designed as a solid structure to withstand the high amount of forces acting on them. But the larger gears, with such a large mass, do not need to be full of material between the hub and the root circle of the gears. This extra material present contributes to the dead torques due to increased inertia of the gears. Therefore, in this step the cam gear and the fuel pump gear, which have a large pitch circles, need to be stripped off the excess material by designing web and the pockets on the gear body so that the inertia of the gears could be reduced. This reduction in inertia of the gears will reduce the dead torques of the gears. This is done by FEA modelling of gears in ANSYS workbench and then calculating the stresses on the gear web using Goodman criteria tool in ANSYS itself. Further the fatigue margins will be calculated according to the equivalent fully reversed (EFR) limit of the material of the gear. The model is subjected to every force that is acting on every teeth of the gear in the forward direction first and then in the reverse direction and then the fatigue margins are calculated for the forward and reverse loading separately. After this the model is also is subjected to the combined forward and reverse loading, which is a case that would seldom occur. It is done so that if the fluctuating loads suddenly reverses due to knocking in the engine, or some other factor, the gear teeth can withstand the forces and not fail under influence of abnormal loading.

3.11 Joint Capacity Analysis

Joint capacity analysis is done to ensure that the joint between the shaft and the gear hub can sustain the torques that the gears are experiencing. This is done to ensure that there is no slippage in between the shaft and the gear hub so that the torques from the gears can be efficiently transferred to the shafts.

There are two types of joints used to sustain the gears in position in this design. The first one is press fit that is employed on the crank, cam and the lube pump gear and idler. The second one used is the taper joint which uses a nut that is pre-torqued to the gear face to push it into a tight fit with the tapered shaft.

The press fit is one of the types of interference fit which can be used to fit the shaft on shaft with high interferences. This can be used to sometimes eliminate the use of keyways or can also be used with keyways. The torque capacities were calculated using the standard formulae form [**Budynas & Nisbett, 2011**] for interference fit and then the 3D model was analysed using FEA in ANSYS. The calculation of the torques were done as per the formulae presented in the Eqs. (3.45 – 3.47)

$$p_{\mathrm{i}} = \frac{\delta_{\mathrm{i}}}{\frac{d_{\mathrm{n}}}{E_0}\left(\frac{d_0^2 + d_{\mathrm{n}}^2}{d_0^2 - d_{\mathrm{n}}^2} + \nu_0\right) + \frac{d_{\mathrm{n}}}{E_{\mathrm{i}}}\left(\frac{d_{\mathrm{n}}^2 + d_{\mathrm{i}}^2}{d_{\mathrm{n}}^2 - d_{\mathrm{i}}^2} + \nu_{\mathrm{i}}\right)} \tag{3.45}$$

$$F_{\mathrm{f}} = f p_{\mathrm{i}} \pi d_{\mathrm{n}} l \tag{3.46}$$

$$T = F_{\mathrm{f}} \frac{d}{2} \tag{3.47}$$

The Table 3.10 shows the calculated values of the contact pressure, frictional force and the torque capacity of the joint using the above formulae.

The calculations of the torque capacities for the taper joints was done assuming the taper fit similar to the cone clutch. The calculation methodology of the cone clutch was taken from design of machine elements [**Bhandari, 2010**]. The uniform pressure theory was applied as the base formula. As this theory does not consider the material properties, the torques calculated by this method were very high. Therefore, a Cummins proprietary MATLAB code was used to determine the torque capacities and then verified using FEA in ANSYS. The uniform pressure theory is the basics of the code

and the simulation in ANSYS and can be represented as in Eq. (3.48) and the Fig. 3.15 shows the schematic of a taper fit assembly.

The bolt preload is to be calculated as we know the pre-torque value of the bolt and not the force that is being applied. The preload value can be calculated as given in Eq. (3.49). The Table 3.10 shows the values of the nut factors for various conditions.

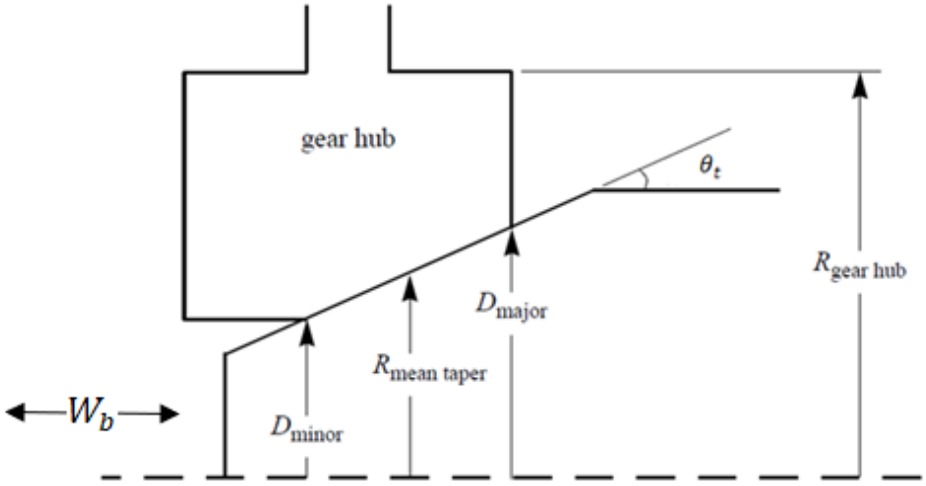

Fig. 3.15 Schematic showing the taper fit assembly [**Cummins Technologies India Pvt. Ltd.**]

$$T = \left(\frac{W_{\text{b}} \times \mu}{3\ sin\ \theta_{\text{t}}}\right)\left(\frac{D^3_{\text{Major}} - D^3_{\text{Minor}}}{D^2_{\text{Major}} - D^2_{\text{Minor}}}\right) \tag{3.48}$$

$$W_{\text{b}} = \frac{T_{\text{n}}}{kD_{\text{b}}} \tag{3.49}$$

For the FEA analysis of the gears, the models were given a displacement in the tangential direction on the pitch circle in successive increments starting from zero. The movement of the gears in their axial direction were restricted by another displacement. A hole was made inside the shaft to add a remote displacement and restrict all six degrees of freedom of the shaft. A frictional contact was provided between the gear hub and the shaft for the press fit models and for the taper fit model the contacts given were frictional between the shaft and the hub, bonded between the nut and the shaft and nut and the washer and frictionless contact was provided between the washer and the gear hub. The simulation was performed and the displacement at which either the torque became constant or decreased was taken as the point of slip and the torque was termed as the torque capacity of the gears.

Table 3.10 Normalized values of calculated contact pressure, frictional force and torque capacity of press fit joint

Gear	**Contact pressure (MPa)**	**Frictional force (N)**	**Torque capacity (N-m)**
Crank	0.31	0.58	0.90
Cam	1.00	1.00	1.00

Table 3.11 The values of nut factor for various coatings [**Fastenal, 2005**]

Nut Coating	***k***
No plating	$0.20 - 0.30$
Plated with zinc	$0.17 - 0.22$
Lubrication provided	$0.12 - 0.16$
Plated with cadmium	$0.11 - 0.15$

In this research, a methodology was followed to obtain a viable solution for the problem of the cam gear walk off. The solution was obtained in the form of changing the existing timing gear train from helical to spur. This involved the gear design, dynamic analysis and the structural analysis of the gears so that the gears can rectify the cam gear walk off problem and are manufacturable. This section of the research shows the results obtained at every step in the design process as per the followed methodology.

4.1 Results for Addendum Modification of the Spur Gears

After modifying the gears using the addendum modification coefficient, the gears were modelled in Creo software for the 3D representation. Fig. 4.1 shows the addendum modification done on cam gear by superimposing the 3D computer aided design (CAD) model of a standard spur gear over an addendum modified spur gear. The grey gear is the standard gear and the red one is the addendum modified gear. This shows the effects of positive modification on the gear teeth. It is evident from Fig. 34 that the positive modification on gear teeth increases the tooth thickness, addendum, base diameter, pitch diameter and all the other standard gear parameters.

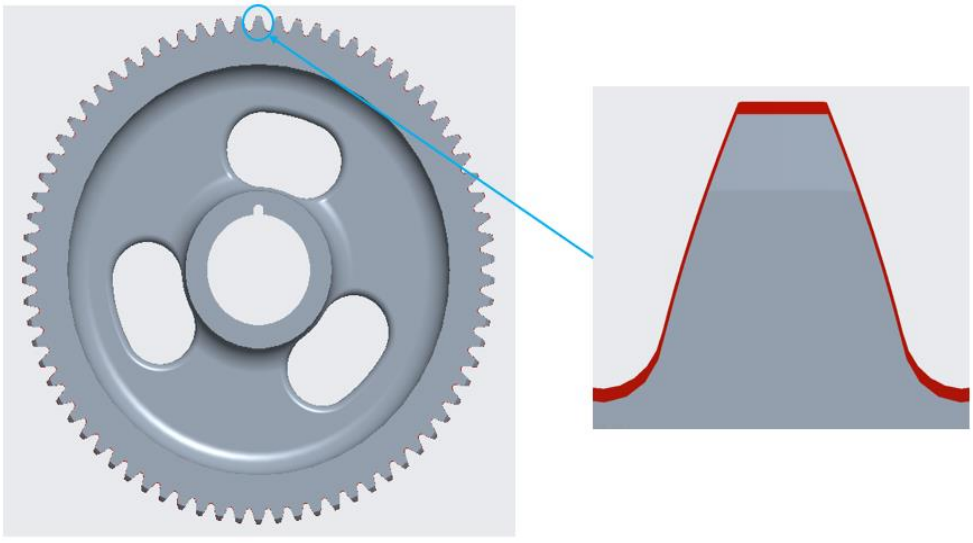

Fig. 4.1 3D CAD model showing the effect of addendum modification

The Fig. 6.2 shows that the gears mesh more closely with conjugate action as compared to in the Fig. 3.2 which was just the standard gears without addendum

modification. This means that now there will be less amount of backlash introduced due to the variation in centre distance consequently having less amount of TE and noise. Moreover, it seems that the contact stresses will also be less due to the less amount of the space in between the consecutive teeth of the gears. Thus, the gears would work more effectively and have a conjugate action between their movement which would provide a much smoother action between the gears mesh.

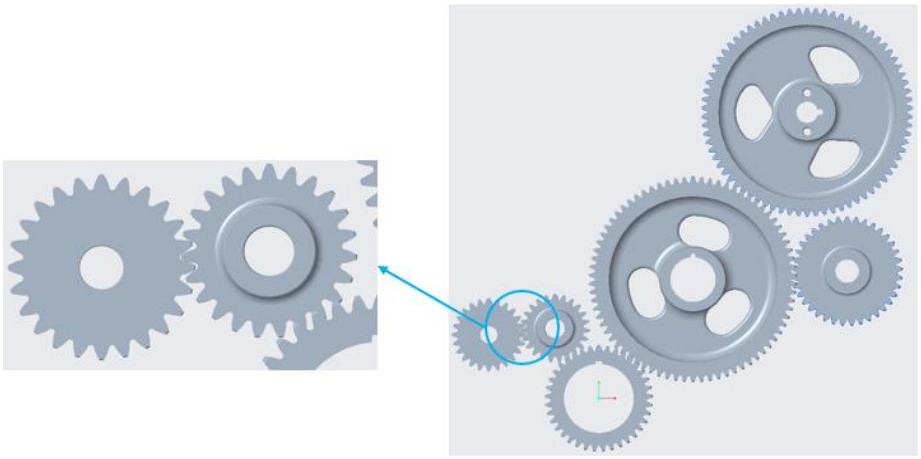

Fig. 4.2 3D CAD model showing gear train employing addendum modified spur gears

4.2 Without Lash Dynamic Response of the Gear Model Using GT-Suite

After the addendum modification of the gears, it was important to ascertain the dynamic characteristics of the gear pairs. But before it could be done for the newly modelled spur gears it was important to make a new dynamic model map for the already existing helical gears and confirming the outputs of the new helical gear model with the already available contact forces of helical gear which was considered as the base model. The contact forces of the crank-cam, cam-fuel pump (FP) and cam-air compressor (AC) pairs only have been documented as the forces in crank-lpi (lube pump idler) and lpi-lpg (lube pump gear) pairs are of highly fluctuating nature and magnitude is also very less. The contact forces without backlash for the comparison of the re-constructed model with the old helical model are shown in Fig. 4.3 (a), (b) and (c) and through the graphs it is evident that the contact forces of the base model and the re-constructed model are in unison except for some peaks. The difference in the shape and the appearance angle of some peaks are different because of the change in the stiffness and the damping used as the new model is based on the theoretical calculations and the old helical model is based on the calibration data.

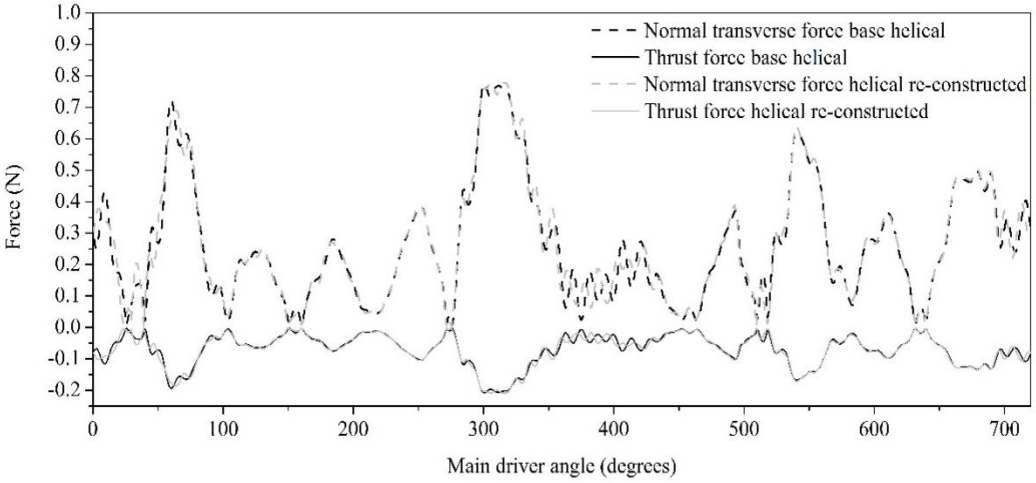

(a)

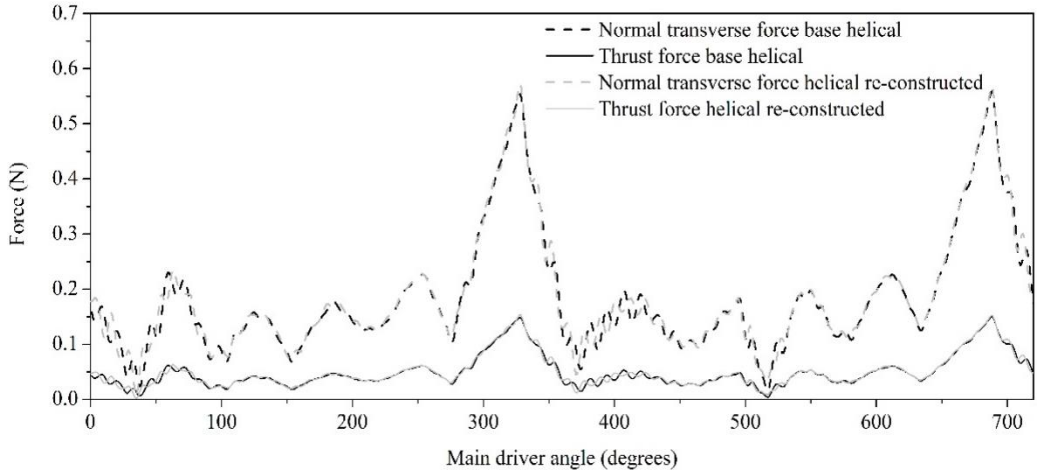

(b)

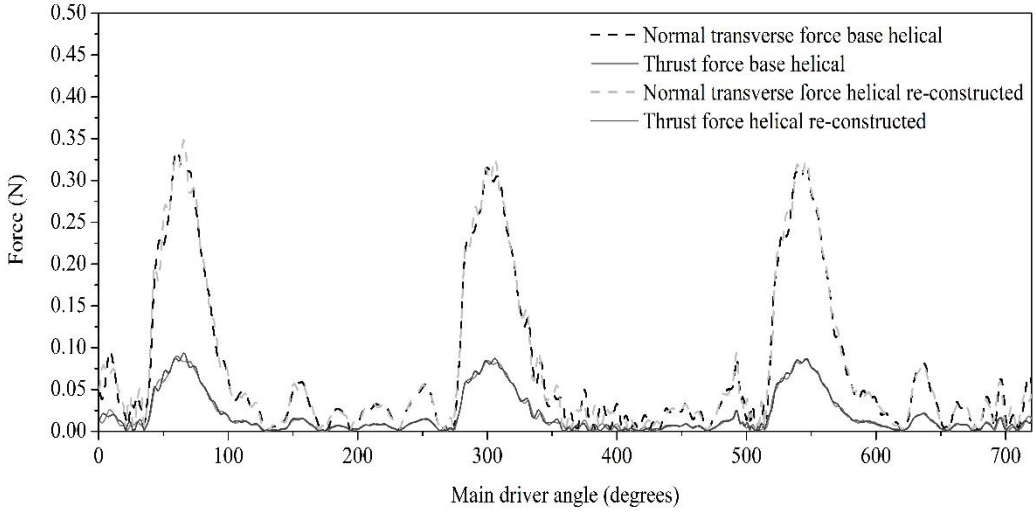

(c)

Fig. 4.3 Without backlash contact forces comparison for base helical model and re-constructed helical model (normalized) of (a) Crank-cam pair, (b) Cam-ac pair and (c) Cam-fp pair

Now, when it was confirmed that the new model is correct, the model was changed from the helical model to addendum modified gear model. This new addendum modified gear model was to be checked for the dynamic characteristics independently to ascertain whether the contact forces are in limit. Also, it was compared with the new model of the helical gear to find that by how much factor does the contact forces increase or decrease in the spur gears. The Fig. 4.4 (a), (b) and (c) shows the comparison of the contact forces without backlash in the helical and the spur crank-cam, cam-ac and cam-fp gear pairs. From the graphs it is ascertained that the normal transverse dynamic forces for the addendum modified spur gear train also follows a similar trend to the normal transverse dynamic contact forces of the helical gear train. Moreover, it is seen that the contact forces on the spur gear does not exceed the specified limit anywhere in the operating cycle, in fact, the normal transverse contact force of the addendum modified spur gear train is almost the same as the helical gear train which is a good result.

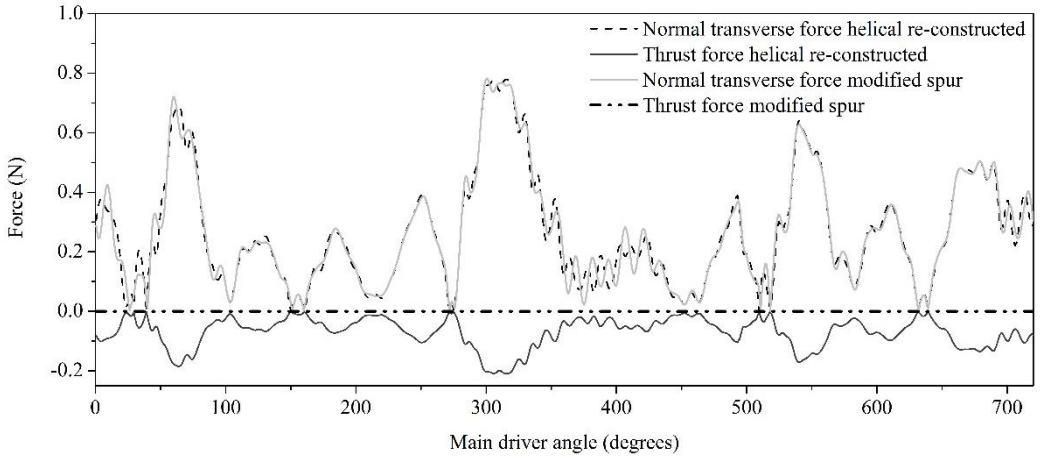

(a)

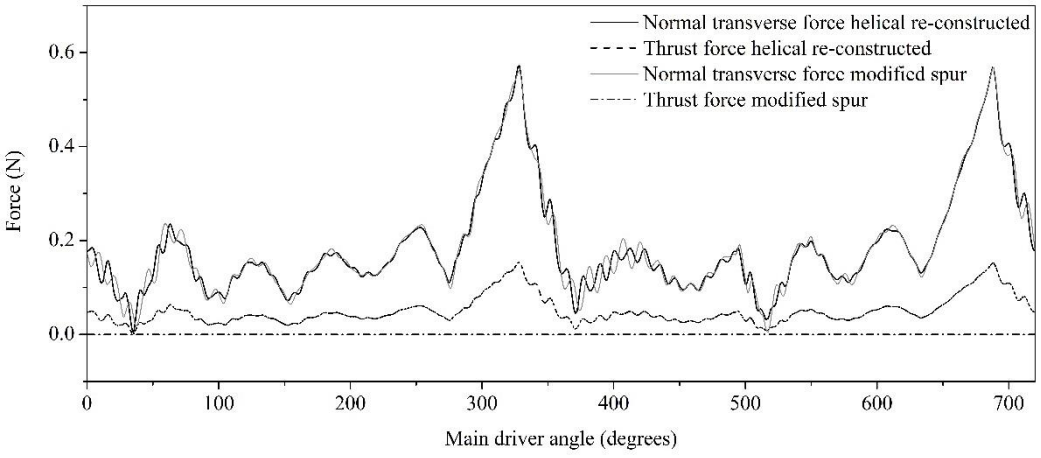

(b)

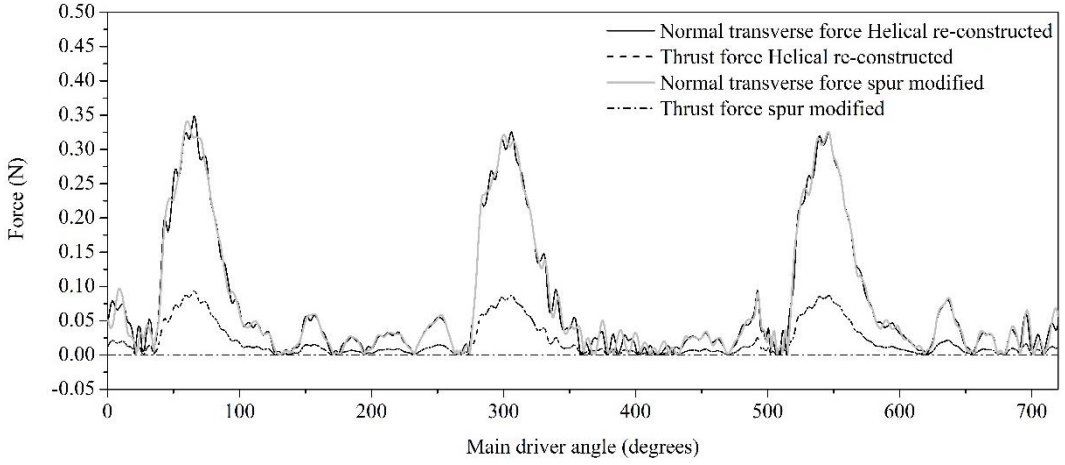

(c)

Fig. 4.4 Without backlash contact forces comparison for re-constructed helical model and addendum modified spur gear model (normalized) of (a) Crank-cam pair (b) Cam-ac pair and (c) Cam-fp pair

In the Fig. 4.4 (a), (b) and (c) it is apparent that the thrust forces for the spur gears have reduced to zero which marks the main objective of this research, the elimination of the cam gear walk-off by eliminating the thrust forces acting on it. Although the dynamin forces show that the gear would not move from its position due to the dynamic forces, but, there can be many more causes of the failure of the gear train if all the aspects of the gear design are not completed.

4.3 With Lash Dynamic Response of the Gear Model Using GT-Suite

The lash dynamic response Fig. 4.5 (a), (b) and (c) of the gear pair is analysed to obtain the characteristics and the amount of contact forces which will act on the gear teeth in the real life. This analysis shows that how the forces will rise or fall when there is backlash present on the gears.

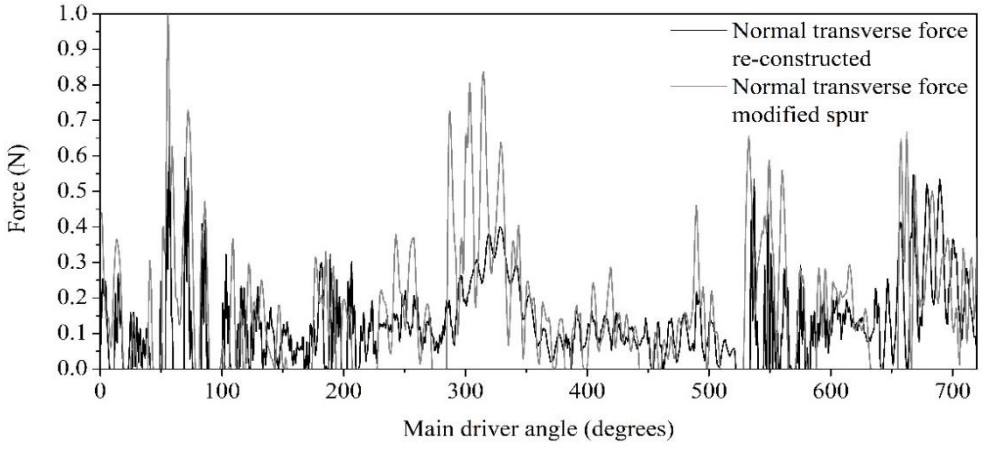

(a)

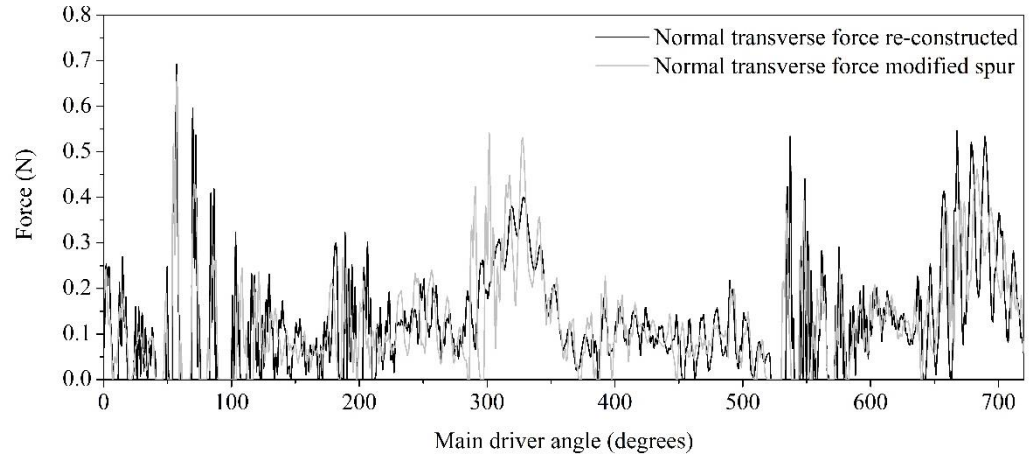

(b)

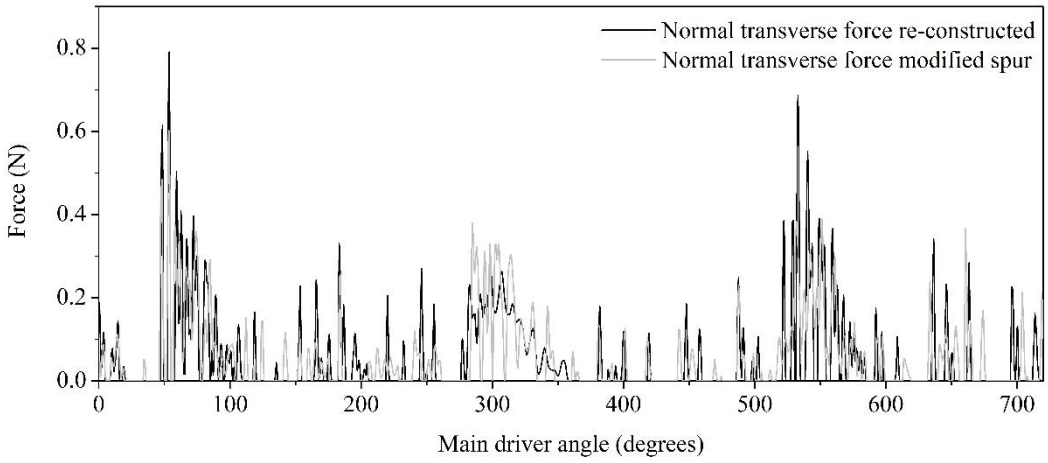

(c)

Fig. 4.5 With backlash contact forces comparison for re-constructed helical model and addendum modified spur gear model (normalized) of (a) Crank-cam pair (b) Cam-ac pair and (c) Cam-fp pair

From the above graphs it is evident that in the real-life scenario *i.e.* when the backlash is present on the gears, the contact forces will shoot to almost double the values of the contact forces when there is no backlash present. Also, the highly fluctuating nature of the graphs show the instability of the data due to which the data with backlash cannot be used to calculate a constant amount of the torques that the gears are experiencing during operation. Therefore, the torques on the gears are calculated only using the dynamic forces which do not consider the backlash. The data with no backlash gives the constant torques as their result which are further used to study the transmission error, root stresses, contact stresses, load intensity distribution and temperature distribution using the Windows LDP tool. Also, these torques also gives us the benchmark for the torque capacity analysis of the gear and the shaft joints.

4.4 Root Stress (Von-Mises) Evaluation for the Addendum Modified Gears using Windows LDP and ANSYS

Cummins used Ansys as the tool to calculate the root stresses of the gear teeth. But, in this research microgeometries were to be analysed which meant the changing of the root stresses on the gears as well which meant that LDP should be the one to ascertain the root stresses of the gears as well. Therefore, to determine whether LDP gives a comparable result of root stress to the one obtained by ANSYS, the addendum modified gears were used to compare the root stresses given by the two softwares and these were compared to the hand calculated root stresses which were obtained by Lewis equation. This was only done for the crank-cam and the cam-fp pair as these were having higher forces on them. The Fig. 4.6 (a), (b), (c) and (d) shows the Von-Mises root stress that the crank gear is experiencing in crank-cam pair. Similarly, Fig. 4.7 (a), (b), (c), and (d) and Fig. 4.8 (a), (b), (c) and (d) also show the Von-Misses root stresses as experienced by the cam gear due to crank-cam forces and the FP gear due to cam-fp forces. The cam gear root stress was not analysed for the cam-fp forces as already cam gear can withstand the higher forces exhibited by the crank-cam pair.

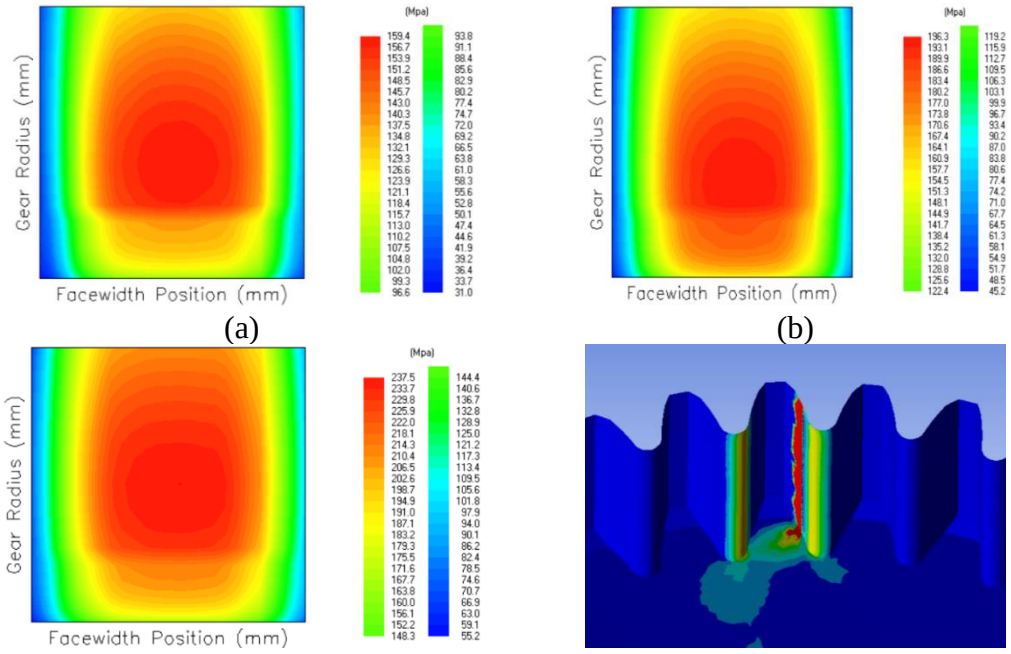

Fig. 4.6 Comparison of root stresses (von-mises) on the gear teeth of crank gear using the forces on the crank-cam pair (a) Tensile root stress LDP, (b) Compressive root stress LDP, (c) Maximum root stress LDP and (d) Tensile and compressive root stress ANSYS

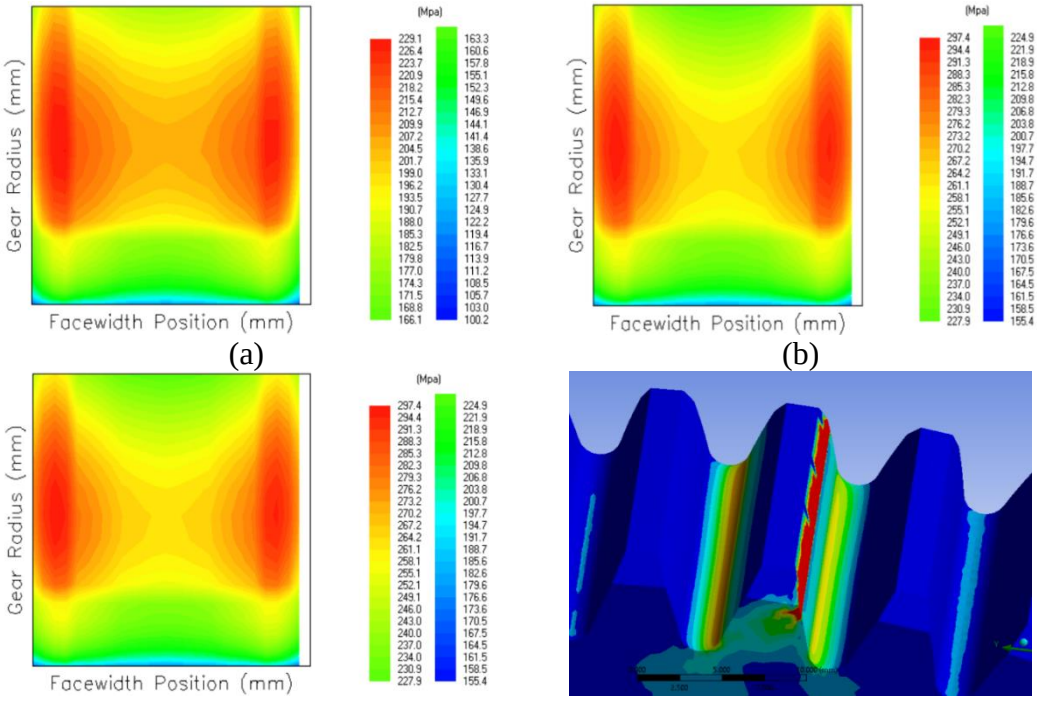

Fig. 4.7 Comparison of root stresses (von-mises) on the gear teeth of cam gear using the forces on the crank-cam pair (a) Tensile root stress LDP, (b) Compressive root stress LDP, (c) Maximum root stress LDP and (d) Tensile and compressive root stress ANSYS

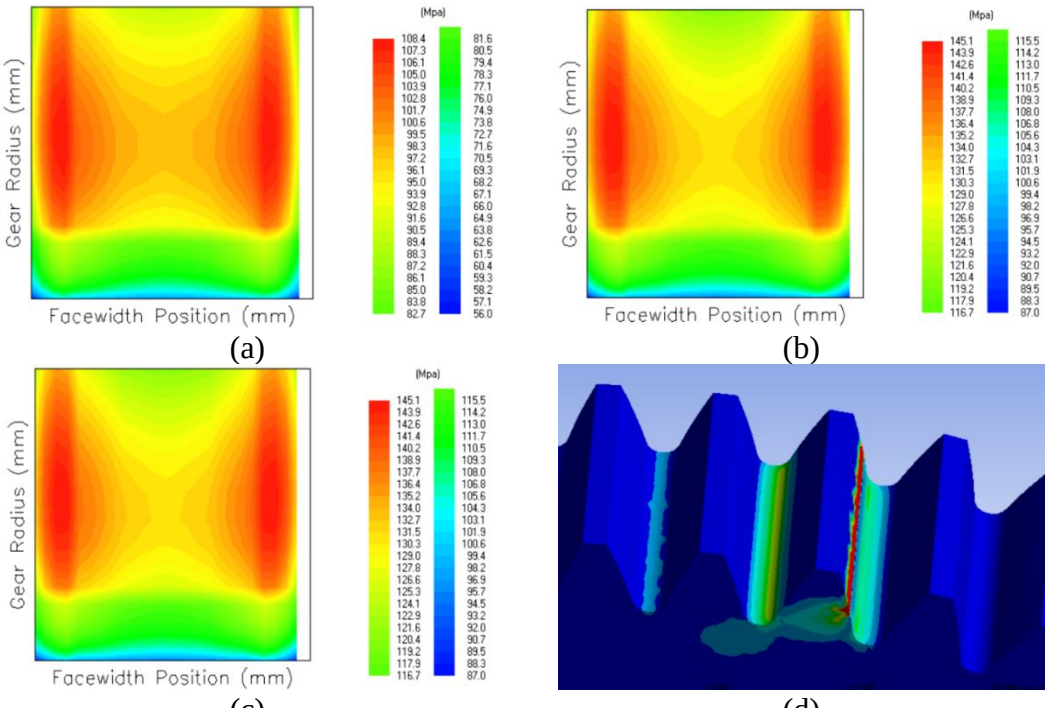

Fig. 4.8 Comparison of root stresses (von-mises) on the gear teeth of fp gear using the forces on the cam-fp pair (a) Tensile root stress LDP, (b) Compressive root stress LDP, (c) Maximum root stress LDP and (d) Tensile and compressive root stress ANSYS

From Figs. (4.6 – 4.8) it is evident that tensile and compressive root stress from LDP matches the tensile root stress form ANSYS with ANSYS overestimating or underestimating with respect to LDP. This is because ANSYS only considers a single tooth in loading whereas LDP calculates the root stress at various mesh positions and gives different root stress on teeth at different mesh positions. Also, the maximum stress on the gear as predicted by LDP is much higher than any of the tensile or compressive stress predicted, this is because the stresses may be higher at some other meshing positions. Therefore, it can be concluded form here that the LDP tool is much more effective to be used than ANSYS for the root stresses as LDP can measure root stresses at each position of the meshing. Also, the microgeometries could not be captured in the 3D model of the gears therefore, once the microgeometries have been modified, the root stresses from ANSYS will become obsolete and LDP will only be used.

Also, while looking at the stress map from LDP shows that the maximum stresses for cam and FP occur at the extreme of the face widths which may lead to the damage of the corners of the teeth as the corners are the weakest in strength. This is also one of the main reasons why microgeometry modification is to be done to bring the maximum stresses in the middle of the face width and minimise the probability of chipping off the corners.

4.5 Effect of Microgeometry Modification on the Gears and their Comparison with their Helical and Unmodified Counterparts

The microgeometry modification was done on the spur gears with the aim of reducing the transmission errors (noise reduction) while keeping the stresses and the temperatures below the specified limit. Although the microgeometry modification is a trade off between the transmission error reduction and the reduction in the contact and the root stresses and the surface temperature distribution, here the objective was to reduce the noise produced by the spur gears along keeping the stresses and the surface temperatures under the specified limit of the material. The microgeometries were optimised for all the gear pairs except the crank-lpi and lpi-lpg because these gears are very small in size and the torques on these gears are very less which does not contribute much to the noise of the gear train. Also, the evaluation of root stresses is not important for these gears because of the less amount of torque they are subjected to.

4.5.1 Crank-Cam Pair

The Fig. 4.9 (a), (b) and (c) shows the transmission error plot of unmodified spur, baseline helical and modified spur crank-cam gear pair. It is to be noticed that the helical has the smoothest operation between the three whereas the unmodified has a sudden jump in the graph which would become the cause of the noise. Moreover, the higher the peak-to-peak value is, the higher will be the noise produced by the gear pair. It is apparent by Fig. 4.9 (c) that the peak-to-peak value has been drastically reduced by the microgeometry modification. Although the modifications provided to the gear pair were unable to reduce the peak-to-peak values of spur gears below the helical gears, the reduction provided by them is enough to reduce the amount of noise in the spur gear pair.

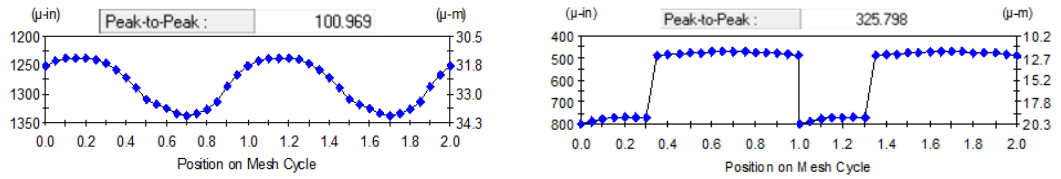

(a)

(b)

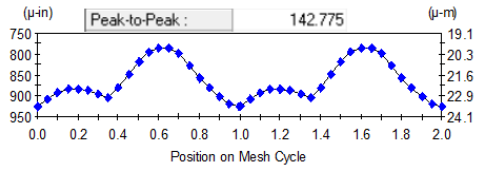

(c)

Fig. 4.9 Comparison of TE between the crank-cam gear pair (a) TE plot of baseline helical, (b) TE plot of unmodified spur and (c) TE plot of microgeometry optimized spur

The Fig. 4.10 (a), (b) and (c) shows the contact stress distribution (CSD) plot of unmodified spur, baseline helical and modified spur crank-cam gear pair. It is the Hertz stress that results in pitting, wear and surface deterioration.

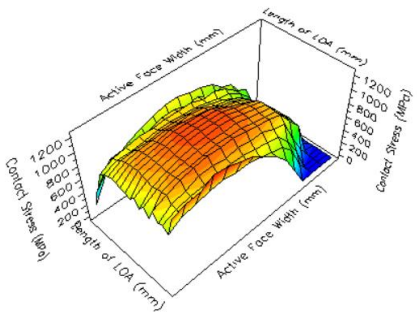

(a)

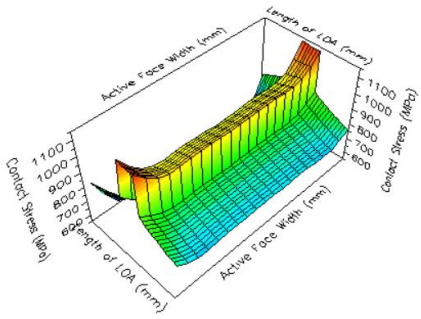

(b)

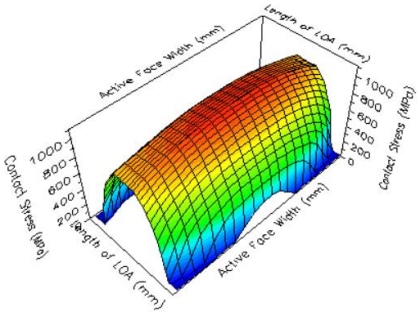

(c)

Fig. 4.10 Comparison of CSD between the crank-cam gear pair (a) CSD plot of baseline helical, (b) CSD plot of unmodified spur and (c) CSD plot of microgeometry optimized spur

If the modifications are not adequate, there will be an abnormally high stress at the entering and leaving corners of the face width in Fig. 4.10. This is not the case with the modified gear. The maximum stress concentration lies at the centre of the face width with a lower value of contact stress than the unmodified as well as the helical gear. This means that the gears will last much longer in wear.

The Fig. 4.11 (a), (b) and (c) shows the load intensity distribution (LID) plot of unmodified spur, baseline helical and modified spur crank-cam gear pair. This is a practical plot since it normalizes load to length of each contact segment and shows the intensity of the load per millimetre (mm) of the face width. It can be inferred from these plots that the value of load per mm is lesser than even the helical gear and is far more less than the unmodified spur gear. This means that the tooth has a more uniform loading all over the face which decreases the risk of micro pitting. There were corner contacts present on the non-modified spur gear which posed a threat of overloading of the corner points of the gear tooth and subsequent breakage of the teeth from the ends. The microgeometry modified gear pair has no such issue and has the maximum value of LID in the middle of the face width of the tooth.

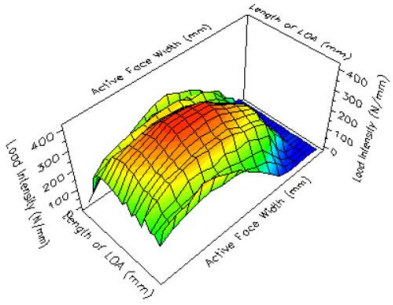

(a)

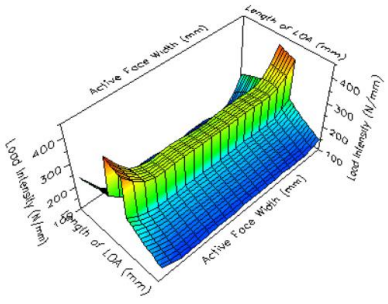

(b)

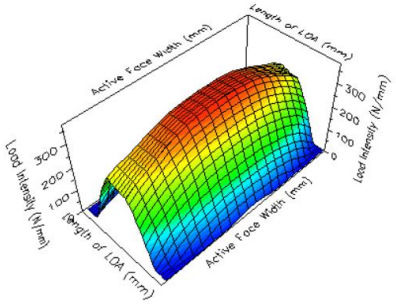

(c)

Fig. 4.11 Comparison of LID between the crank-cam gear pair (a) LID plot of baseline helical, (b) LID Plot of unmodified spur and (c) LID plot of microgeometry optimized spur

The Fig. 4.12 (a), (b) and (c) shows the temperature distribution (TD) plot of unmodified spur, baseline helical and modified spur crank-cam gear pair. The surface temperature that is graphed is the sum of the material bulk temperature that is input by the user and the flash temperature that is calculated with the AGMA equation. It is observed that the maximum surface temperature occurs at the point where the product of sliding velocity and contact stress is a maximum. Where contact is close to the pitch point and sliding velocity approaches zero, a very low surface temperature is observed. This is because at that point the involutes are in pure rolling which means the temperature due to the friction is not generated.

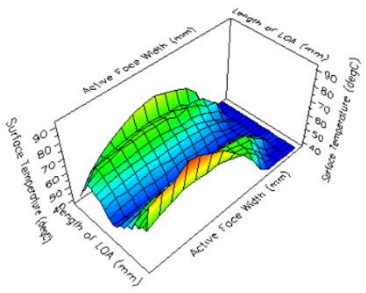

(a)

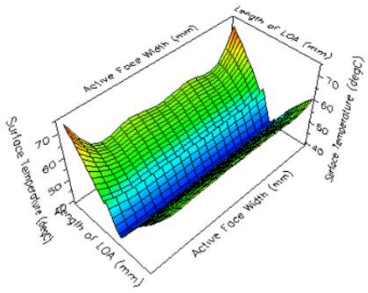

(b)

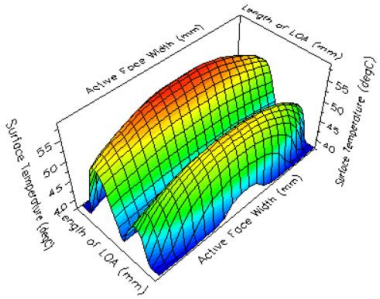

(c)

Fig. 4.12 Comparison of TD between the crank-cam gear pair (a) TD plot of baseline helical, (b) TD plot of unmodified spur and (c) TD plot of microgeometry optimized spur

In Fig. 4.12 it is observed that the maximum temperature occurring on the surface of the tooth of the modified spur gear is far lesser than the ones on the non-modified spur gear or even the helical gear. This means that there is lesser sliding on the involutes of the gear teeth and the wear due to the sliding friction. Also, the thermal deformations of the teeth will also become less dominant and need for lubrication will also decrease.

The Fig. 4.13 (a), (b) and (c) shows the FEA root stress plot for crank gear of unmodified spur, baseline helical and modified spur crank-cam gear pair. It is evident from the plots that the unmodified plot had a better distribution of the root stress and a lower maximum value than the modified crank gear. But this was expected as the aim of microgeometry modification was to reduce the transmission error and not the stresses. It can be seen that the maximum stress on the root of the helical gear and the modified spur gear is almost identical in the value but the stresses are much more distributed along the face width on the modified spur gear, which is a good result.

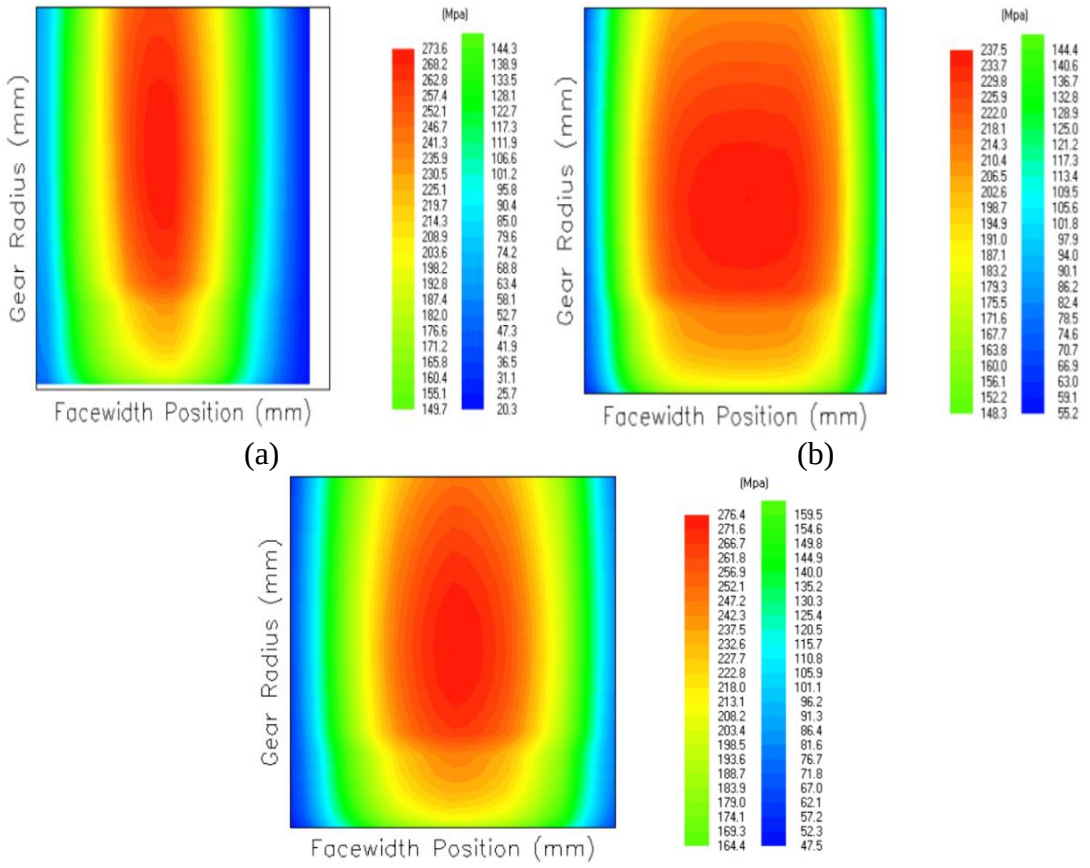

Fig. 4.13 Comparison of maximum root stress (von-mises) of crank gear between the crank-cam gear pair (a) Root stress plot of baseline helical, (b) Root stress plot of unmodified spur and (c) Root stress plot of microgeometry optimized spur

The Fig. 4.14 (a), (b) and (c) shows the FEA root stress plot for cam gear of unmodified spur, baseline helical and modified spur crank-cam gear pair. From the plots it can be seen that the helical gear has less value of maximum root stress than any of the others, the unmodified gear had the maximum root stress concentrated on the tips of the face width which could have weakened the corners and ultimately lead to chipping off. Therefore, using the lead crowning the stresses were made to be much more distributed in the centre of the gear tooth, where it is much stronger. Although the maximum stresses in the modified cam gear are higher than in its helical counterpart, the total stresses are well below the threshold limit of the material of the gears.

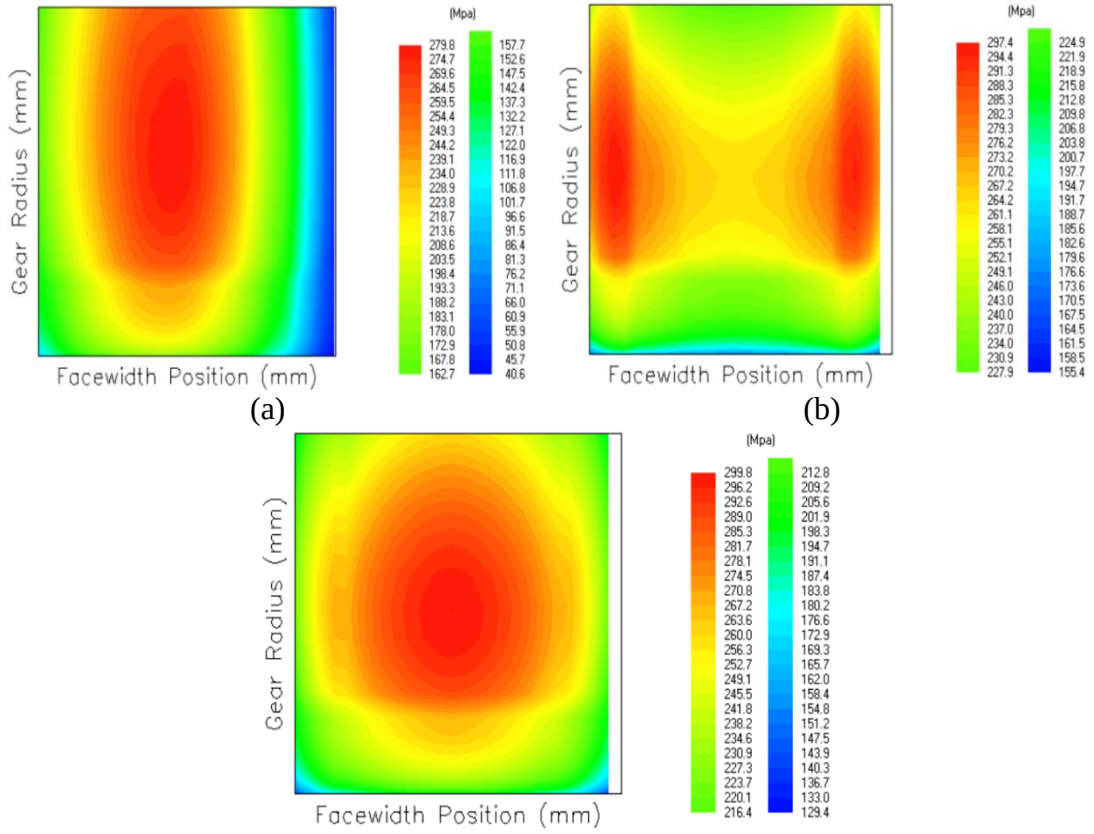

Fig. 4.14 Comparison of maximum root stress (von-mises) of cam gear between the crank-cam gear pair (a) Root stress plot of baseline helical, (b) Root stress plot of unmodified spur and (c) Root stress plot of microgeometry optimized spur

As a conclusion to the result of the microgeometry modification in the spur gear, the Fig. 4.15 portrays percentage change in maximum value of attributes by microgeometry optimization in crank-cam pair for modified gear pair vs helical gear pair and non-modified gear pair. The negative y-axis means the percent reduction and vice-versa.

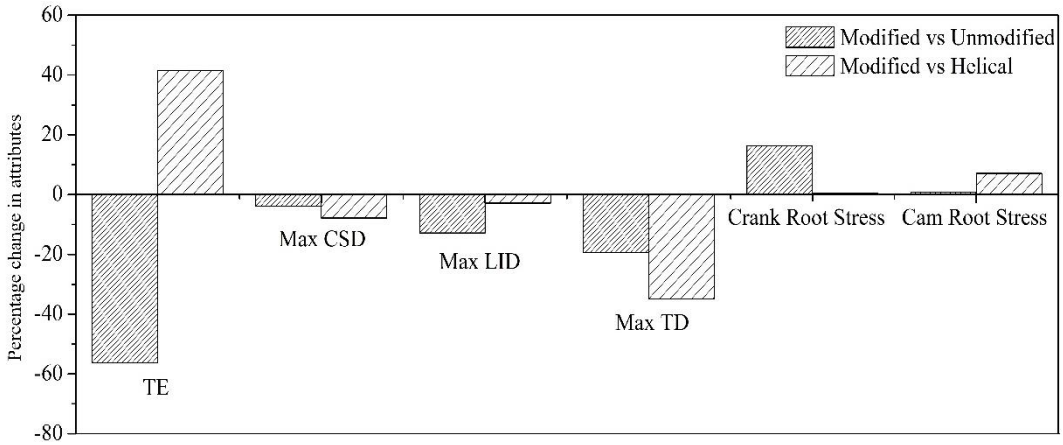

Fig. 4.15 Percentage change in maximum value of analyzed attributes by microgeometry optimization in crank-cam pair

4.5.2 Cam-AC Pair

The Fig. 4.16 (a), (b) and (c) shows the transmission error plot of unmodified spur, baseline helical and modified spur cam-ac gear pair. The helical gear train here also has the smoothest meshing. But the peak-to-peak TE of the modified spur has the lowest value of them all which means that it would be far quieter than the helical as well.

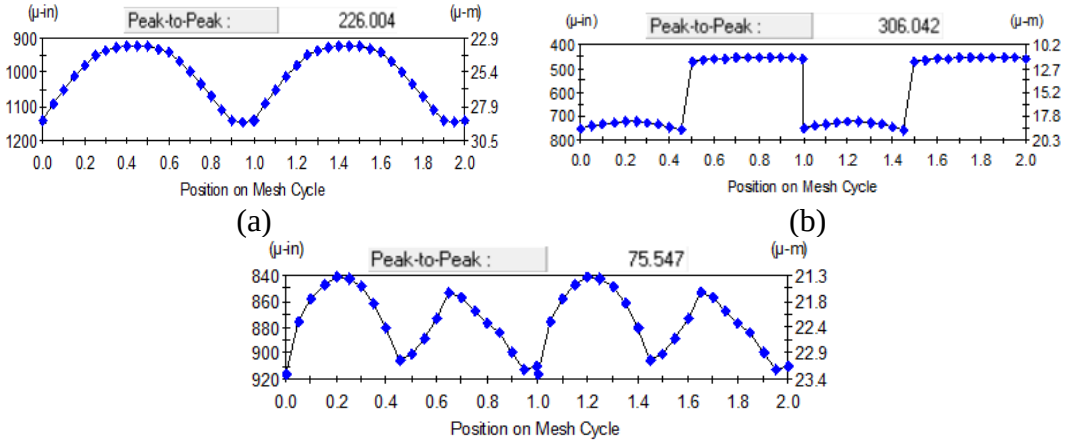

Fig. 4.16 Comparison of TE between the cam-ac gear pair (a) TE plot of baseline helical, (b) TE plot of unmodified spur and (c) TE plot of microgeometry optimized spur

The Fig. 4.17 (a), (b) and (c) shows the CSD plot of unmodified spur, baseline helical and modified spur cam-ac gear pair. The modification shows that the maximum value of the CSD has decreased considerably and the stresses are more evenly distributed over the tooth face rather than concentrating at one side of the face as in the unmodified gear.

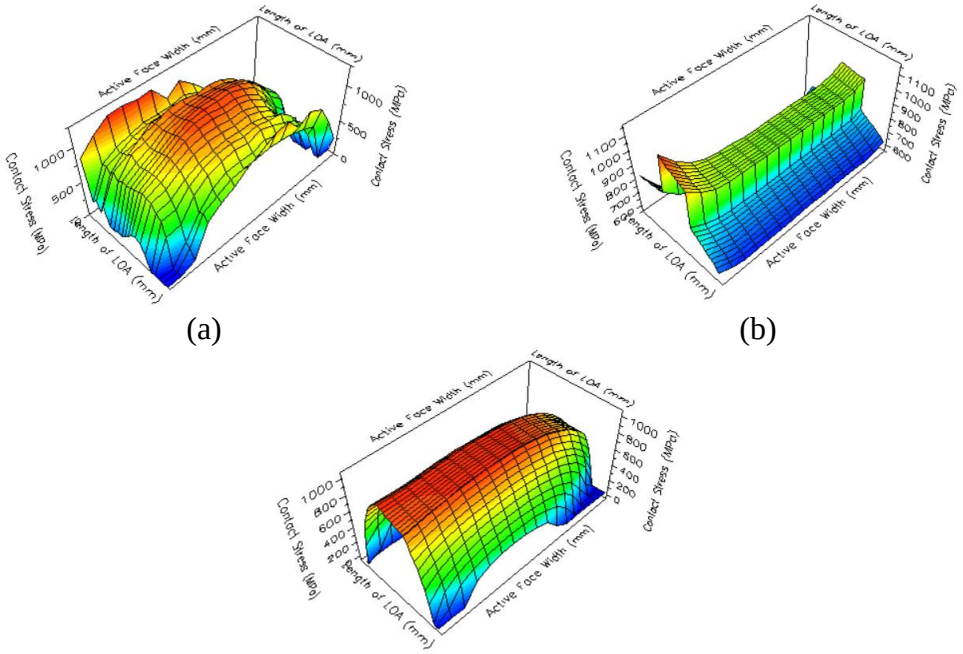

(a) (b)

(c)

Fig. 4.17 Comparison of CSD between the cam-ac gear pair (a) CSD plot of baseline helical, (b) CSD plot of unmodified spur and (c) CSD plot of microgeometry optimized spur

The Fig. 4.18 (a), (b) and (c) shows the LID plot of unmodified spur, baseline helical and modified spur cam-ac gear pair.

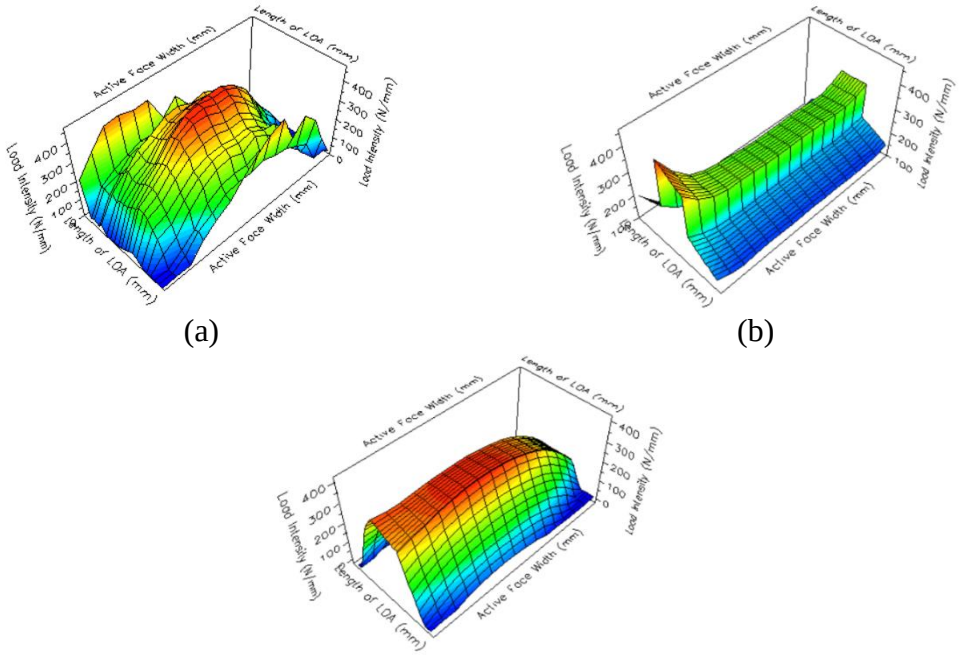

(a) (b)

(c)

Fig. 4.18 Comparison of LID between the cam-ac gear pair (a) LID plot of baseline helical, (b) LID plot of unmodified spur and (c) LID plot of microgeometry optimized spur

It is certain that in the unmodified gear pair all the load is acting on the corners of the face width which may lead to chipping. Therefore, the lead modification helped in bringing the LID into the centre of the face width and also reducing its maximum value by around a 100 N/mm which is an excellent improvement over the helical and unmodified spur gear pairs.

The Fig. 4.19 (a), (b) and (c) shows the TD plot of unmodified spur, baseline helical and modified spur cam-ac gear pair. The temperatures for the helical gear pair can be seen running quite high which is not the case with the unmodified spur and the modified spur. They run relatively cooler than the helical.

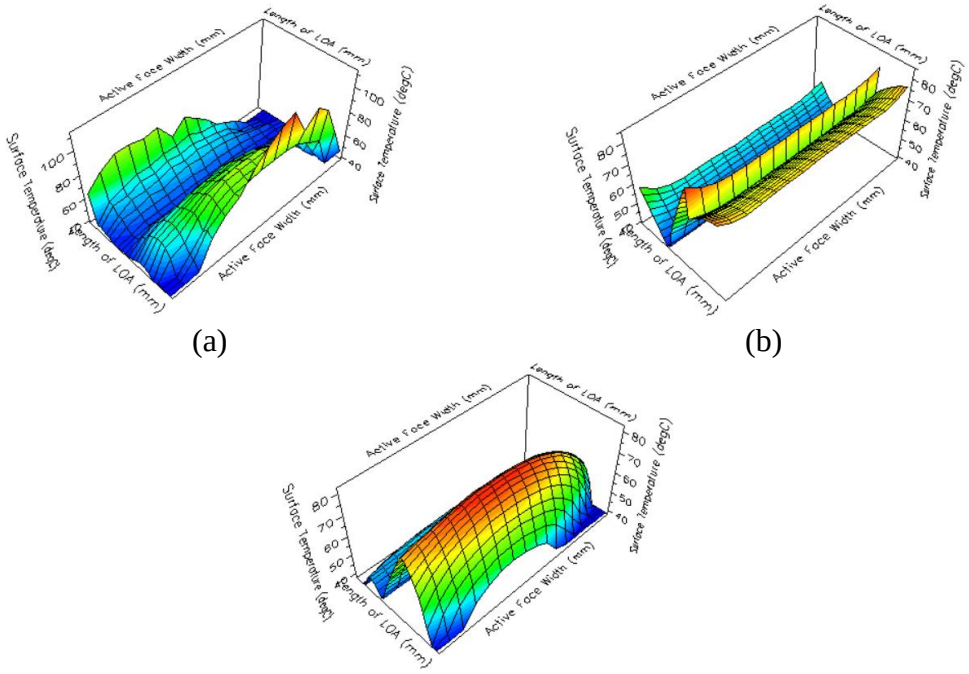

Fig. 4.19 Comparison of TD between the cam-ac gear pair (a) TD plot of baseline helical, (b) TD plot of unmodified spur and (c) TD plot of microgeometry optimized spur

The unmodified spur gear has a sudden jump in the temperatures in at a point on the line of action whereas the modified gear has a smoother transition and the temperatures are also distributed across the face width and the length of LOA.

The Fig. 4.20 (a), (b) and (c) shows the FEA root stress plot for cam gear of unmodified spur, baseline helical and modified spur cam-ac gear pair. From the Fig. 4.20 it is evident that the unmodified gear has the least max root stress, but the root

stress is present at the corner of the face width which may cause the crack initiation at the tip. Therefore, the modified gear despite of having the increased maximum root stress, is a better option as he stresses have been shifted to the middle of the tooth face width.

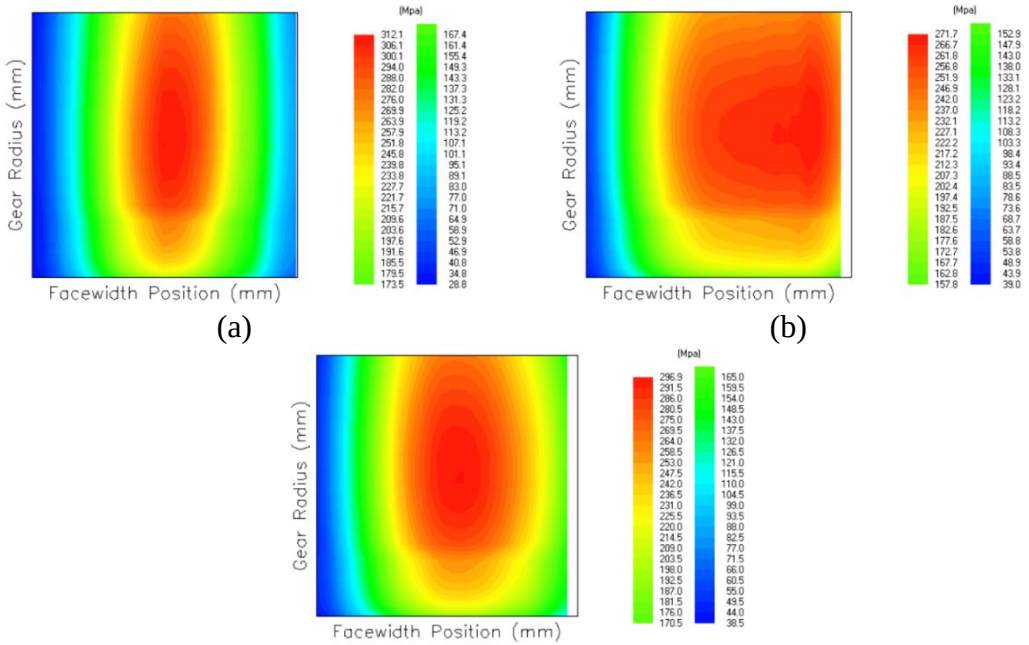

Fig. 4.20 Comparison of maximum root stress (von-mises) of cam gear between the cam-ac gear pair (a) Root stress plot of baseline helical, (b) Root stress plot of unmodified spur and (c) Root stress plot of microgeometry optimized spur

The Fig. 4.21 (a), (b) and (c) shows the FEA root stress plot for ac gear of unmodified spur, baseline helical and modified spur cam-ac gear pair. In the ac gear also, the microgeometry optimization shifts the location of the maximum stresses from the corners towards the centre of the face width and distributes it on a larger area rather than concentrating them. The Fig. 4.22 shows the change in the attributes when the microgeometries of the spur gear are modified.

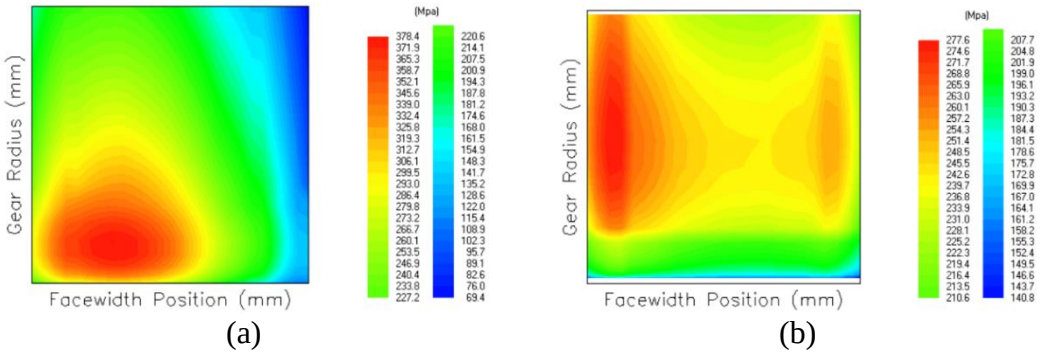

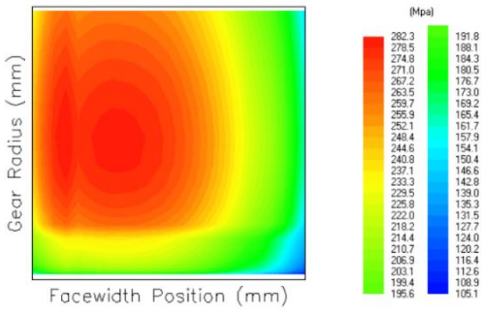

(c)

Fig. 4.21 Comparison of maximum root stress (von-mises) of ac gear between the cam-ac gear pair (a) Root stress plot of baseline helical, (b) Root stress plot of unmodified spur and (c) Root stress plot of microgeometry optimized spur

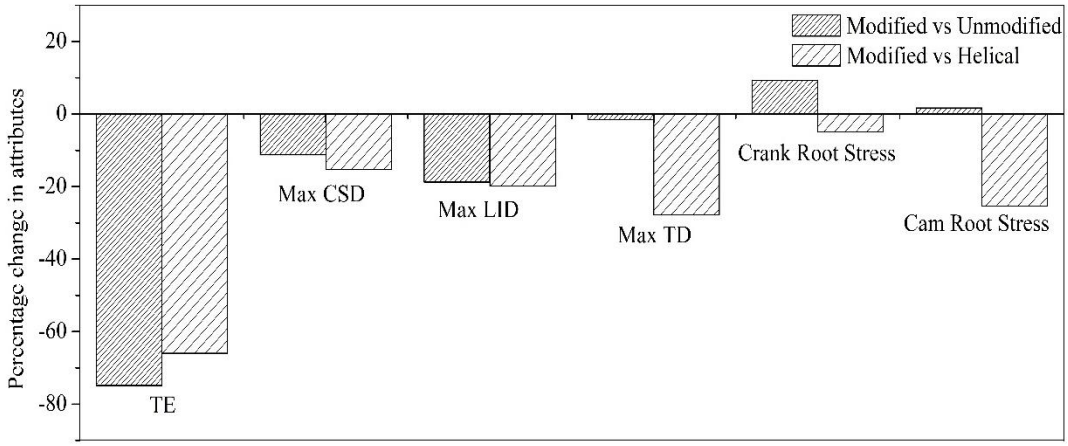

Fig. 4.22 Percentage change in maximum value of analyzed attributes by microgeometry optimization in cam-ac pair

4.5.3 Cam-FP Pair

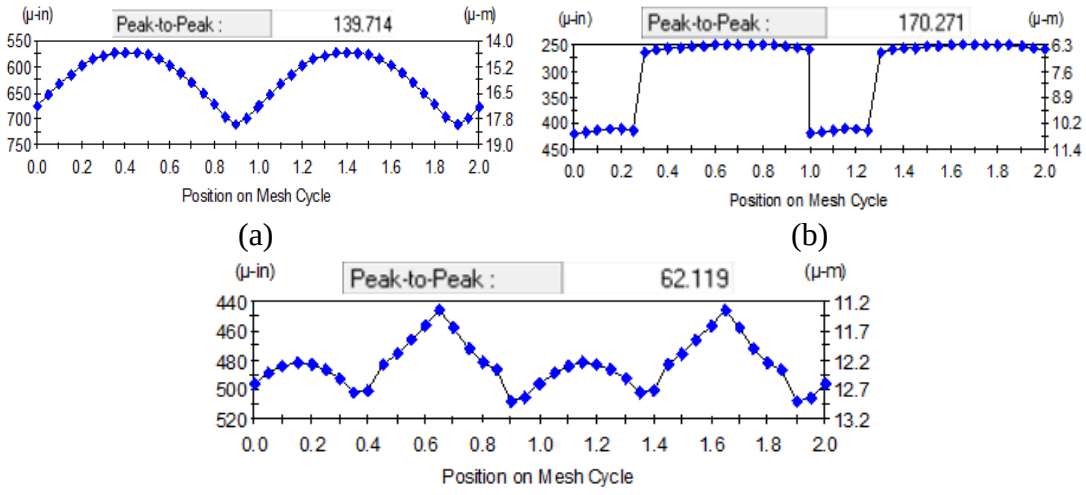

Fig. 4.23 Comparison of TE between the cam-fp gear pair (a) TE plot of baseline helical, (b) TE plot of unmodified spur and (c) TE plot of microgeometry optimized spur

The Fig. 4.23 (a), (b) and (c) shows the transmission error plot of unmodified spur, baseline helical and modified spur cam-fp gear pair. Here also the results are the same as the cam-ac pair and the peak-to-peak TE is far lesser than the helical and the unmodified which means that the noise will be less.

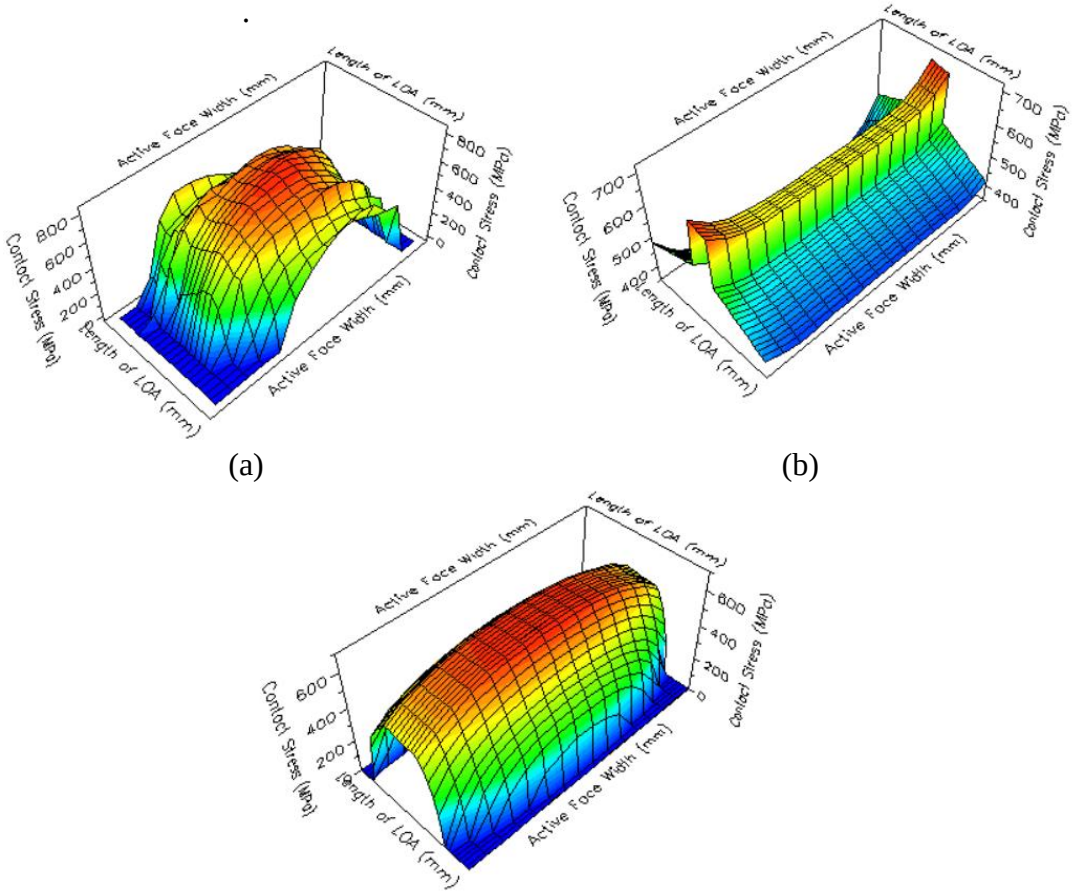

(a) (b)

(c)

Fig. 4.24 Comparison of CSD between the cam-fp gear pair (a) CSD plot of baseline helical, (b) CSD plot of unmodified spur and (c) CSD plot of microgeometry optimized spur

The Fig. 4.24 (a), (b) and (c) shows the CSD plot of unmodified spur, baseline helical and modified spur cam-fp gear pair. Here also the same pattern is followed as was in the cam-ac pair by distributing the load in the middle of the face width after modification.

The Fig. 4.25 (a), (b) and (c) shows the LID plot of unmodified spur, baseline helical and modified spur cam-ac gear pair. The LID is shifted from the corners to the middle of the gear tooth after the modification and the maximum value is also far less than the helical counterpart.

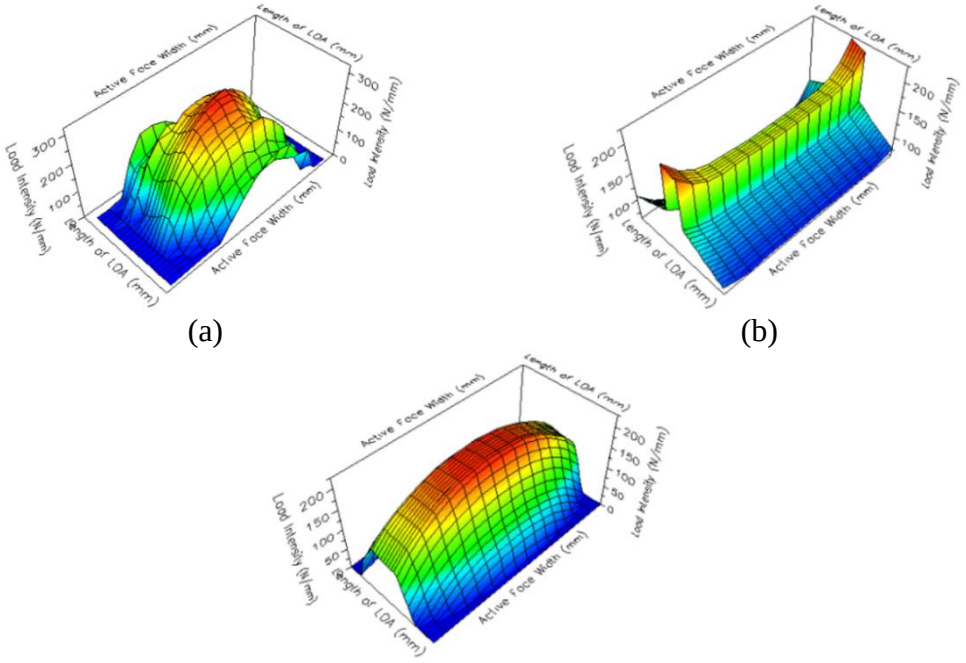

(a) (b)

(c)

Fig. 4.25 Comparison of LID between the cam-fp gear pair (a) LID plot of baseline helical, (b) LID plot of unmodified spur and (c) LID plot of microgeometry optimized spur

The Fig. 4.26 (a), (b) and (c) shows the TD plot of unmodified spur, baseline helical and modified spur cam-ac gear pair.

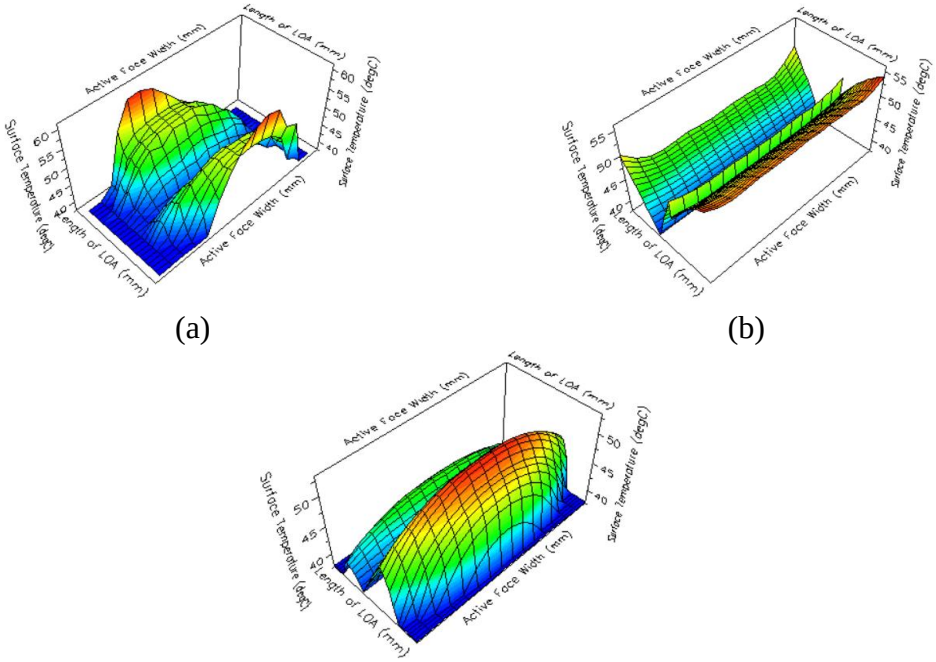

(a) (b)

(c)

Fig. 4.26 Comparison of TD between the cam-fp gear pair (a) TD plot of baseline helical, (b) TD plot of unmodified spur and (c) TD plot of microgeometry optimized spur

The temperatures in this gear pair does not run hot as the torque experienced by this pair is quite low.

The Fig. 4.27 (a), (b) and (c) shows the FEA root stress plot for cam gear of unmodified spur, baseline helical and modified spur cam-ac gear pair. From the Fig. 52 it is evident that the unmodified gear has the least max root stress and the more perfect distribution of the stresses.

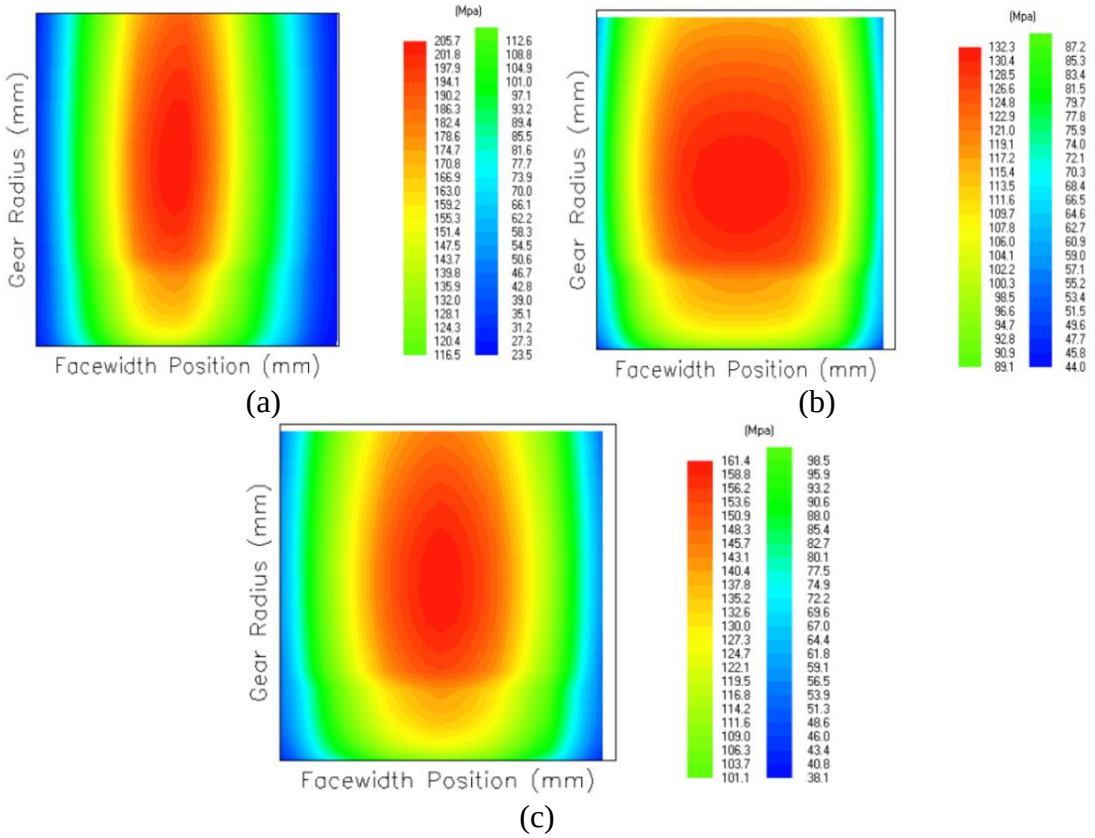

Fig. 4.27 Comparison of maximum root stress (von-mises) of cam gear between the cam-fp gear pair (a) Root stress plot of baseline helical, (b) Root stress plot of unmodified spur and (c) Root stress plot of microgeometry optimized spur

The helical gear has the maximum amount of the root stress concentrated at the centre and the modified spur gear also has a central distribution of the stresses but with a lesser maximum value than the helical.

The Fig. 4.28 (a), (b) and (c) shows the FEA root stress plot for fp gear of unmodified spur, baseline helical and modified spur cam-fp gear pair. Th concentration of the maximum stresses has been shifted to the middle of the gear with an increase in the maximum value of the root stress in the fp gear.

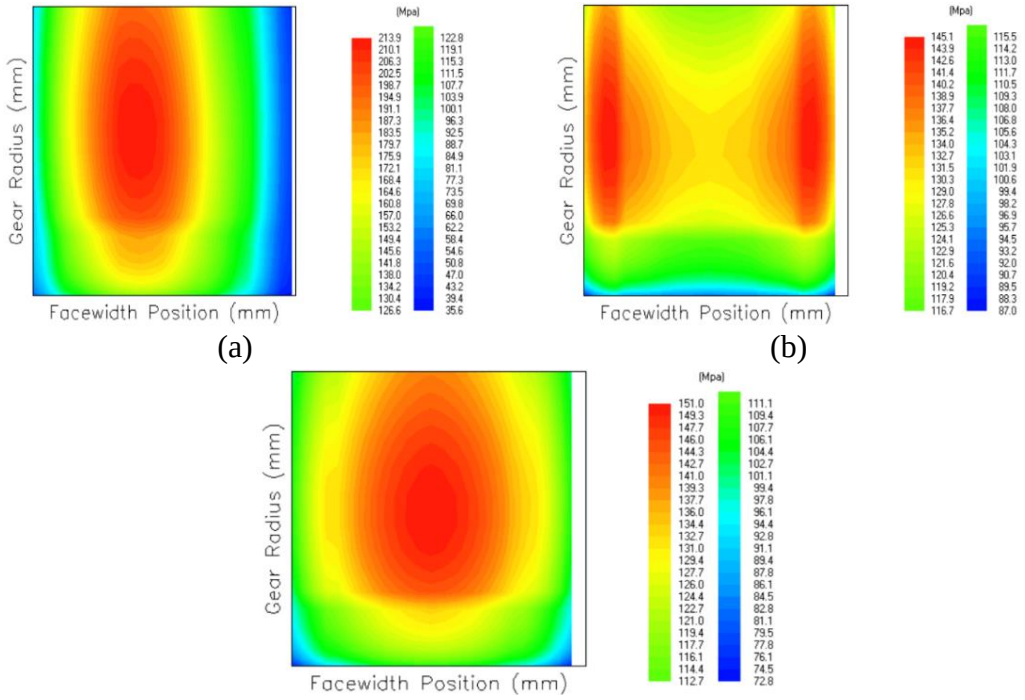

Fig. 4.28 Comparison of maximum root stress (von-mises) of fp gear between the cam-ac gear pair (a) Root stress plot of baseline helical, (b) Root stress plot of unmodified spur and (c) Root stress plot of microgeometry optimized spur

The Fig. 4.29 shows the change in the attributes in the cam-fp pair when the microgeometries of the spur gear are modified.

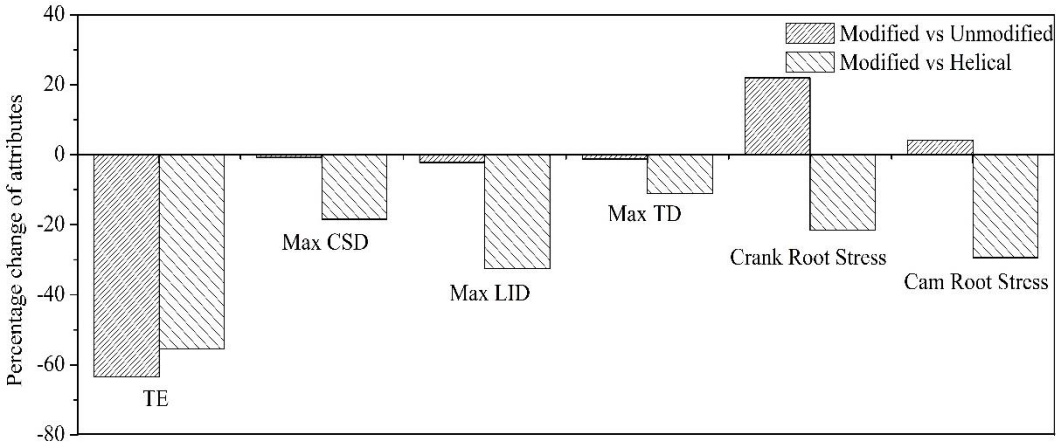

Fig. 4.29 Percentage change in maximum value of analyzed attributes by microgeometry optimization in cam-fp pair

4.6 Gear Web Fatigue Analysis

The aim of this analysis was to check the web and the pocket design on the cam and FP gears for the fatigue loading. To pass the fatigue loading test, the maximum stress any

point on the web of the gears should be less than the yield strength of the gear material and the fatigue margin should be greater than 1.

The Figs. (4.30 & 4.31) shows the maximum Von-Mises stress that the webs of cam gear and the FP gear respectively experience. The stresses were found out to be well under the yield strength of the material which meant that there would be no chances of yielding in the normal operation of the gears.

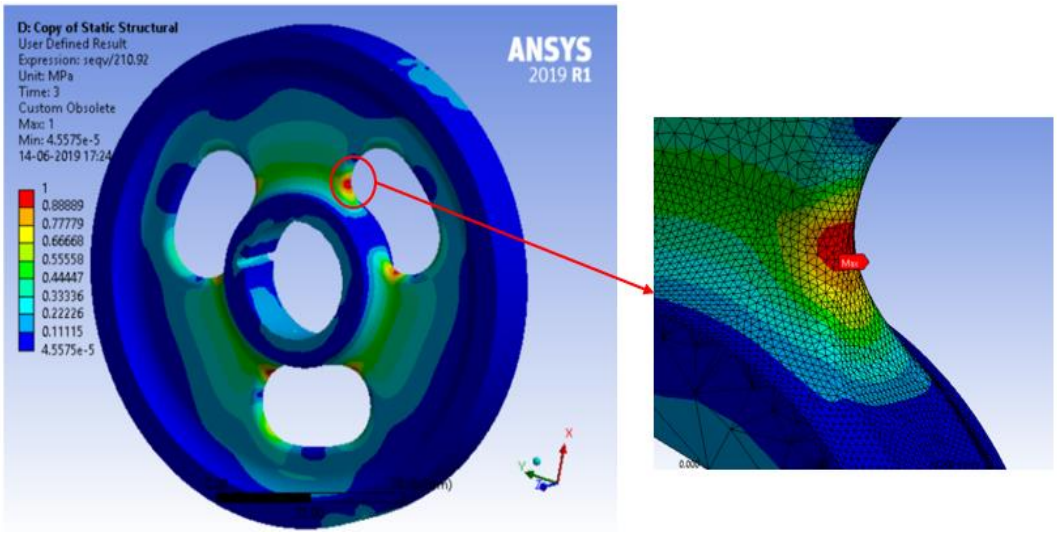

Fig. 4.30 Von-mises stresses (normalized) on the cam gear web due to loading on the teeth

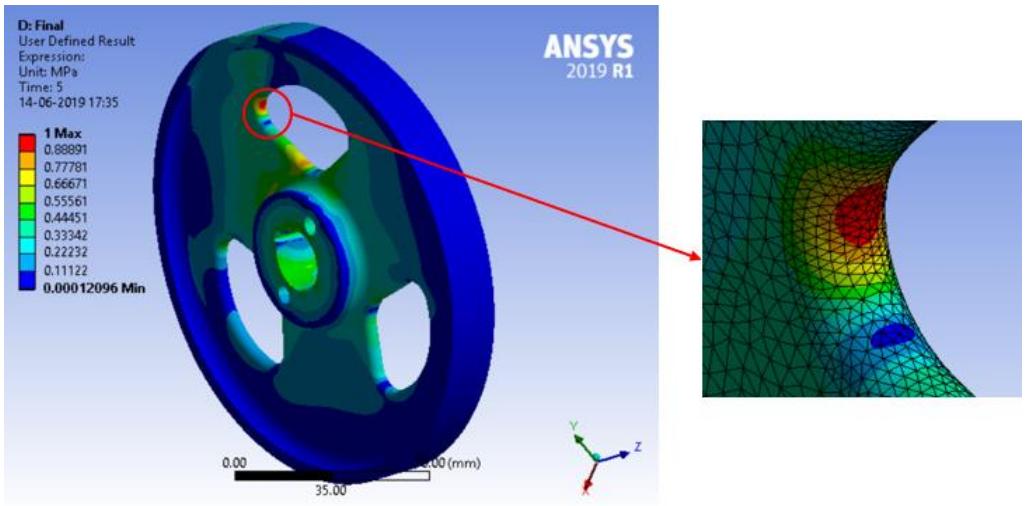

Fig. 4.31 Von-mises stresses (normalized) on the fp gear web due to loading on the teeth

The Fig. 4.32 (a) & (b) shows the EFR stress field on the gear web during the forward loading of the gears, Fig. 4.32 (c) & (d) shows the Goodman stress field on the gear web during the reverse loading of the gears and Fig. 4.32 (e) & (f) shows the EFR

stress field on the gear web during the forward and reverse loading of the gears. The calculation of the fatigue margin according to the obtained EFR stresses was carried out and the design had the margin well above the value 1.

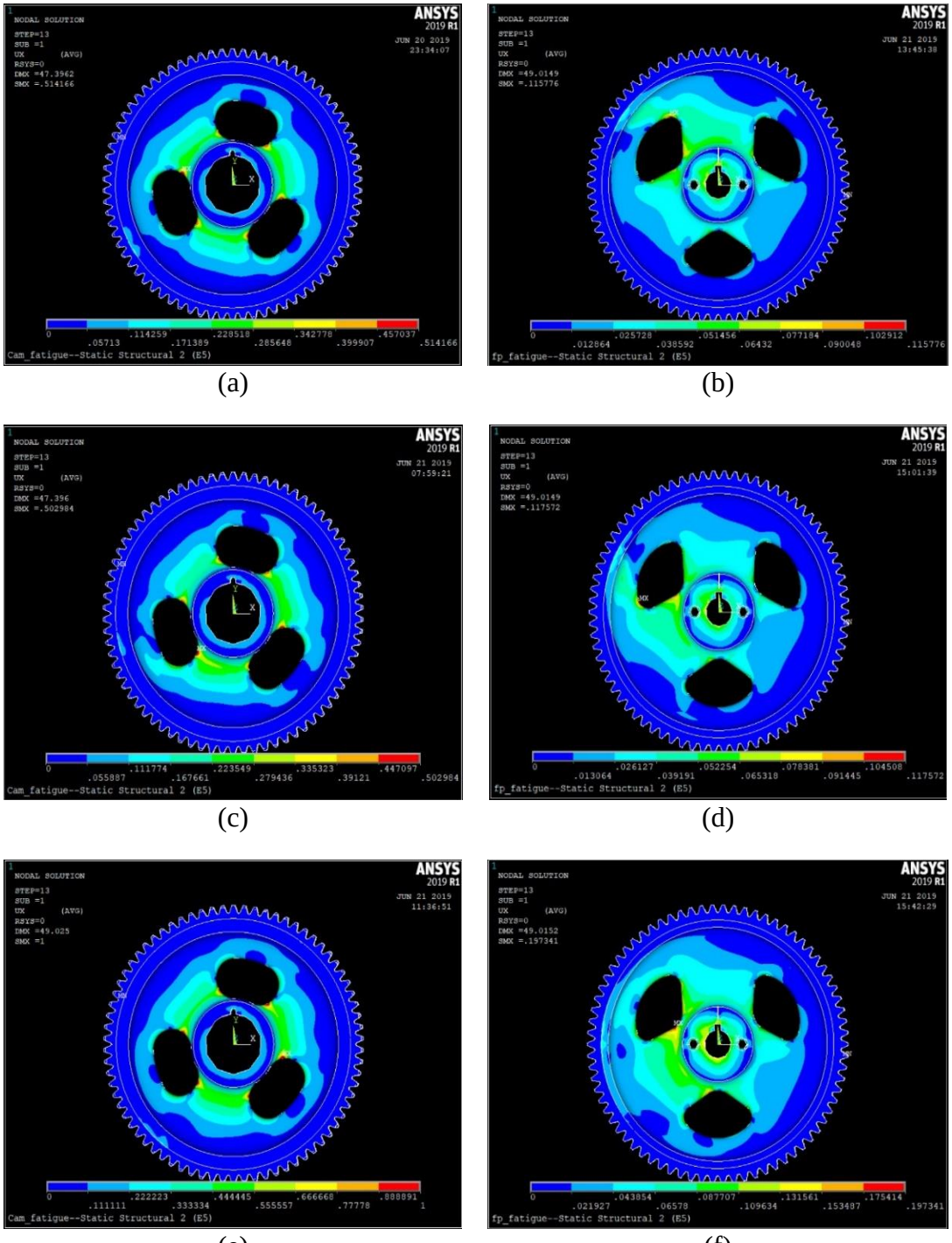

Fig. 4.32 EFR stress field (normalized) during (a) Forward loading of cam gear, (b) Forward loading of fp gear, (c) Reverse loading of cam gear, (d) Reverse loading of fp gear, (e) Forward-reverse loading of cam gear and (f) Forward-reverse loading of fp gear

4.7 Determination of Torque to Slip Capacity of the Gear and the Shaft Joints

The torque to slip capacity analysis was done to calculate the maximum amount of the torque a gear and shaft joint could sustain. The gears were fit onto the shaft using two methods for different gears. The analysis for the torque to slip capacity for both the methods have been discussed in this section. This analysis was only carried out for the crank, cam, ac and fp gears and not for the lpi and lpg gears as the lpi and lpg gears experience very low torque.

4.7.1 Press Fitted Joints in Crank and Cam Gears

The crank and the cam gears were analysed in this section as these were the only two gears having the press fitted joints. The torque capacity was analysed using the standard formulae for press fit mentioned in Section 5.10. and were further analysed using FEA in ANSYS software. All the torque capacity graphs are normalized by taking the maximum torque of the crank gear as the reference.

The Fig. 4.33 shows the normalized graph for the torques obtained from the simulation for crank gear which shows that the torque decreases instantly and goes to zero, which means the gear has slipped off the shaft and is rotating freely after the torque capacity has reached. Also, the torque that has been obtained for FEA is the same that was obtained from the formula which means that shaft on shaft interference fit formulae suits for the calculation of the torque capacity if the gear is a solid piece without any webs or holes to reduce inertia.

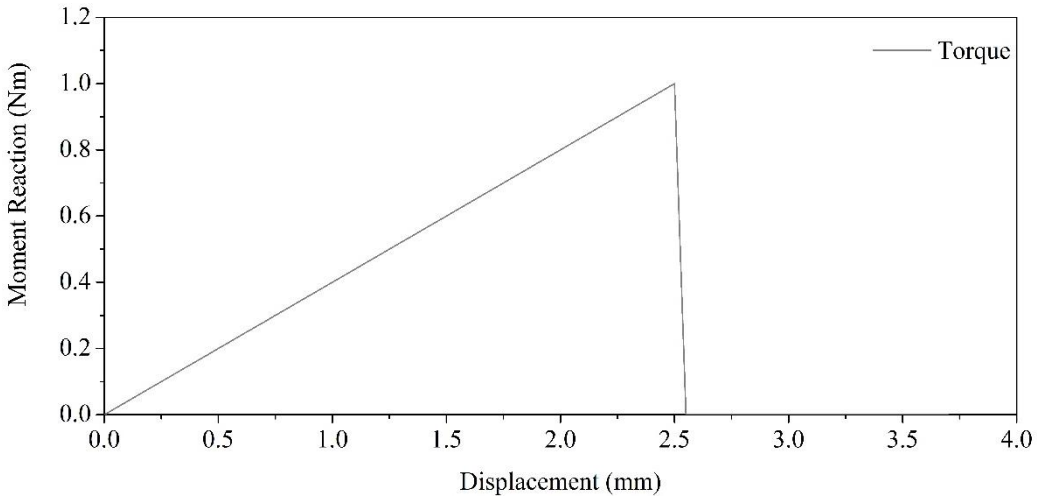

Fig. 4.33 Torque carrying capacity (normalized) for crank gear press fit joint

The Fig. 4.34 shows the normalized graph of for the torques obtained from the simulation showing the torque capacity for the cam gear. It is evident that the torques in the cam gear rise in a linear fashion up till the point where the gear experiences a slip from the shaft and then the torque becomes constant. This means that the gear still stays on the shaft and the continues to rotate while slipping. For the cam gear, the torque capacity calculated with the standard formulae is not valid as the gear has web cut into it. Therefore, the torque capacity can only be calculated through FEA in this case.

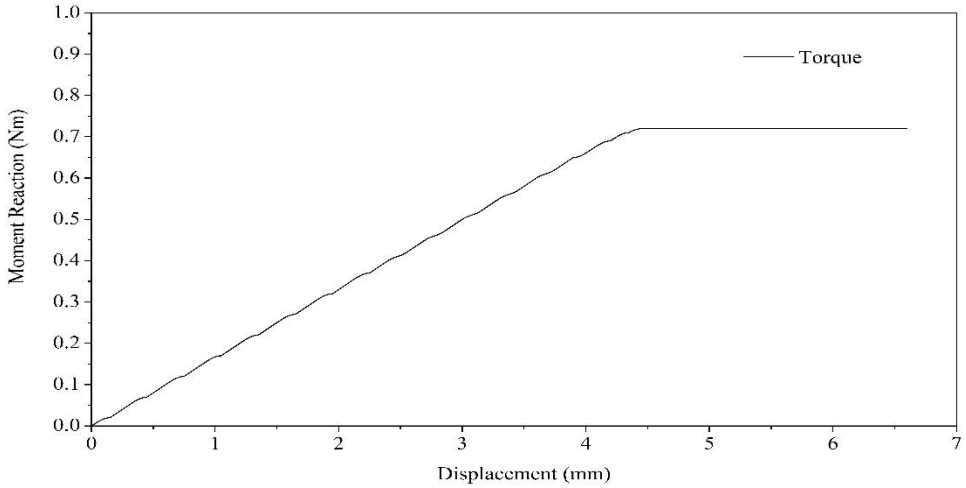

Fig. 4.34 Torque carrying capacity (normalized) for cam gear press fit joint

These gears are also provided with keys as a failsafe and to locate the proper position of the gears if at any time the replacement is to be made.

4.7.2 Taper Fit Joints in AC and FP Gears

The AC and the FP gears are using taper fit to instead of the press fit as while performing the press fit, the force of the press could damage the vital components of the small parts inside the fuel pump and the compressor. The torque capacities were calculated for the AC and the FP joints using the Cummins proprietary MATLAB tool and then verified using FEA in ANSYS.

The Fig. 4.35 shows the normalized torque capacity curve, obtained using FEA, for the AC taper joint. The curve begins to slope down gradually after a peak point is reached. This peak point is taken as the torque capacity of the ac gear as this is when the gear hub begins to slip on the shaft of the compressor. Also, the torque capacity value from the MATLAB tool confirms with the torque capacity from FEA simulation.

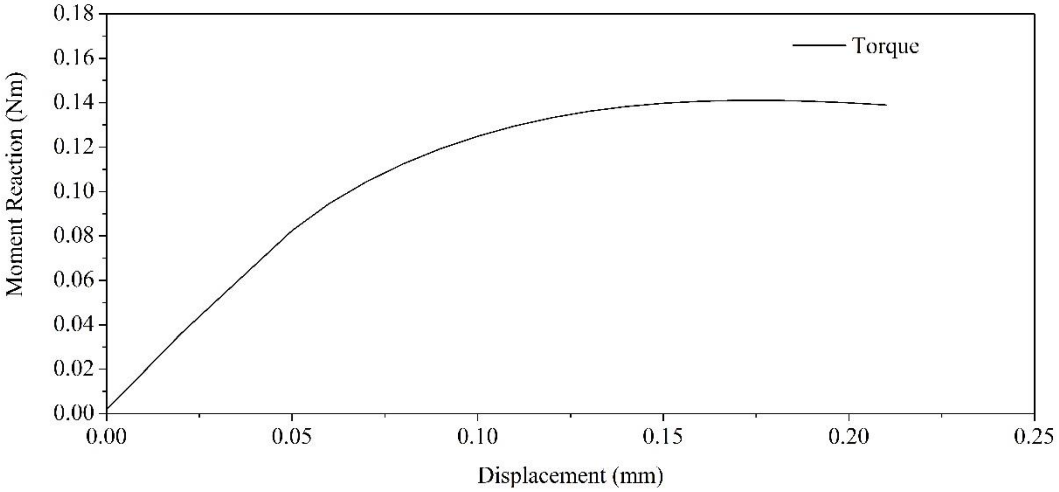

Fig. 4.35 Torque carrying capacity (normalized) for ac gear taper fit joint

The Fig. 4.36 shows the normalized torque capacity curve, obtained using FEA, for the FP taper joint. The curve becomes constant after a particular displacement where the hub slips off the shaft of the fuel pump. This also confirms the torque capacity obtained from MATLAB.

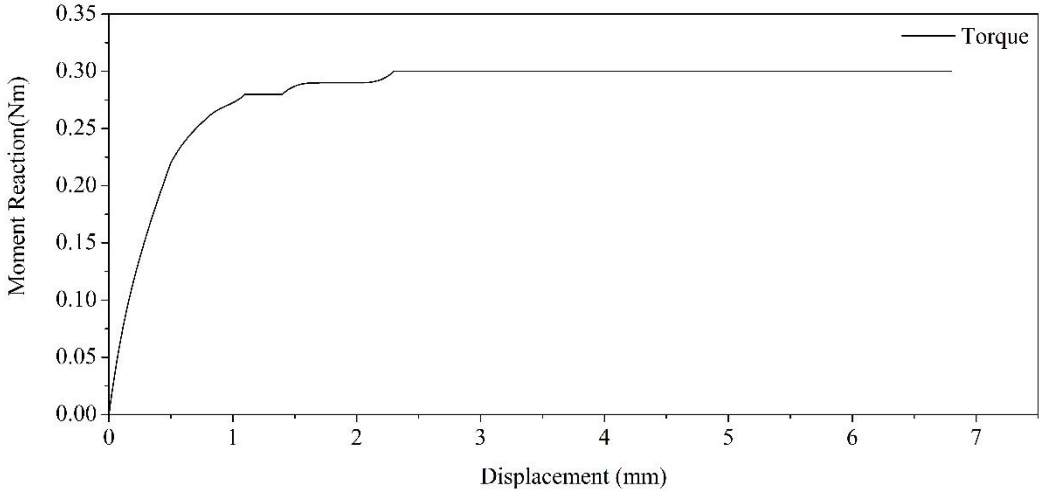

Fig. 4.36 Torque carrying capacity (normalized) for fp gear taper fit joint

The analysis for the taper joint for both the above gears showed lesser value of the design margins, therefore the pre-torque of the nuts was recommended to be increased. The other ways that the torque capacity of the gears could be increased were by increasing the taper length or the taper angle or by changing the size of the nuts.

5.1 Conclusions

This dissertation aimed at the design of the spur gear train in place of the existing helical gear train to address the failure of cam gear walk-off in the timing system of the diesel engine. The result summary in this dissertation is discussed as per the author's point of view. Some conclusions that can be drawn from the study are

- The macro geometry of the new gears was designed in the space that was available in the gear cover. The discrepancies in the centre distance between the gears were addressed by modifying the addendum of the gears using the international standards, which proved to be fruitful modification as it helped in reducing the backlash and the transmission error in the macro geometry itself
- The dynamic analysis, using the GT-Suite software, was carried out and the lash and no-lash dynamic response was ascertained. This helped in predicting the amount of forces the gear tooth of each gear experienced during the continuous meshing which in turn helped the further design process of the gears. The dynamic analysis also helped in visualising the amount of backlash which the gears were experiencing in the real time. Dynamic analysis proved that there will be no thrust forces produced by the spur gear train which means that there will be no failure of cam gear walk-off
- The comparison of the root stress in LDP and ANSYS shows that the FEA most of the time overestimates the stresses and the root stresses analysed we found to be below the yield strength of the material
- The microgeometries were calculated and optimised using the Windows LDP tool for the optimization of the gear noise while keeping contact stresses, load distribution and the surface temperature distribution under the limits. For the noise reduction, the PPTE was reduced and the transmission error was transformed to a smooth graph using sufficient profile modifications on the gear teeth and the stress distributions were controlled using the lead modifications
- The webs were designed on the larger gears to reduce the inertia of the gears. The webs were designed by continuously evaluating the gears by FEA and after

final creation the Von-Mises stresses were calculated on the web which were found to be well below the yield strength of the material. Further the EFR stresses were calculated on the gears for the cyclic loading which were also found under the limit

- Lastly, the gear joints with the shaft were checked for their torque to slip capacity using FEA. The results of this analysis showed that the torque to slip capacity for every gear is well above the dynamic torques experienced by the gears during their normal operation

The results prove that the gear train is well designed to fit the constraints of the gear cover and is also is manufacturable with the gear hobbing process. The results also show that the gear transmission error has been reduced which implies that the gears will produce less noise almost comparable to the helical gears while not producing any amount of axial thrust. Also, the stresses like contact stresses, root stresses and EFR stresses on the gears are well under the threshold limit of the material which means that the gear will not go under extreme wear and tear, hence, increasing their life.

5.2 Future Work

- A final experimental validation can be carried out to fortify the results of the research
- The microgeometry analysis here is done on windows LDP tool which is capable only to model a single gear pair at a time. Therefore, microgeometry analysis for the whole gear train can be run on software like SMT MASTA or KISSsoft which are capable to run the analysis of the whole gear train in a single go
- The misalignments due to the shaft deflections in the LDP tool were ignored. Therefore, the test can be carried out by including the shaft data and getting real-time results
- A MATLAB tool can be made employing design of experiments (DOE) and machine learning to quickly determine the best possible microgeometries of the gear teeth instead of calculating the tip relief by hand and applying trial and error method for the profile and lead crown modification

REFERENCES

Andrews, J. D., 1991. A Finite Element Analysis of Bending Stresses Induced in External and Internal Involute Spur Gears. *The Journal of Strain Analysis for Engineering Design*, 26(3), pp. 153−163.

Bennett, S., 2010. *Modern Diesel Technology: Diesel Engines.* New York: Cengage Learning.

Bhandari, V. B., 2010. *Design of Machine Elements.* 3rd ed. New Delhi: Tata Mc-Graw Hill.

Bibel, G. D., Reddy, S. K., Savage, M. & Handschuh, R. F., 1994. Effects of Rim Thickness on Spur Bending Stress. *Journal of Mechanical Design*, 116(4), pp. 1157−1162.

Budynas, R. G. & Nisbett, J. K., 2011. *Shigley's Mechanical Engineering Design.* 9th ed. New York: McGraw-Hill.

Chong, T., Bae, I. & Kubo, A., 2001. Multiobjective Optimal Design of Cylindrical Gear Pairs for the Reduction of Gear Size and Meshing Vibration. *JSME International Journal Series C*, 44(1), pp. 291−298.

Coy, J. J. & Zaretsky, V. E., 1975. *Life Analysis of Helical Gear Sets Using Lundberg-Palmgren Theory,* Washington, United States: NASA Technical Notes.

Croker, M. D., Amphlett, S. A. & Barnard, A. I., 1995. Heavy Duty Diesel Engine Gear Train Modelling to Reduce Radiated Noise (No. 951315). *SAE Technical Paper Series*, pp. 663−667.

Farhani, A. D., 1994. Evaluation Methodology of Gear Systems by Dynamic Real Time Non-linear F.E.M. Analysis. *SAE Transactions,* Volume 103, pp. 169−177.

Fastenal, 2005. *Technical Reference Guide.* [Online] Available at: https://www.fastenal.com/content/documents/FastenalTechnicalReferenceGuide.pdf [Accessed 11 May 2019].

Foltz, A., Wasfy, T., Ostergaard, E. & Piraner, I., 2016. Multibody Dynamics Model of a Diesel Engine and Timing Gear Train With Experimental Validation. *ASME 2016 International Mechanical Engineering Congress and Exposition*, Volume 4B; Dynamics, Vibration and Control, pp. V04BT05A003 − V04BT05A003.

Gopinath, K. & Mayuram, M. M., 2010. *Module-2 Gears, Lecture-7 Spur Gear Design.* [Online] Available at: https://nptel.ac.in/courses/112106137/pdf/2_7.pdf [Accessed 9 April 2019].

GT-Suite, 2018. *ContactGear - Gear-to-Gear Contact,* Software: GT-Suite.

Gunay, D., Ozer, H. & Alpay, A., 1996. The Effect of Addendum Modification Coefficient. *Mathematical and Computational Applications,* 1(1), pp. 36−43.

Guo, J., Zhang, W. & Zhang, X., 2015. Modeling and Analysis of the Transient Vibration of Camshaft in Multi-Cylinder Diesel Engine. *Advances in Mechanical Engineering,* 7(11), pp. 1−14.

Harianto, J. & Houser, D. R., 2007. A Methodology for Obtaining Optimum Gear Tooth Microtopographies for Noise and Stress Minimization Over a Broad Operating Torque Range. *ASME 2007 International Design Engineering Technical Conferences and Computers and Information in Engineering Conference,* Volume Volume 7: 10th International Power Transmission and Gearing Conference, pp. 289−303.

Hariss, S. L., 1958. Dynamic Loads on the Teeth of Spur Gears. *Proceedings of the Institution of Mechanical Engineers,* 172(1), pp. 87−112.

Hassan, A. R., 2009. Contact Stress Analysis of Spur Gear Teeth Pair. *World Academy of Science, Engineering and Technology,* 58(1), pp. 597−602.

Houser, D. R., 2006. *Gear Mesh Misalignment.* [Online] Available at: http://gear solutions.com/features/gear-mesh-misalignment/ [Accessed 16 March 2019].

Houser, D. R., Oswald, F. B., Valco, M. J. & Drago, R. J., 1994. *Comparison of Transmission Error Predictions with Noise Measurements for Several Spur and Helical Gears.* Indianapolis, 30th AIAA/ASME/SAE/ASEE Joint Propulsion Conference.

Hu, Z. & Mao, K., 2017. An Investigation of Misalignment Effects on the Performance of Acetal Gears. *Tribology International,* Volume 116, pp. 394−402.

International Organization for Standardization, 1982. *ISO/ TR 4467 − 1982 (E) Addendum modification of the teeth of the cylinderical gears for speed-reducing and speed-increasing gear pairs.* Geneva.

International Organization for Standardization, 2007. *ISO 21771:2007(E) Gears — Cylindrical involute gears and gear pairs — Concepts and geometry.* Geneva

Joshi, Y. & Kelleher, J., 2014. Gear Train Mesh Efficiency Study: The Effects of an Anti-Backlash Gear. *SAE International Journal of Commercial Vehicles,* 7(1), pp. 271−277.

KHK Stock Gears, 2015. *Gear Nomenclature.* [Online] Available at: https://khkgears .net/new/gear_knowledge/gear-nomenclature.html [Accessed 25 April 2019].

KHK Stock Gears, 2015. *Gear Types and Characteristics.* [Online] Available at: https://khkgears.net/new/gear_knowledge/abcs_of_gears-b/gear_types_and_character istics.html [Accessed 15 April 2019].

Kissling, U., 2010. *Effects of Profile Corrections on Peak-to-Peak Transmission Error.* [Online] Available at: http://kadkraft.com/wp-content/uploads/2015/06/Rcvd-2012-

01-01-E-Ulrich_Kissling-Effects_of_proifle_corrections_on_peak_to_peak_transmission_error.pdf [Accessed 6 Feburary 2018].

Kissling, U., 2015. *Layout of the Gear Micro Geometry.* [Online] Available at: http://gearsolutions.com/features/layout-of-the-gear-micro-geometry/ [Accessed 21 March 2019].

Kuhr, R. R., 2009. *Noise Reduction in Plastic Gears.* [Online] Available at: http://gearsolutions.com/features/noise-reduction-in-plastic-gears/ [Accessed 6 February 2019].

Litvin, F. L., Zhang, J., Chaing, W. S., Coy, J. J. & Handschuh, R. F., 1987. Crowned Spur Gears: Optimal Geometry and Generation. *Gear Technology,* 5(5), pp. 9−15.

Madhusudan, G. & Vijayasimha, C., 1987. Approach to spur gear design. *Computer-Aided Design*, 19(10), pp. 555−559.

Maiti, R. & Roy, A. K., 1996. Minimum Tooth Difference in Internal-External Involiute Gear Pair. *Mechanism and Machine Theory,* 31(4), pp. 475−485.

Maitra, G. M., 2008. *Handbook of Gear Design.* 2nd ed. New Delhi: Tata Mc-Graw Hill.

Malviya, D. & Sharma, P. K., 2014. Transmission Error in Gear. *International Journal of Modern Engineering Research,* 4(1), pp. 35−37.

Marjanovic, N., Isailovic, B., Marjanovic, V., Milojevic, Z., Blagojevic, M. & Bojic, M., 2012. A Practical Approach to the Optimization of Gear Trains With Spur Gears. *Mechanism and Machine Theory,* Volume 53, pp. 1−16.

Marković, K. & Vrcan, Ž., 2016. Influence of Tip Relief Profile Modification on Involute Spur Gear Stress. *Transactions of Famena,* 40(2), pp. 59−70.

Mehta, G., Somani, M., Babu, T. & Watts, T., 2018. Contact Stress Analysis on Composite Spur Gear using Finite Element Method. *Materials Today: Proceedings*, 5(5), pp. 13585−13592.

Munro, R. G., 1990. A Review of the Theory and Measurement of Gear Transmission Error. *Gearbox Noise and Vibration*, pp. 3−10.

Munro, R. G., Yildrim, N. & L, H. D., 1990. Optimum Profile Relief and Transmission Error in Spur Gears. *Gearbox Noise and Vibration*, pp. 35−42.

Okamura, H. & Yamashita, K., 1997. *Influence of the Valve and Accessory Gear Train on the Crankshaft Three-Dimensional Vibrations in High Speed Engines.* USA, SAE Technical Paper No. 971967, pp.773−782.

Palmer, D. & Fisch, M., 2010. Evaluation of Methods for Calculating Effects of Tip Relief on Transmission Error, Noise and Stress in Loaded Spur Gears. *American Gear*

Manufacturers Association Fall Technical Meeting, October, Volume 2010, pp. 112−126.

Pedrero, J. I., Artes, M. & Garcia-Prada, J. C., 1996. Determination of Addendum Modification Faactors for Gears with Pre-Established Contact Ratio. *Mechanism and Machine Theory,* 31(7), pp. 937−945.

Prayoonrat, S. & Walton, D., 1988. Practical approach to optimum gear train design. *Computer-Aided Design,* 20(2), pp. 83−92.

Radzevich, S. P., 2012. *Dudley's Handbook of Practical Gear Design and Manufacture.* 2nd ed. Boca Raton: Taylor & Francis Group.

Ramamurti, V., Gautam, P. & Kothari, A., 1997. Computer-aided design of a two-stage gearbox. *Advances in Engineering Software,* 28(1), pp. 73−82.

Recurdyn, 2019. *Modification.* [Online] Available at: https://functionbay.com/documentation/onlinehelp/default.htm#!Documents/modification.htm[Accessed 8 March 2019].

Rivola, A. & Troncossi, M., 2014. Dynamic Analysis of a Motorbike Engine Timing System: Experimental and Numerical Investigation of the Geartrain. *Mechanical Systems and Signal Processing,* 48(1-2), pp. 325−338.

Sato, O., Shimojima, H. & Inano, S., 1985. Dynamic torsional analysis of Gear Train System. *Bulletin of JSME,* 28(242), pp. 1756−1760.

Shiau, T., Chang, J., Huang, K., Cheng, C. & Wang, C., 2011. Non-Linear Dynamic Analysis of a Multi-Gear Train With Time-Varying Mesh Stiffness Including Modification Coefficient Effect. *ASME 2011 Turbo Expo: Turbine Technical Conference and Exposition,* 6(Structures and Dynamics, Parts A and B), pp. 1115−1125.

Shim, S. B., Park, Y. J. & Kim, K. U., 2008. Reduction of PTO Rattle Noise of an Agricultural Tractor using and Anti-Backlash Gear. *Biosystems Engineering,* 100(3), pp. 346 − 354.

Tamminana, V., Kahraman, A. & Vijayakar, S., 2007. A Study of the Realtionship Between the Dynamic Factors and the Dynamic Transmission Error of Spur Gear Pairs. *Journal of Mechanical Design,* Volume 129, p. 75.

Tharmakulasingam, R., 2010. *Transmission Error in Spur Gears: Static and Dynamic Finite-Element Modeling and Design Optimization,* Brunel University: Doctoral Dissertation, Brunel University School of Engineering and Design PhD Thesis.

Warner, J., 2017. *A Look at Belt, Chain and Gear Drive Technology.* [Online] Available at: https://www.powertransmission.com/blog/a-look-at-belt-chain-and-gear-drive-technology/ [Accessed 15 April 2019].

Wikipedia, 2018. *Gear*. [Online] Available at: https://en.wikipedia.org/wiki/Gear [Accessed 15 November 2018].

Wilhelm, M., Laurin, S., Schmillen, K. & Spessert, B., 1990. Structure Vibration Excitation by Timing Geat Impacts. *SAE Transactions,* 99(1), pp. 1−13.

Wright, M., 2018. *Engine Ignition and Cam Timing for the Novice.* [Online] Available at: https://www.thoughtco.com/engine-ignition-and-cam-timing-281468 [Accessed 04 October 2018].

Yang, D. & Sun, Z., 1985. A Rotary Model for Spur Gear Dynamics. *Journal of Mechanisms Transmissions and Automation in Design,* 107(4), pp. 529−535.

Yu, W., Mechefske, C. & Timusk, M., 2017. Influence of the addendum modification on spur gear back-side mesh stiffness and dynamics. *Journal of Sound and Vibration,* Volume 389, pp. 183−201.

naval

ORIGINALITY REPORT

5%	2%	3%	4%
SIMILARITY INDEX	INTERNET SOURCES	PUBLICATIONS	STUDENT PAPERS

PRIMARY SOURCES

1	studentsrepo.um.edu.my Internet Source	<1%
2	Submitted to Cranfield University Student Paper	<1%
3	Encyclopedia of Tribology, 2013. Publication	<1%
4	Submitted to Modern Education Society's College of Engineering, Pune Student Paper	<1%
5	Submitted to Universiti Tunku Abdul Rahman Student Paper	<1%
6	bura.brunel.ac.uk Internet Source	<1%
7	Submitted to Indian Institute of Technology, Madras Student Paper	<1%
8	www.quickspline.com Internet Source	<1%

9	Submitted to Associatie K.U.Leuven Student Paper	<1%
10	Submitted to University of Newcastle upon Tyne Student Paper	<1%
11	Adam D. Foltz, Tamer M. Wasfy, Erik Ostergaard, Ilya Piraner. "Multibody Dynamics Model of a Diesel Engine and Timing Gear Train With Experimental Validation", Volume 4B: Dynamics, Vibration, and Control, 2016 Publication	<1%
12	Submitted to University of Birmingham Student Paper	<1%
13	Jyh-Cheng Yu. "DESIGN OPTIMIZATION FOR ROBUSTNESS USING QUADRATURE FACTORIAL MODELS", Engineering Optimization, 1998 Publication	<1%
14	S.B. Shim, Y.J. Park, K.U. Kim. "Reduction of PTO rattle noise of an agricultural tractor using an anti-backlash gear", Biosystems Engineering, 2008 Publication	<1%
15	Wang, Jian, Hou Liang, Shanming Luo, and Ray Y. Wu. "Active design of tooth profiles using parabolic curve as the line of action", Mechanism and Machine Theory, 2013.	<1%

	Publication	
16	www.nrel.gov Internet Source	<1%
17	Submitted to University of Warwick Student Paper	<1%
18	Submitted to National Institute of Technology, Silchar Student Paper	<1%
19	polymerinfo.com Internet Source	<1%
20	Submitted to University of Queensland Student Paper	<1%
21	involute.pro Internet Source	<1%
22	Qi Zhang, Jaihwa Kang, Wei Dong, Sungki Lyu. "A study on tooth modification and radiation noise of a manual transaxle", International Journal of Precision Engineering and Manufacturing, 2012 Publication	<1%
23	Submitted to University of Leicester Student Paper	<1%
24	Li, S., and A. Kahraman. "Influence of dynamic behaviour on elastohydrodynamic lubrication of spur gears", Proceedings of the Institution of	<1%

	Mechanical Engineers Part J Journal of Engineering Tribology, 2011. Publication	
25	eprints.mdx.ac.uk Internet Source	<1%
26	Wasiq A.M. Abdul, Timothy L. Krantz, Iqbal Shareef. "Influence of tip modification on performance characteristics of involute spur gears", Australian Journal of Mechanical Engineering, 2018 Publication	<1%
27	J.I Pedrero, M Artés, J.C García-Prada. "Determination of the addendum modification factors for gears with pre-established contact ratio", Mechanism and Machine Theory, 1996 Publication	<1%
28	Submitted to University of Sheffield Student Paper	<1%
29	Submitted to KTH - The Royal Institute of Technology Student Paper	<1%
30	"Quantum Chromodynamics", Springer Nature, 2007 Publication	<1%
31	espace.curtin.edu.au Internet Source	<1%

32	Stephen P. Radzevich. "Technological methods for noise/vibration reduction in driveline/transmission of trucks and all-wheel-drive vehicles", International Journal of Vehicle Noise and Vibration, 2006 Publication	<1%
33	Jia-Hung Liu. "Design and manufacture of plunge shaving cutter for shaving gears with tooth modifications", The International Journal of Advanced Manufacturing Technology, 10/29/2008 Publication	<1%
34	J. Hong, D. Talbot, A. Kahraman. "A semi-analytical load distribution model for side-fit involute splines", Mechanism and Machine Theory, 2014 Publication	<1%
35	repository.tudelft.nl Internet Source	<1%
36	Submitted to Queen Mary and Westfield College Student Paper	<1%
37	www.abarth.it Internet Source	<1%
38	Shan Chang, Donald R. Houser, Jonny Harianto. "Tooth Flank Corrections of Wide Face Width Helical Gears That Account for	<1%

Shaft Deflections", Volume 4: 9th International Power Transmission and Gearing Conference, Parts A and B, 2003
Publication

39	Antonio Acinapura, Gionata Fragomeni, Pasquale Francesco Greco, Domenico Mundo, Giuseppe Carbone, Guido Danieli. "Design and Prototyping of Miniaturized Straight Bevel Gears for Biomedical Applications", Machines, 2019 Publication	<1%
40	kar.kent.ac.uk Internet Source	<1%
41	Submitted to Engineers Australia Student Paper	<1%
42	Zedong Hu, Ken Mao. "An investigation of misalignment effects on the performance of acetal gears", Tribology International, 2017 Publication	<1%
43	Hsi Lin, H.. "Dynamic loading of spur gears with linear or parabolic tooth profile modifications", Mechanism and Machine Theory, 199411 Publication	<1%
44	Sheng Li. "An Investigation on the Influence of Misalignment on Micro-pitting of a Spur Gear Pair", Tribology Letters, 2015 Publication	<1%

Exclude quotes	On	Exclude matches	< 10 words
Exclude bibliography	On		